NASA/CR—2015-218390

Design Concepts for Cooled Ceramic Composite Turbine Vane

Robert J. Boyle, Ankur H. Parikh, and Vinod K. Nagpal
N&R Engineering and Management Services, Parma Heights, Ohio

February 2015

NASA STI Program . . . in Profile

Since its founding, NASA has been dedicated to the advancement of aeronautics and space science. The NASA Scientific and Technical Information (STI) program plays a key part in helping NASA maintain this important role.

The NASA STI Program operates under the auspices of the Agency Chief Information Officer. It collects, organizes, provides for archiving, and disseminates NASA's STI. The NASA STI program provides access to the NASA Aeronautics and Space Database and its public interface, the NASA Technical Reports Server, thus providing one of the largest collections of aeronautical and space science STI in the world. Results are published in both non-NASA channels and by NASA in the NASA STI Report Series, which includes the following report types:

- TECHNICAL PUBLICATION. Reports of completed research or a major significant phase of research that present the results of NASA programs and include extensive data or theoretical analysis. Includes compilations of significant scientific and technical data and information deemed to be of continuing reference value. NASA counterpart of peer-reviewed formal professional papers but has less stringent limitations on manuscript length and extent of graphic presentations.

- TECHNICAL MEMORANDUM. Scientific and technical findings that are preliminary or of specialized interest, e.g., quick release reports, working papers, and bibliographies that contain minimal annotation. Does not contain extensive analysis.

- CONTRACTOR REPORT. Scientific and technical findings by NASA-sponsored contractors and grantees.

- CONFERENCE PUBLICATION. Collected papers from scientific and technical conferences, symposia, seminars, or other meetings sponsored or cosponsored by NASA.

- SPECIAL PUBLICATION. Scientific, technical, or historical information from NASA programs, projects, and missions, often concerned with subjects having substantial public interest.

- TECHNICAL TRANSLATION. English-language translations of foreign scientific and technical material pertinent to NASA's mission.

Specialized services also include organizing and publishing research results, distributing specialized research announcements and feeds, providing information desk and personal search support, and enabling data exchange services.

For more information about the NASA STI program, see the following:

- Access the NASA STI program home page at *http://www.sti.nasa.gov*

- E-mail your question to *help@sti.nasa.gov*

- Phone the NASA STI Information Desk at 757-864-9658

- Write to:
  NASA STI Information Desk
  Mail Stop 148
  NASA Langley Research Center
  Hampton, VA 23681-2199

NASA/CR—2015-218390

Design Concepts for Cooled Ceramic Composite Turbine Vane

Robert J. Boyle, Ankur H. Parikh, and Vinod K. Nagpal
N&R Engineering and Management Services, Parma Heights, Ohio

Prepared under Contract NNX11CA49C

National Aeronautics and
Space Administration

Glenn Research Center
Cleveland, Ohio 44135

February 2015

Acknowledgments

We would like to acknowledge the helpful discussions we had with Michael Vinup, Kin Poon, and Edward Zurmehly of Honeywell International Inc., and with Michael Halbig, Ramakrishna Bhatt, James DiCarlo, and Jerry Lang of the NASA Glenn Research Center. Michael Halbig was the contract monitor for this work.

Level of Review: This material has been technically reviewed by technical management.

Available from

NASA STI Information Desk
Mail Stop 148
NASA Langley Research Center
Hampton, VA 23681-2199

National Technical Information Service
5301 Shawnee Road
Alexandria, VA 22312

Available electronically at http://www.sti.nasa.gov

Table of Contents

Design Concepts for Cooled Ceramic Composite Turbine Vane

Robert J. Boyle, Ankur H. Parikh, and Vinod K. Nagpal
N&R Engineering and Management Services
Parma Heights, Ohio 44130

1.0 - Summary

The objective of this work was to develop design concepts for a cooled ceramic vane to be used in the first stage of the High Pressure Turbine(HPT). To insure that the design concepts were relevant to the gas turbine industry needs, Honeywell International Inc. was subcontracted to provide technical guidance for this work. The work performed under this contract can be divided into three broad categories. The first was an analysis of the cycle benefits arising from the higher temperature capability of Ceramic Matrix Composite(CMC) compared with conventional metallic vane materials. The second category was a series of structural analyses for variations in the internal configuration of first stage vane for the High Pressure Turbine(HPT) of a CF6 class commercial airline engine. The third category was analysis for a radial cooled turbine vanes for use in turboshaft engine applications. The size, shape and internal configuration of the turboshaft engine vanes were selected to investigate a cooling concept appropriate to small CMC vanes.

Cycle benefits. The benefits to the engine cycle from using CMC vanes in the HPT are improved efficiency and reduced NOx. The higher temperature capability of CMC materials compared to conventional metallic vane materials results in less required vane coolant when the rotor inlet temperature is unchanged. The higher temperature capability of CMC materials provide the greatest cycle benefits when these materials are used in the first HPT stage. In a cycle analysis most vane cooling air is non-chargeable air, in that this air is available to do work in the first stage rotor. Even if all vane cooling air is considered as non-chargeable air, reduced vane cooling improves vane efficiency. With the same cooling approach for CMC and metallic vanes the calculated reduction in required cooling was nearly 5.5% of the compressor discharge flow rate over a wide range of conditions. The 5.5% reduction in compressor discharge air represents approximately a one-third to one-half reduction in required vane coolant. The calculated improvement in cycle efficiency due to reduced first stage vane coolant was 0.4%. Cooling air introduced into the main gas flow path downstream of the vane throat is sometimes considered chargeable air. Cooling air ejected from the vane trailing edge falls into this category, since it is introduced into the main gas flow path downstream of the vane throat. There is a reduction in trailing edge ejection air when CMC vanes replace metallic vanes. If this air is considered to be chargeable air, the additional improvement in cycle efficiency is 0.6% It is expected that CMC vanes can eliminate second stage HPT vane coolant. When this is done the calculated additional improvement in cycle efficiency was between 0.3 and 0.5%, depending on the compressor extraction location for second stage cooling air. In summary, the calculated cycle efficiency, and thus specific fuel consumption, improvement was as much as 1.5% due to replacing conventional metallic vanes with CMC vanes in both stages of the HPT. The largest improvement in cycle efficiency occurs when both vanes and rotors have higher temperature capability. The calculated improvement in

cycle efficiency was between 5 and 6% when the first stage rotor sees an increased inlet temperature. Raising the rotor inlet temperature while still using metallic rotor blades yields little or no efficiency benefits. Rotor cooling air rapidly increases as rotor inlet temperature is raised, and all rotor cooling air is chargeable air.

The production of NOx in gas turbine combustion is a major concern, and NOx production is a non-linear function of the fuel-to-air ratio. As vane cooling decreases, and rotor inlet temperature remains constant, the combustor outlet temperature, and thus the fuel-to-air ratio decreases. If there was no vane coolant, the combustor outlet and rotor inlet temperatures would be equal. If vane coolant is 10% of mainstream flow, the combustor outlet temperature, and thus the fuel-to-air ratio, would increase by approximately 5%. The 5% reduction in vane coolant was calculated to reduce combustor outlet temperature by $50°C(90°F)$. Experimental data from different sources show that this temperature reduction yields a NOx reduction between 15 to 40%.

Replacing first stage metallic vanes and rotor blades with CMC components in order to raise the rotor inlet temperature was calculated to improve cycle efficiency by at least 5%. A 5% increase in efficiency would reduce CO2 emissions by 5%. However, NOx emissions would not be reduced, since T_{40} increases as T_{41} increases.

Full size vane Steady state aerothermal and structural analyses were done for a first stage HPT vane, and this vane was sized to be consistent with vanes in CF6 class engines. While alternate external vane shapes were identified as likely candidates to reduce maximum stresses, only internal modifications to the reference vane shape were structurally analyzed. Analyses were performed for both pressure and temperature loads. Stresses were determined when only pressure loads were applied, and when only thermal loads were applied. Stresses were also determined when both pressure and thermal loads were simultaneously applied. Pressure loads were determined assuming gas and coolant total pressures of 50 atm. Thermal loads arose from temperature gradients, which varied with the cooling scheme. Even though the total pressure was greater than in current engines, stresses from thermal loads generally exceeded those due to pressure loads. Stresses were calculated using the ANSYS computer code with the linear static modeling assumption, so that creep effects were not included in the analysis. Three stress components: (1) through thickness; (2) hoop; and (3) spanwise, are discussed for each case. While shear stresses were calculated, they are not discussed. The material properties used in the analysis were those of the N24A SiC/SiC CMC system developed under the NASA's Enabling Propulsion Materials (EPM) program. The N24A material is formed from balanced two-dimensional woven plies. The CMC fiber orientation was assumed such that the strength of the CMC was the same in the hoop and spanwise directions. The material strength in the through thickness direction was less than one-tenth of the strength in the other two directions. The through thickness direction was perpendicular to the plane of the weave.

Perhaps the most significant conclusion from this work is that stresses which exceeded design goals were seen for cooling configurations which resembled those used to cool current metallic vanes. However, peak stresses were often highly localized. Significantly lower maximum stresses were identified for configurations without trailing edge ejection, which is a feature of current metallic vanes. However, these configurations required as much cooling as metallic vanes, even though maximum CMC temperatures were much higher than the maximum metal temperatures. A path was identified to reduce maximum CMC stresses,

while maintaining the 5% reduction in required vane coolant. Stress analysis comparisons are given for twenty five pairs of cases. The initial comparisons were done for configurations without trailing edge ejection. For these configurations a rib connecting the suction and pressure surfaces, as well as having a minimum pressure surface wall thickness, was beneficial in terms of reduced maximum stresses. With trailing edge ejection pressure side, as opposed to centerline, trailing edge coolant ejection resulted in lower maximum stresses. By moving the location of the rear of the vane impingement cooling cavity forward, maximum stresses were reduced when trailing. edge ejection was used.

The results from the structural analysis identify where future work is needed. The highly localized regions of maximum stresses indicate that a creep analysis is likely to show reduced maximum stresses. This is especially true for configurations with trailing edge ejection tubes. Maximum tensile and minimum compressive stresses were often seen within the tube, and relatively close to each other. Internal configurations that increased radii in either the rib or fork region showed reduced maximum stress. Alternate external vane shapes which allow for larger radii in high stress regions, and provide acceptable aerodynamics, should be investigated.

Radial cooled vane Current cooling schemes rely on impingement and film cooling to achieve acceptable temperatures. Radial cooling has been proposed for small CMC vanes, such as would be found in turboshaft engine applications. With radial cooling the impingement scheme is replaced by using several cooling tubes, oriented in the spanwise or radial direction. Without film cooling, air flowing through the radial tubes absorbs the entire heat flux due to the gas-to-wall temperature difference. With film cooling, air is extracted from the tubes and is used to reduce the external heat flux by insulating the wall with a film of cooler air. For the same coolant amount, when film cooling air is extracted from the tubes the average tube heat transfer coefficient is lower than when no film cooling is used. Two configurations were analyzed. One was multi-tube radial cooling. The other was a single cavity configuration. This single cavity configuration could be viewed as a single radial tube, or, if there was enough space, as an impingement cooled vane. The single cavity configuration always was coupled with trailing edge ejection tubes.

The thermal and aerodynamic performance was determined for two vane external configurations. One was a half scale version of the vane used for the full size vane structural analysis. The other was a vane shape specified by Dr. Jerry Lang at the NASA Glenn Research Center. Both had acceptable aerodynamics in that calculated vane efficiency was consistent with the full size vane. Neither vane could be effectively cooled using only radial cooling. Film cooling was required to be used in conjunction with multi-tube radial cooling. With film and multi-tube radial cooling, or single cavity and trailing edge ejection cooling, the aggressive future engine goals of NASA's Large Civil Tilt Rotor(LCTR) program could be achieved. These goals are a gas temperature of $1927°C(3500°F)$, and a coolant temperature of $594°C(1100°F)$. The gas temperature includes a pattern factor to account for temperature variations at the combustor outlet. The coolant temperature is significantly warmer than ambient due to a takeoff pressure of 30 atm.

2.0 - Acknowledgments

We would like to acknowledge the helpful discussions we had with Michael Vinup, Kin Poon, and Edward Zurmehly of Honeywell International Inc., and with Michael Halbig, Ramakrishna Bhatt, James DiCarlo, and Jerry Lang of the NASA Glenn Research Center. Michael Halbig was the contract monitor for this work.

3.0 - Introduction

Ceramic Matrix Composite(CMC) vane and rotor blades can significantly improve gas turbine efficiency, due to their higher temperature capability compared to conventional metallic blades. The CMC consists of Silicon Carbide(SiC) fibers in a SiC matrix. Using CMC vanes in the first stage of the High Pressure Turbine(HPT) provides the greatest benefit in terms of reduced vane coolant. Reduced vane coolant results in improved vane and turbine stage efficiency, which results in lower CO2 emissions. If rotor inlet temperature is unchanged when CMC vanes are used, NOx emissions are reduced because the combustor outlet temperature is lowered. However, vane pressure and thermal loads are also at a maximum in the first stage of the HPT. CMC materials have directionally dependent properties, as well as directionally dependent strengths or load bearing capability. CMC have significantly lower strength in the interlaminar direction, compared to their strength in the plane of the fibers. This report gives stress analysis results which account for directionally dependent material properties.

To illustrate the benefits and challenges associated with CMC vanes the report is divided into three sections. The first section addresses the benefits in terms of improved efficiency and reduced NOx emissions from using CMC vanes and blades. The second section presents the results of stress analyses for a vane with varying internal configurations. In this section component stresses in the through thickness, hoop, and spanwise directions are shown. This vane analyzed is suitable for a large engine application. The third section presents the results of a thermal analysis of cooled small size vanes suitable for a turboshaft engine application. This section also gives details of the thermal analysis used for both the small and large engine size vanes.

The benefits of replacing conventional metallic vanes with CMC vanes arise from the higher temperature capability of CMC vanes. For the same rotor inlet temperature, T_{41}, CMC vanes require less coolant than conventional metallic vanes. Vane efficiency increases as the amount of cooling air decreases. Hartsel[1] gave a correlation to estimate the improvement in vane efficiency due to reduced coolant. Increasing vane efficiency increases cycle efficiency, and thus reduces CO2 emissions and fuel consumption. From a cycle standpoint reducing cooling air ejected from the vane trailing edge may be more important than reducing the overall amount of vane cooling air. Trailing edge ejection air is sometimes considered chargeable air. Chargeable air is unavailable to do work in the first HPT stage. NOx emissions are reduced when the combustor outlet temperature is reduced. When T_{41} is held constant, and vane cooling air is reduced, the temperature difference between T_{41} and the combustor outlet temperature, T_{40} is reduced, since the coolant temperature, T_3 is much less than T_{41} A reduced temperature difference between T_{40} and T_{41} results in a lower T_{40}, since T_{41} is unchanged with reduced coolant. Reducing T_{40} reduces the combustor fuel-to-air ratio, and a small change in the fuel-to-air ratio has a disproportionately large change in NOx production. The benefits analysis also includes the consequences of replacing both conventional metallic vanes and rotor blades with CMC vanes and rotor blades. It will be shown that replacing both vanes and rotor blades yields a much greater improvement in cycle efficiency, and thus CO2 emissions, than just replacing metallic vanes with CMC vanes. The efficiency improvement is achieved by raising the rotor inlet temperature, T_{41}. Since raising T_{41} also raises T_{40}, the benefits of reduced NOx emissions are not available when CMC rotor blades

are used.

Stress analyses were done for a vane sized for a CF6 engine size application. Component stresses were evaluated. The component directions were the through thickness or interlaminar, the hoop or circumferential, and the spanwise or radial directions. The vane internal configuration was varied, while the external geometry was held constant for the stress analyses. Stress analyses were done for vanes with and without trailing edge ejection tubes. Thermal analyses showed that trailing edge ejection was needed to achieve the reductions in vane coolant. Without trailing edge ejection, excessive amounts of film cooling were needed if film cooling rows were avoided for the aft portion of the suction surface.

The feasibility of manufacturing CMC vanes have been discussed in several references. CMC vanes have been designed, fabricated, and tested, as discussed by Verrilli et al.[2], Vedula et al.[3], Brewer et al.[4], Watanabe et al.[5], and Nakamura et al.[6]. Marshall and Cox[7] discussed the use of ceramic textiles in gas turbine components. These references discuss the desirability of using film cooling, since current design maximum gas temperatures exceed the expected temperature capability of the Environmental Barrier Coating(EBC) used to shield the CMC. The presence of film cooling rows was not included in the stress analysis. This is not a short coming, since results showed that most of the vane can accommodate the stress augmentation from film cooling rows without causing excessive stresses.

In the stress analysis section comparisons illustrating the effects of vane internal geometric variations, property variations, and modeling assumptions are given. The vane external geometry is that given by Halila et al.[8]. The effects of a rib connecting the pressure and suction surfaces will be examined. The effects of using a thinner pressure surface wall thickness will be examined, The effects of centerline and pressure side trailing edge ejection will be examined. The effects of material property and boundary conditions, as well as the effects of mesh refinement studies will be examined. Stresses due only to pressure loads, and stresses due only to temperature gradients, as well as stresses due to combining these loads will be given. Stresses due to individual loads are shown because, in a specific application, loads different than those used for the analysis are likely to be applied. For example, if the inlet pressure was half of the 50 atm. used, and the pressure distribution was similar, stresses due to pressure loads would be nearly halved. Two stress components, through thickness and hoop, will be discussed in detail. The strength of woven CMC materials in the interlaminar or through thickness direction is substantially lower than the strength in the hoop or fiber direction. For the majority of cases examined the maximum spanwise stress was less than the maximum hoop stress. Detailed stress distributions are not given for spanwise stress, but the maximum spanwise stress is given for each case. The chosen CMC material was N24A. The properties of N24A were given by Mital et al.[9]. This material is a two dimensional balanced weave. It was assumed that material properties in the spanwise or radial direction were the same as those in the hoop direction.

Pressure loads were determined from the vane static pressure distribution. A pressure of 50 atm. was assumed for both the internal pressure, and the external total pressure. Thermal loads were calculated assuming film cooling and impingement cooling for vane cavities. Heat transfer in the trailing edge ejection tubes was calculated from a correlation.

The third section of this report discusses thermal analyses for two vane geometries suitable for the first HPT stage of a turboshaft engine. Vanes for turboshaft engines are approximately half the size of the vanes for a large commercial aircraft engine. One vane geometry

was a half scale version of the full size vane used for the stress analysis. The other vane geometry was specified by Dr. Jerry Lang of the NASA Glenn Research Center. This vane is referred to as the NASA vane. Two cooling configurations were analyzed for each vane. The first configuration was for radial cooling, where tubes are aligned in the spanwise direction. Air flowing through these tubes absorbs heat from the mainstream gas. Thermal analysis was done for radial cooling with and without film cooling. The other cooling configuration was for a single cavity in the forward part of the vane, and trailing edge ejection tubes to cool the aft portion of the vane. Two sets of boundary conditions were analyzed. One was for a gas temperature of $1700°K(2600°F)$ and an inlet total pressure of 17 atm. The other was for a gas temperature of $2200°K(3500°F)$ and an inlet total pressure of 30 atm. This temperature and pressure are consistent with NASA's goals for the Large Civil Tilt Rotor Aircraft(LCTR) program[10].

One objective of this work was to determine if vane radial cooling was a viable cooling approach. In the radial cooling approach tubes are oriented in the spanwise or radial direction. Internal cooling is provided by flow in the radial tubes, and no impingement cooling is used. This cooling approach is relatively easy to implement, and small size vanes may not have room for even a single impingement cooling insert. Since the vanes are smaller than for the full size vane, thermal resistance is lower for HPT vanes of a turboshaft engine than the thermal resistance of vanes used in a large commercial engine.. The analysis included film cooling. It was found that radial cooling without film cooling was unable to keep vane temperatures within acceptable limits. Another objective of this work was to determine if a vane with a single cavity and having trailing edge ejection tubes could be sufficiently cooled when the gas temperature was $2200°K(3500°F)$. The procedure used to determine vane temperatures is discussed in section 4. The same procedure was used to determine vane temperatures for both the full size vane and for the radial cooled vane.

This work addresses the benefits and challenges associated with using CMC vanes to replace conventional metallic vanes in the high pressure turbine. The work was undertaken in consultation with Honeywell International Inc. personnel to insure that it is relevant to industry needs. It is recognized that the trailing edge thickness of a CMC vane may need to be greater than the relatively thin trailing edge of this metal vane.

The purpose of this report is to comprehensively present the results of the work done under the SBIR contract. Previous reports[11-13] covered aspects of the work, but the results presented here cover aspects of the work not presented in any of the references.

4.0 - Benefits from CMC vanes and blades

Typical CMC materials have higher temperature capabilities than conventional metallic vanes, and this leads to less required coolant for the same gas temperature. When only metallic vanes are replaced by CMC vanes rotor inlet temperature, T_{41} is unlikely to increase. Wilcock et al.[14] showed that raising T_{41} for current HPT blades is unlikely to improve thermodynamic efficiency because the additional required rotor cooling air negates the gain in efficiency from raising T_{41}. Rotor cooling air is unavailable to do work in the stage for which it is introduced. If current metallic blades are replaced by CMC blades T_{41}, and thus thermodynamic efficiency, can increase, since rotor cooling need not increase as T_{41} is increased. Even if only current metallic vanes are replaced with CMC vanes there is an improvement in thermodynamic efficiency, since vane efficiency increases as vane cooling requirements decrease. Perhaps as importantly, when only the vanes are made from CMC materials reduced vane coolant is expected to reduce NOx production, since reduced vane coolant reduces the temperature difference between the combustor outlet, T_{40}, and the rotor inlet, T_{41}. If CMC vanes and rotors are used raise cycle efficiency by raising T_{41}, CO2 emissions are reduced, but NOx emissions are not reduced.

4.1 - SFC Improvement from CMC vanes.

Less vane coolant is required when metallic vanes are replaced by CMC vanes. Less vane coolant improves vane aerodynamic efficiency, and stage efficiency further improves because the amount of coolant air ejected from the vane trailing edge is also decreased. If the trailing edge ejection air is considered to be chargeable air, a reduction in this air increases stage output work, with no increase in fuel flow or compressor work. Figure 4.1.1 compares material properties for a selected CMC material and MA754, which is an alloy suitable for HPT vanes(Halila et al.[8]). The MA754 properties were obtained from the Special Metals web site[15]. The properties of the CMC material(N24A), a balanced 2D weave, were obtained from Mital et al.[9]. As discussed by DiCarlo et al.[16] this is a fiber reinforced SiC/SiC material with an upper use temperature of $1316°C(2400°F)$. While the ratio of the Proportional Limit(PL) strength to the Ultimate Tensile Strength(UTS) is lower for N24A than for MA754, N24A maintains its strength to a much higher temperature. This figure shows that for N24A the UTS in the through thickness or interlaminar direction is nearly a order of magnitude lower than the UTS in the plane of the weave.

Thermal properties and stiffness are given in figure 4.1.2 for both the CMC material and the reference metallic material. At high temperatures N24A has lower thermal conductivity and coefficient of thermal expansion than MA754. In the comparative thermal analysis a thin EBC layer was applied over the CMC vane and was assumed to have a temperature capability of $1483°C(2700°F)$. This EBC layer had a thermal conductivity of $1W/m-K$. The EBC material was described by Lee et al.[17]. For the comparative thermal analysis a Thermal Barrier Coating(TBC) having the same thermal conductivity, but a lower temperature capability of $1316°C(2400°F)$. was applied to the metallic vane.

Figure 4.1.3 shows typical maximum temperatures for the CMC and the protective low conductivity EBC layer. These temperatures are the midspan outer temperatures of each layer. A surface distance of zero corresponding to the leading edge stagnation point. Since

CMC materials require an EBC, comparisons were made assuming that both the metal and CMC vanes had prime reliant 0.25mm(10mil) Thermal Barrier Coatings(TBC). A relatively thick EBC or TBC layer, reduces the temperature gradients in the vane walls. The desirability of reducing the wall temperature gradient will be shown.

The calculations shown in figure 4.1.3 were done using data from Reiss and Bolcs[18] for the leading edge region film effectiveness and heat transfer, and the correlation developed by Boyle and Ameri[19] for film cooling effectiveness. Local film cooling effectiveness was calculated assuming superposition from upstream cooling rows. The outer temperatures show a saw tooth pattern, and temperature minimums indicate the location of film cooling rows. No suction surface film cooling rows were downstream of the vane throat, since doing so causes excessive aerodynamic losses. The relatively thick barrier coatings resulted in the outer coatings reaching their maximum temperatures, while most of the vane temperatures were less than their maximum values. Using a thick barrier coating lessened the vane through thickness temperature gradients, which lowered vane thermal stresses.

Figure 4.1.4 shows calculated vane coolant fractions, (vane coolant-to-compressor discharge, $(w_C/w_{2.5})$ ratio) for both the metal and CMC vanes. Comparisons were made at constant rotor inlet temperature, T_{41}. These comparisons show that the reduction in vane coolant when using CMC vanes is approximately 5% over a wide range of rotor inlet temperatures, T_{41}. The calculated coolant fractions included both film cooling and cooling using trailing edge ejection. The portion of the cooling air fraction attributable to trailing edge ejection was found using internal heat transfer correlations and appropriate pressure losses.

The approximately 5.5% reduction in required cooling air improves cycle efficiency because vane aerodynamic efficiency increases when vane cooling is reduced. Stage output increases when vane trailing edge ejection air is reduced. Improved cycle efficiency reduces CO2 emissions. The improvement in vane aerodynamic efficiency due to reduced coolant was calculated using the correlation given by Hartsel[1] Calculations using this correlation showed that a 5.5% reduction in vane coolant air increased the total pressure at the rotor inlet by 0.86%. Even though this increase in total pressure is less than 1%, there is a resulting increase in turbine output of 0.2%. This 0.2% increase in turbine output results in a cycle efficiency increase of approximately 0.4%.

Most first stage HPT vane cooling air is non-chargeable air, and is available to do work in the first stage rotor. However, air ejected from the trailing edge of the first HPT stage vane may be considered as chargeable air. Even if this air is not considered to be chargeable air the first stage performance is likely to decrease since trailing edge ejection air causes increased aerodynamic loss. Assuming first stage vane trailing edge ejection cooling air is fully chargeable air gives a significant improvement in SFC. Calculations showed that there was a 5.5% reduction in required vane coolant from using CMC vanes. Trailing edge ejection air was reduced by 1.2% of mainstream air, or nearly a quarter of the overall 5.5% reduction. This 1.2% reduction in first stage vane chargeable air improved SFC by 0.6% for a highly efficient two stage HPT with equal work splits, and an equal work split between the HPT and Low Pressure Turbine. If trailing edge ejection air is not considered to be chargeable air, it still benefits stage performance to reduce trailing edge ejection air. Trailing edge ejection air only partially fills in the vane wake, and there is a large rotor incidence variation when the rotor passes through the vane wake. The incidence variation decreases rotor, and therefore stage, performance.

If using CMC material reduces first stage HPT coolant requirements, cooling can be eliminated for the second stage HPT vane. This also improves SFC. In the design report of Halila et al.[8] the second stage HPT vane cooling flow was 1.85%, of which 0.75% was used for purge air. It is conservative to assume a 1.1% reduction in stage two vane cooling air due to using CMC vanes. While second stage air is chargeable air, it may come from an intermediate compressor stage, and thus is not fully chargeable air. On the other hand, according to Honeywell International Inc. personnel, in small engine applications, it is sometimes desirable to extract HPT cooling air for both stages from the compressor exit. A 1.1% reduction in second stage HPT vane cooling air improves cycle efficiency by 0.55%, when this air is compressor discharge air. It is estimated that the SFC improvement would be about 0.3% when second stage vane cooling air is extracted from and intermediate compressor stage. The Hartsel[1] correlation gives only a small reduction in second stage vane pressure loss due to the elimination of cooling air.

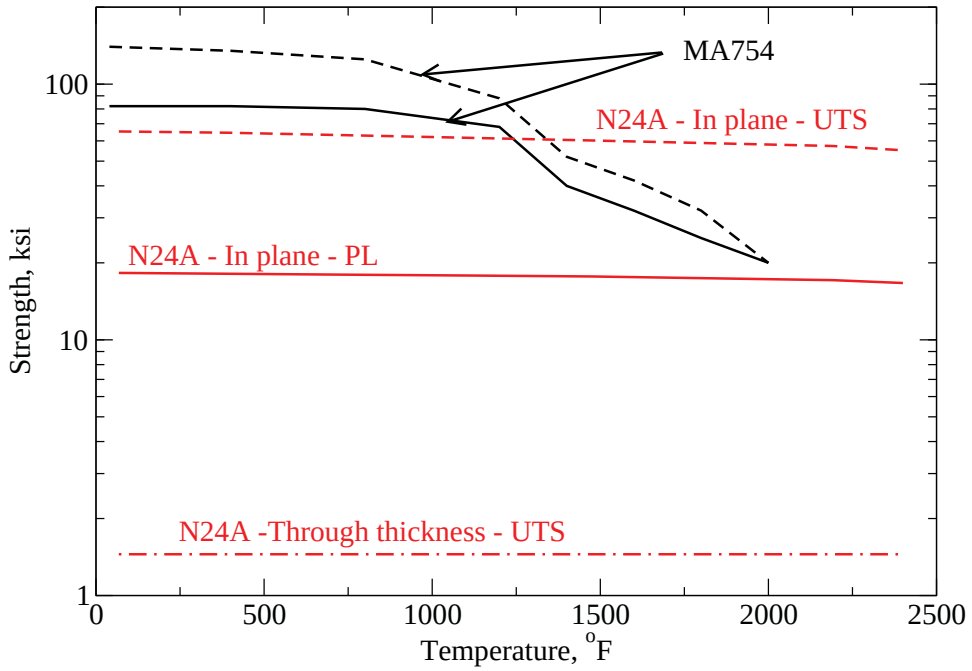

Fig. 4.1.1 Strength properties of CMC material N24A and conventional metallic vane material MA754

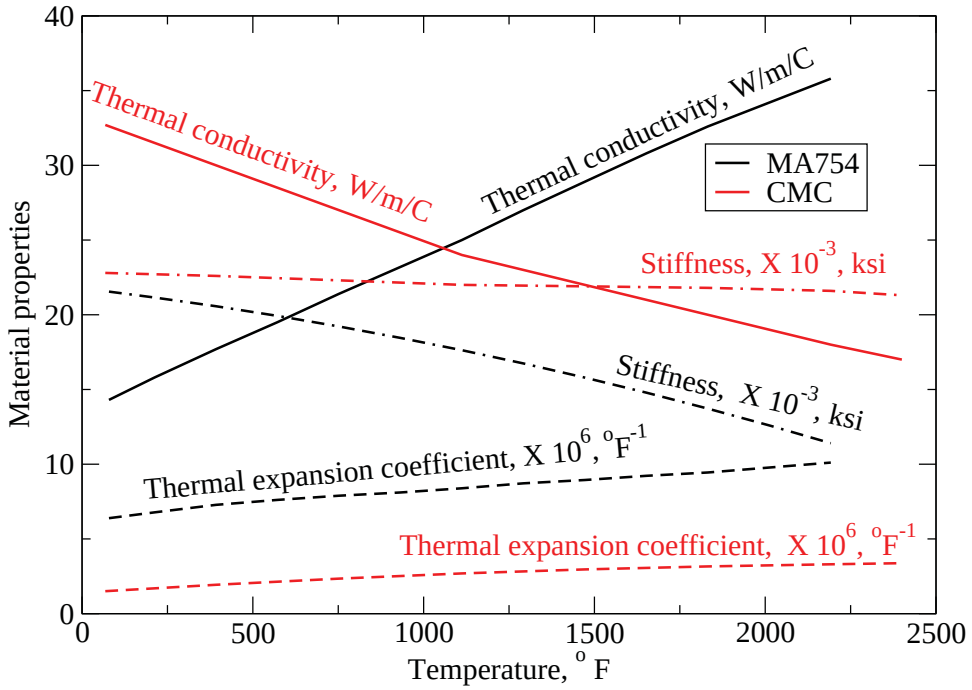

Fig. 4.1.2 Material properties for N24A and MA754

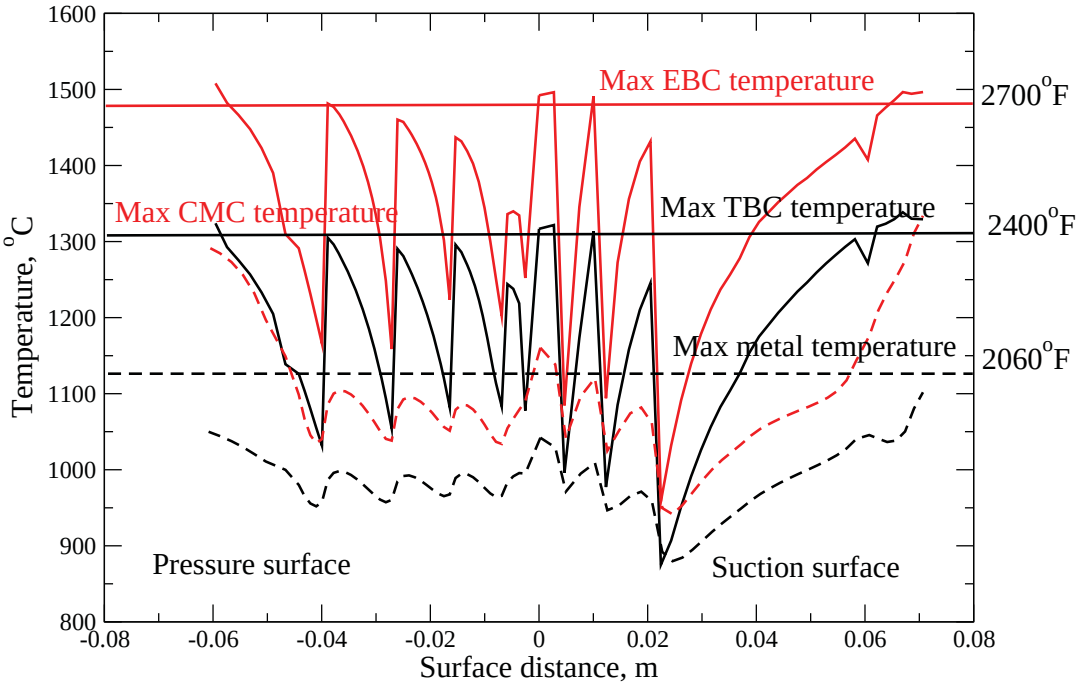

Fig. 4.1.3 Maximum vane and EBC/TBC temperatures for CMC and metallic vanes

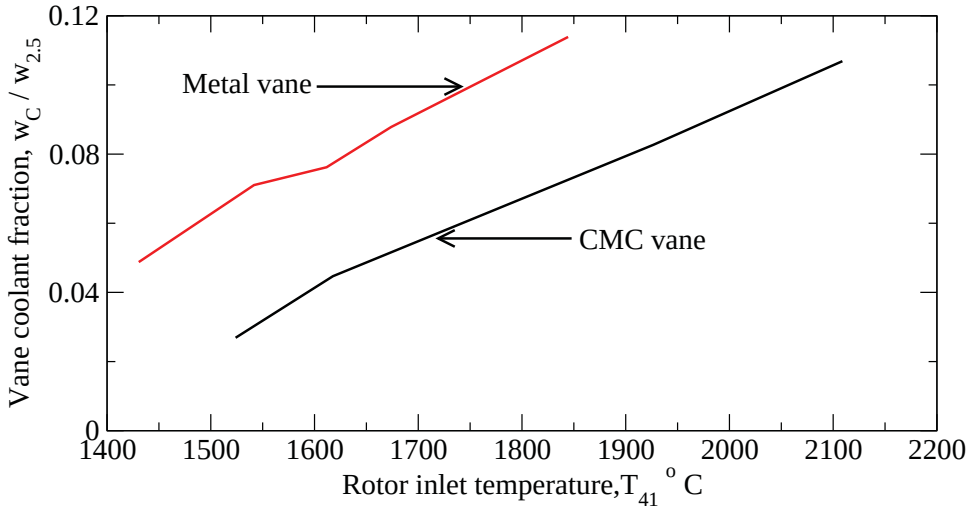

Fig. 4.1.4 Coolant fractions for CMC and metallic vanes

4.2 - NOx reduction from CMC vanes.

Because CMC vanes use less cooling air than metal vanes for the same rotor inlet temperature, T_{41}, the combustor outlet temperature, T_{40}, is lower when CMC vanes replace conventional metallic vanes. Since most vane cooling air is non-chargeable air, the turbine output is nearly the same when CMC vanes replace metallic vanes.

Data show that a small reduction in T_{40} significantly reduces NOx. A constant specific heat thermal balance across the vane row gives:

$$T_{41}(1 + w_C/w_{40}) = T_{40} + w_C T_C$$

where w_C/w_{40} is the vane coolant fraction, and T_C is the coolant temperature. While T_{41} and T_C vary depending on the application, a typical difference between these two temperatures is $1000°C(1800°F)$. For this temperature difference a 5% reduction in w_C/w_{40} results in a $50°C(90°F)$ reduction in T_{40}.

Several references showed that the amount of NOx produced is very sensitive to T_{40}. Figure 4.2.1, from Tacina et al.[20], shows the amount of NOx produced per kilogram of fuel as a function of the flame temperature. NOx is strongly dependent on the combustor configuration, and the red line data is for the configuration with the lowest NOx at high temperature. The peak gas temperature, T_G, which corresponds to the flame temperature is over $2000°K(3140°F)$ and is expected to be more than $200°C(360°F)$ hotter than T_{40}. An extrapolation of the curve shows that NOx is reduced by nearly 15% when the flame temperature is reduced by $50°C(90°F)$.

The straight lines in figure 4.2.2, which is from Harth et al.[21] show that the relative sensitivity of NOx to the adiabatic combustor temperature is independent of this temperature. This combustor, like the combustor tested by Tacina et al.[20], is for an aircraft engine application, At the highest combustor pressure and inlet temperature a change of $50°K(90°F)$ in the adiabatic temperature reduces NOx by more than 40%.

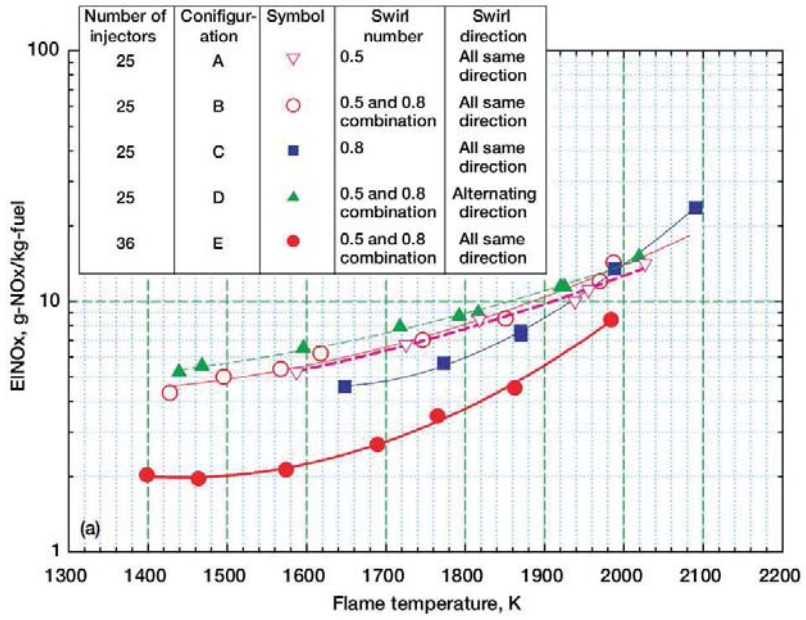

Fig. 4.2.1 NOx as a function fo flame temperature for different combustor geometries, from Tacina et al.[20]

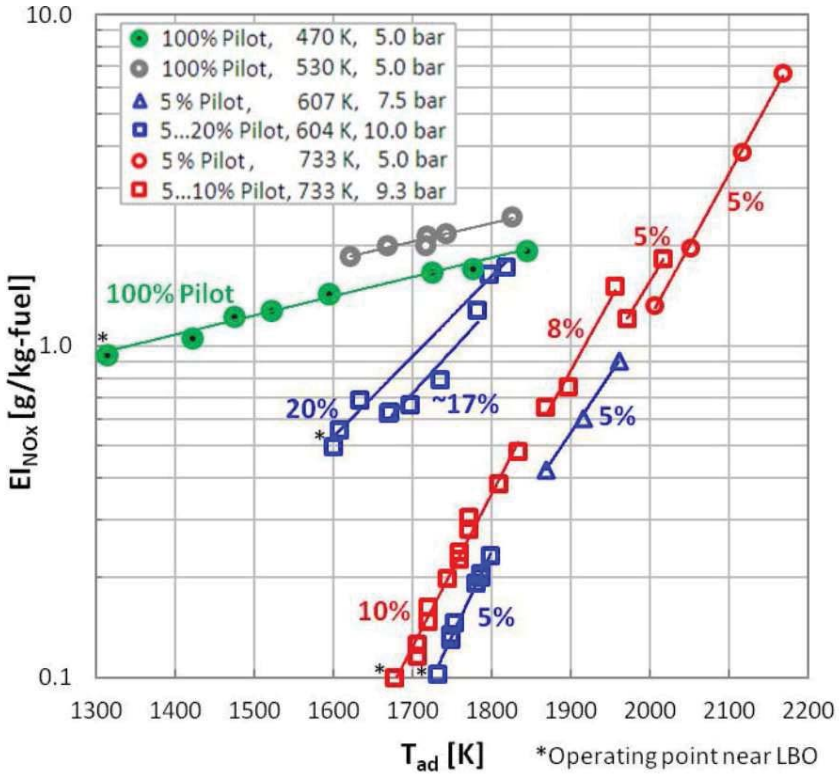

Fig. 4.2.2 NOx as a function of adiabatic temperature for different combustor consitions and fuel splits, from Harth et al.[21]

Fiure 4.2.3, from Dusing et al.[22], shows results similar to those in figure 4.2.2, but for a combustor designed for ground power application. This figure has lines with straight slopes, and shows that a $50°K(90°F)$ reduction in combustor outlet temperature reduces NOx by more than 40lines are approximately parallel for two technology levels, (2006 & 2011). Therefore, it is not likely that future combustor designs will have relative NOx sensitivities significantly lower than current combustor designs. The absolute level of NOx is expected to be lower for future combustors operating at current conditions. However, combustor outlet temperatures and pressures are expected to increase over time, and increases in either of these parameters raises NOx levels. The benefits of lower T_{40} from using CMC vanes provides a means of offsetting the adverse effects of higher temperature and pressure.

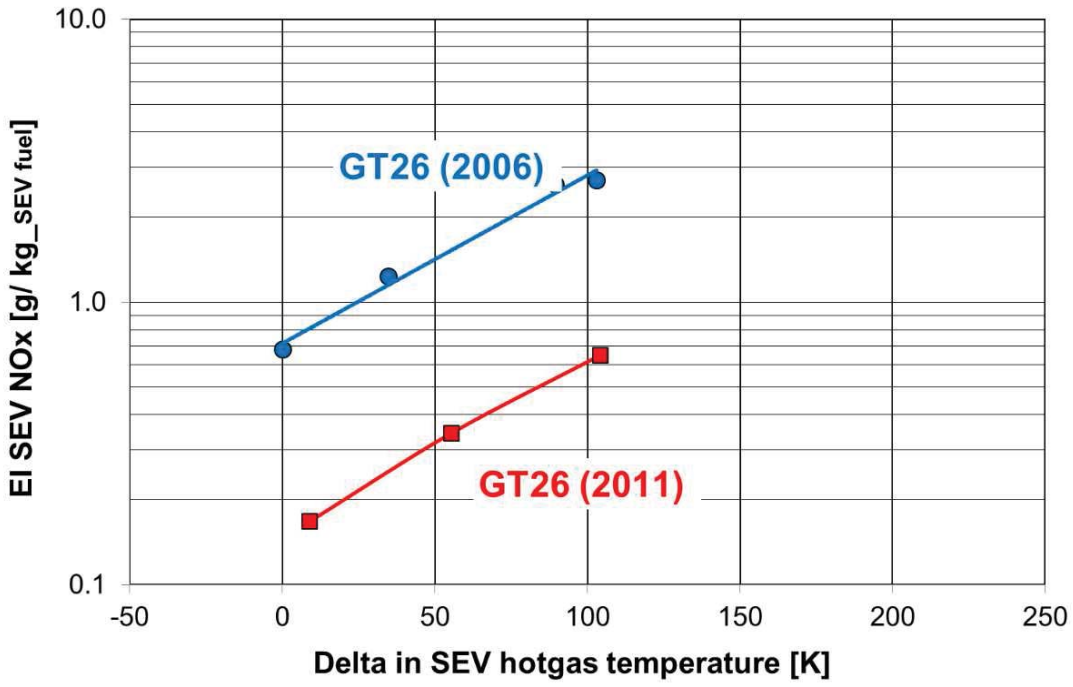

Fig. 4.2.3 NOx as a function fo flame temperature for different combustor geometries, from Dusing et al.[22]

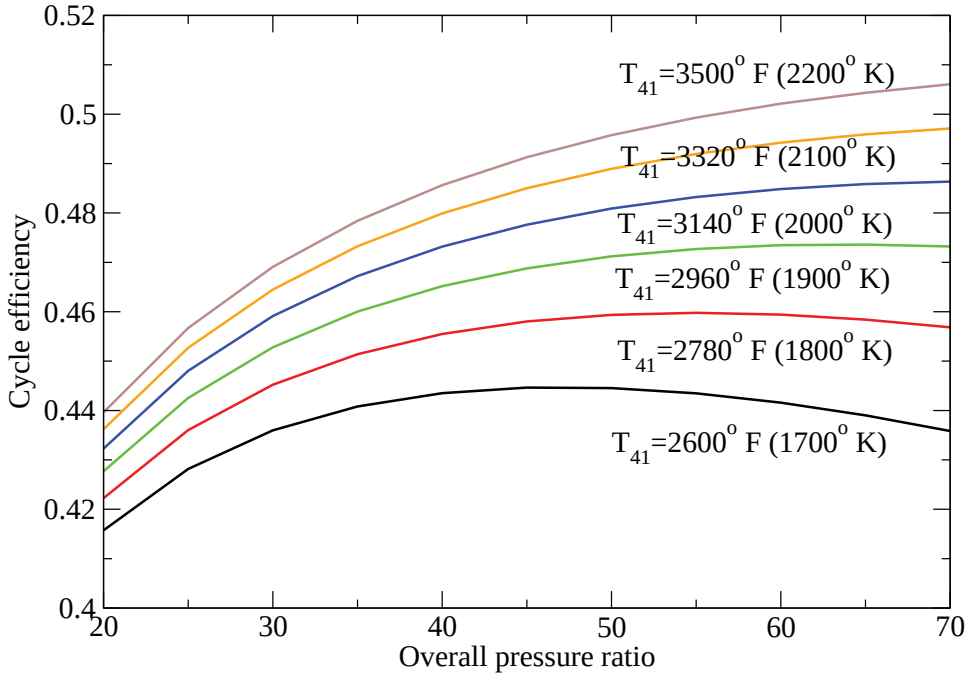

Fig. 4.3.1 Typical cycle efficiency, constant coolant fraction, from Boyle and Jones[23]

4.3 - SFC improvements from CMC vanes and blades

The maximum SFC improvement from replacing metallic airfoils with CMC airfoils is achieved by maintaining the cooling fraction and raising the rotor inlet temperature, T_{41}. Wilcock et al.[14] showed that raising T_{41} for conventional metallic rotor blades does not improve SFC because of the additional cooling air required for the rotor blades. Without penalizing the rotor for additional cooling air, raising T_{41} implicitly assumes both CMC vanes and rotor blades. Figure 4.3.1, from Boyle and Jones[23], shows cycle efficiency for a representative set of conditions, and the assumption that rotor cooling flow fractions are independent of temperature. Higher gas temperatures are achieved by improving the temperature capability of the vane and rotor materials. In reference 24, it was shown that there is no improvement in cycle efficiency with increasing temperature for an ideal cycle, due to the specific heat increasing with temperature. However, this is not the case when stage efficiencies are less than one. At the lowest T_{41}, efficiency decreases for Overall Pressure Ratio(OPR) beyond 45, but efficiency continues to increase with OPR for higher temperatures.

Analyses were also done for the increase in T_{41} when using CMC vanes. Maximum surface temperatures were $2700°F(1756°K)$ for the CMC vane and $2400°F(1589°K)$ for the metal vane. The vane coolant fraction was held constant at 10.6% of compressor discharge air. Coolant air temperature was also held constant. The rotor inlet temperature for the metallic vane was calculated to be $2935°F(1886°K)$. Somewhat surprisingly, the increase in T_{41} was greater than the $300°F(167°C)$ increase in the maximum surface temperature. T_{41} increased by $525°F(292°C)$ when the metallic vane was replaced by a CMC vane. Figure 4.3.1 shows that a $300°(540°F)$ increase in T_{41} produces a relative increase in cycle efficiency of at least 3% at constant OPR when the OPR is between 40 and 50. The minimum relative

increase is at high T_{41} values. When the increase in T_{41} is accompanied by an increase in OPR, as has been the historic trend, a 300° increase in T_{41} yields even greater efficiency gains. Going from $T_{41} = 1900°K(2960°F)$ and an OPR of 40 to a $T_{41} = 2200°K(3500°F)$ and an OPR of 50 results in a relative cycle efficiency gain of over 6%. It is conservative to expect a gain of 5% in cycle efficiency due to replacing metallic vanes and rotor blades with CMC components.

4.4 - Conclusions

CMC first stage HPT vanes require 5.5% less vane coolant due to the CMC vanes having higher temperature capabilities for the same cooling configuration. Just replacing metallic vanes with CMC vanes can improve cycle efficiency up to 1.5%. An improvement of 0.4% in efficiency was due to increased first stage vane efficiency. Elimination of second stage vane coolant was estimated to increase cycle efficiency between 0.3 and 0.5%. The lower increase assumed that second stage vane cooling was extracted from an intermediate compressor stage. The higher efficiency increase assumed that second stage vane cooling air was extracted from the compressor exit. With CMC vanes there is a reduction in the required amount of air ejected from the vane trailing edge. Trailing edge ejection air is sometimes considered to be chargeable air in a cycle analysis. If the reduction in trailing edge ejection air, is treated as chargeable air, the additional cycle efficiency improvement was estimated as 0.6% This improvement came from replacing metallic vanes with CMC vanes.

When conventional metallic vanes are replaced with CMC vanes, and the rotor inlet temperature, T_{41} remains the same, the required vane coolant is reduced by approximately 5% of mainstream air ratio. This is due to the higher temperature capability of the CMC materials. The 5% reduction in mainstream air used for vane coolant reduces T_{40} by approximately $50°K(90°F)$. This has a disproportionately large reduction in NOx due to the high sensitivity of NOx to combustor outlet temperature, T_{40}. Experimental data from different sources show a reduction in NOx ranging from 15% to over 40% due to just a $50°K(90°F)$ reduction in T_{40}.

Replacing both conventional metallic HPT vanes and rotor blades with CMC vanes and rotors results in the highest gain in cycle efficiency. It was calculated that the rotor inlet temperature could be raised nearly $300°C(540°F)$ when CMC vanes and rotor blades are used. It was shown that a $300°C$ increase in T_{41} is expected to raise cycle efficiency by at least 5%. A 5% efficiency increase represents a 5% decrease in CO2 emissions. However, NOx emissions will not decrease due to using CMC vanes and blades, since raising T_{41} raises T_{40}.

5.0 - Stress Analysis of CMC Vane

Steady state aerothermal and structural analyses were done to identify approaches to achieving acceptable stress distributions for a specified vane external geometry. This section of the report gives the effects on stress components due to changes in the vane internal geometry, as well as other factors, such as material properties, boundary conditions, and grid density. Figure 4.1.1 shows that allowable stresses for the CMC material are directionally dependent. Consequently, component stresses were calculated. A somewhat arbitrary goal of this work was to identify configurations having through thickness or interlaminar stresses below 1.5ksi(10.5MPa), and having hoop and spanwise stresses below 17ksi(117MPa). This goal was based on the properties of N24A material, and as shown by Engel[25] other CMC materials have significantly higher interlaminar strengths. Detailed results are presented for through thickness and hoop stresses. For the assumed orientation of the reference CMC material(N24A) the allowable stresses in the spanwise or radial direction and in the hoop or vane circumferential direction were the same. Generally, but not for all cases, the maximum spanwise stress in the vane midspan region was lower than the maximum hoop stress in this region. Although a detailed discussion of spanwise stresses is not given, the maximum component stress in all three directions is discussed.

Pressure and thermal loads were determined from Navier-Stokes Computational Fluid Dynamics analyses. Pressure and heat transfer coefficient distributions were calculated using two and three dimensional versions of the Navier Stokes computer analysis codes described in references 26 and 27. A single vane normalized pressure distribution was used. This distribution is for a vane exit Mach number of 0.95. Three dimensional analyses of the vane and flow path of reference vane geometry given by Halila et al.[8] showed little spanwise variation in either pressures or heat transfer coefficients. Consequently, midspan distributions were used for each spanwise vane location.

Heat transfer distributions vary with vane total pressure, and were also obtained using the Navier Stokes analysis. Boundary layer transition was accounted for in determining heat transfer distributions, when film cooling was not used. Data show that, just the presence of film cooling holes causes transition to fully turbulent flow immediately downstream of the film cooling holes. Consequently, when film cooling was used, the flow was assumed to be fully turbulent. The local heat flux is a function of both the heat transfer coefficient and the adiabatic wall temperature. Without film cooling the adiabatic wall temperature is nearly the gas temperature. With film cooling the adiabatic wall temperature approaches the coolant, or compressor discharge, temperature, when the film effectiveness approaches one. The distribution of the vane film cooling effectiveness away from the leading edge was found using the analysis given by Boyle and Ameri[19]. In the leading edge region the film cooling effectiveness, and the increase in the local heat transfer coefficients, were found using the results given by Reiss and Bolcs[18] Internal cooling was either by impingement cooling or by flow through radial cooling tubes. When impingement cooling was assumed, the correlation of Florschuetz et al.[28] for a staggered array of impingement cooling holes was used. When radial cooling was used, the tube heat transfer coefficient was determined by the standard correlation for turbulent flow in a tube[29]. Tube heat transfer, which is a function of the mass flux, was corrected to account for the change in midspan mass flux when film cooling was used in conjunction with radial cooling.

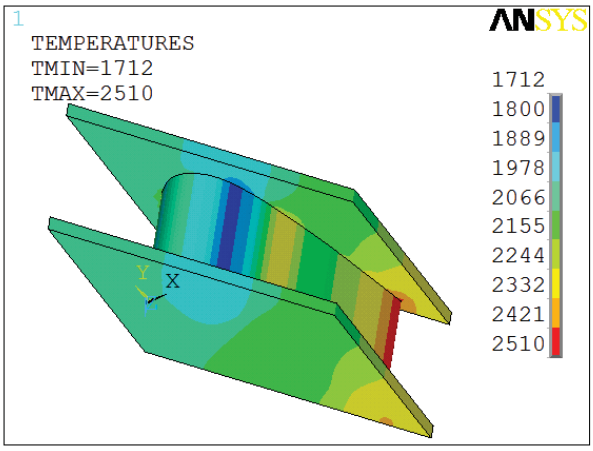

Fig. 5.0.1 Vane with two endplates

Structural analysis was done using the ANSYS code[30]. Component stresses were calculated using the ANSYS linear-static assumptions. CMC materials have higher strengths in the fiber directions. At each point within the CMC material stresses were resolved into three directions. These were the through thickness, hoop, and spanwise directions. The through thickness direction was generally normal to the internal vane surface. Where the vane had no internal surface, typically the aft portion of the vane, the through thickness direction was normal to the vane external surface. The hoop direction was normal to the through thickness direction. Component stresses were calculated using local coordinate systems within the vane and the "as calculated" ANSYS option. Properties of the CMC material, N24A, were also directionally dependent. Even though actual gas turbine vanes are defined by cylindrical coordinates, Cartesian coordinates were used in the analysis. The model vane, shown in figure 5.0.1, has all the necessary features of an actual vane. The vane and end plates show a typical external temperature distribution, where the temperature is in $^{\circ}F$. One of the end plates is fixed, while the other end plate is free to expand in all directions.

While film cooling was assumed to determine vane temperature distributions, film cooling holes were not included in the structural analysis. Film cooling holes have closer spacing in the spanwise direction than in the circumferential or hoop direction. Because of this, hoop stresses are more sensitive than spanwise stresses to stress augmentation due to an area reduction from film cooling holes. It will be shown that peak stresses are highly localized. For most cases there are ample regions where rows of film cooling holes could be located without causing excessive stresses.

The reference vane is shown in figure 5.0.2 The external vane shape is that of the vane of Halila et al.8]. This vane was designed under contract as part of NASA's Energy Efficient Engine(EEE) program. This figure shows a uniform wall thickness of 2mm(80 mil). The vane has an axial chord, C_{X}, of 3.38cm(1.33in), and a true chord nearly twice as long at 6.3cm(2.48in). Three red circles are shown in this figure. The largest circle shows the leading edge region curvature. While the actual leading edge is elliptical in shape, the leading edge radius is approximately 0.3cm(118mil). A smaller circle of 0.076cm(30mil) radius is shown where the inner CMC surfaces come together to form the fork region. Where the inner suction and pressure walls join this radius was used in the stress analysis for the uniform wall thickness cases.. The third circle with a radius of 0.0535cm(21mil) is at the trailing edge. The analysis was done using this radius, even though a thicker trailing edge is likely to be needed for a CMC vane.

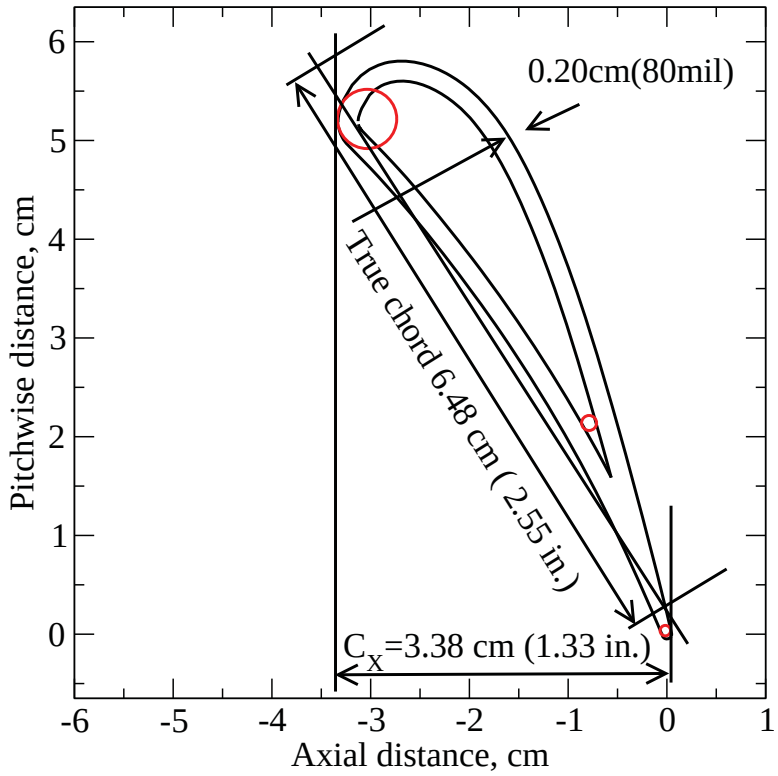

Fig. 5.0.2 Reference vane geometry

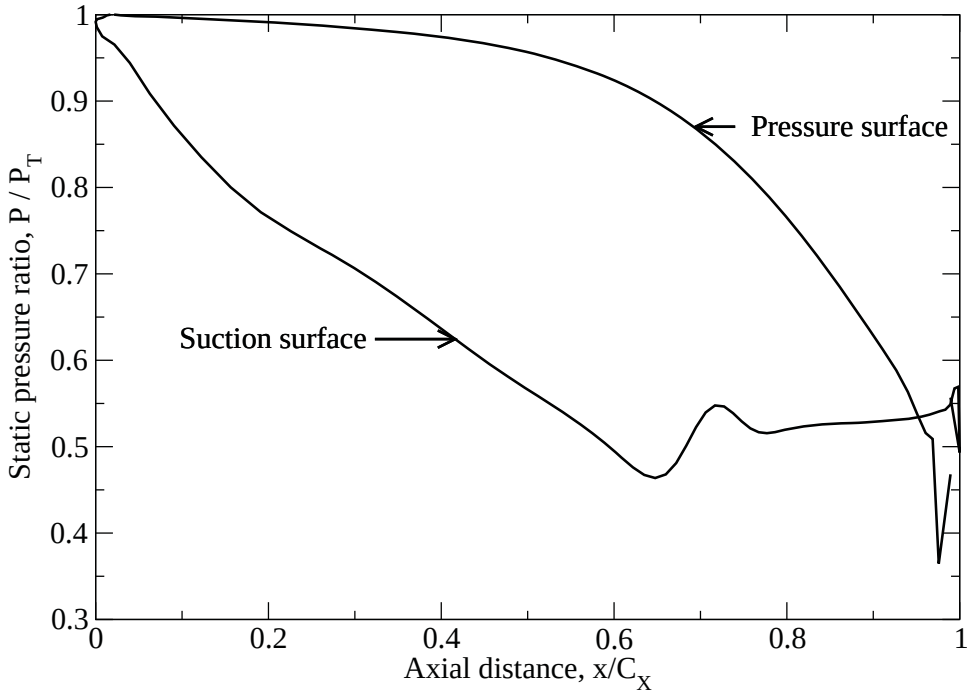

Fig. 5.0.3 Pressure distribution for reference vane

Pressure loads were evaluated using the external pressure distributions shown in figure 5.0.3. Except for one analysis case, there was an internal pressure equal to the external total pressure. The largest pressure differential occurs near mid-chord, where the suction surface pressure is only about half of the inlet total pressure.

Table 5.0.1 gives the list of cases that were analyzed. The case numbering, 1A through 13B, is somewhat arbitrary, but is used to identify cases for comparison purposes. Stresses were calculated for pressure and temperature loads independently, and when pressure and temperature loads were combined. The purpose of each case is given in the table. The majority of cases had a rib connecting the pressure and suction surfaces of the vane, and for most of these cases the rib was insulated. The majority of cases had a differential wall thickness, where the the thickness of the pressure surface and in leading edge were half of the 2mm(80 mil) thickness of the uniform wall thickness cases. Reducing the suction surface wall thickness resulted in very high stresses just due to pressure loads. For most of the cases a non-uniform temperature distribution was used. Nearly half of the cases had either centerline or pressure side trailing edge ejection.

Figure 5.0.4 shows the vane configurations described in Table 5.0.1 This figure show the vane configurations and temperatures for the CMC vane. Only very close to the trailing edge does the vane temperature slightly exceed the desired maximum CMC temperature of $1316°C(2400°F)$. The region is very small, and is approximately the same in each part of the figure. Part a shows the baseline case of single large impingement cavity. Part b shows a vane having a differential wall thickness. The rib is uninsulated, accounting for its relatively cold temperature. Part c shows temperatures through a slice of the vane showing the trailing edge ejection tube. As expected, near the entrance of the tube the surface temperatures are relatively cold. Part d shows temperatures for a single cavity configuration. The end temperatures are shown through the solid section, rather than through the trailing edge ejection tube. This single cavity configuration has the size cavity as the forward cavity shown in part b of figure 5.0.4

Table 5.0.1 - List of Cases

Cases	Load	Purpose	Rib		Wall	CMC	T.E.
			Present	Insulated	Thickness	ΔT	Ejection
1A	Pres	Base line case	No	N.A.	Uniform	N.A.	No
1B	Temp	Uniform ΔT	No	N.A.	Uniform	Uniform	No
1C	Temp	Non-Uniform ΔT	No	N.A.	Uniform	Non-Uniform	No
1D	Comb	Combined loads	No	N.A.	Uniform	Non-Uniform	No
2A	Pres	Connecting rib	Yes	N.A.	Uniform	N.A.	No
2B	Temp	Connecting rib	Yes	No	Uniform	Non-Uniform	No
2C	Comb	Combined loads	Yes	No	Uniform	Non-Uniform	No
3A	Pres	Differential wall thickness	Yes	N.A.	Differential	N.A.	No
3A2	Pres	No internal pressure	Yes	N.A.	Differential	N.A.	No
3B	Temp	Differential wall thickness	Yes	No	Differential	Non-Uniform	No
3C	Temp	Insulating rib	Yes	Yes	Differential	Non-Uniform	No
3D	Comb	Insulating rib	Yes	Yes	Differential	Non-Uniform	No
4A	Pres	Centerline trailing edge ejection	Yes	N.A.	Differential	N.A.	Yes/Cl
4B	Temp	Centerline trailing edge ejection	Yes	Yes	Differential	Non-Uniform	Yes/Cl
4C	Comb	Centerline trailing edge ejection	Yes	Yes	Differential	Non-Uniform	Yes/Cl
5A	Comb	Revised rib shape	Yes	Yes	Differential	Non-Uniform	Yes/Cl
5B	Comb	Reduced coolant	Yes	Yes	Differential	Non-Uniform	Yes/Cl
5C	Comb	Presure side trailing edge ejection	Yes	Yes	Differential	Non-Uniform	Yes/P.S.
5D	Pres	Revised rib shape	Yes	N.A.	Differential	N.A.	No
5E	Pres	Single impingement cavity	No	N.A.	Differential	N.A.	Yes/P.S.
5F	Pres	Pressure side trailing edge ejection	Yes	N.A.	Differential	N.A.	Yes/P.S.
5G	Comb	Single impingement cavity	No	N.A.	Differential	Non-Uniform	Yes/P.S.
6A	Comb	Modulus(E33) change	Yes	Yes	Differential	Non-Uniform	No
6B	Comb	Modulus(E33) change	Yes	Yes.	Differential	Non-Uniform	No
6C	Comb	Revised temperatures	Yes	Yes	Differential	Non-Uniform	No
6D	Comb	Modulus(E33) change	Yes	Yes	Differential	Non-Uniform	No
6E	Comb	Modulus(E33) change	Yes	Yes	Differential	Non-Uniform	Yes/Cl
6F	Temp	Revised temperatures	Yes	Yes	Differential	Non-Uniform	No
6G	Comb	Combined loads	Yes	Yes	Differential	Non-Uniform	No
7A	Comb	End plate thickness	Yes	Yes	Differential	Non-Uniform	No
7B	Comb	Mesh refinement	Yes	Yes	Differential	Non-Uniform	No
7C	Comb	Boundary conditions	Yes	Yes	Differential	Non-Uniform	No
7D	Comb	Square trailing edge	Yes	Yes	Differential	Non-Uniform	No
8A	Comb	Increased CMC conductivity	Yes	Yes	Differential	Non-Uniform	No
10A	Temp	Modified leading edge shape	Yes	Yes	Differential	Non-Uniform	No
10B	Temp	Mesh refinement	Yes	Yes	Differential	Non-Uniform	No
10C	Temp	Hemispherical rib	Yes	Yes	Differential	Non-Uniform	No
10D	Temp	New temperature distribution	Yes	Yes.	Differential	Non-Uniform	No
11A	Pres	Square tube - Hemispherical fork	No	N.A.	Differential	N.A.	Yes/P.S.
11B	Pres	Meshing variation	No	N.A.	Differential	N.A.	Yes/P.S.
11C	Pres	Circular tube	No	N.A.	Differential	N.A.	Yes/P.S.
11D	Pres	Circular tube - mesh refinement	No	N.A.	Differential	N.A.	Yes/P.S.
11E	Pres	Circular tube - meshing variation	No	N.A.	Differential	N.A.	Yes/P.S.
11F1	Temp	Circular tube - meshing variation	No	N.A.	Differential	Non-Uniform	Yes/P.S.
11F2	Comb	Circular tube - meshing variation	No	N.A.	Differential	Non-Uniform	Yes/P.S.
11G1	Temp	Square tube - meshing variation	No	N.A.	Differential	Non-Uniform	Yes/P.S.
11G2	Comb	Square tube - meshing variation	No	N.A.	Differential	Non-Uniform	Yes/P.S.
12A	Comb	E33 variation E33=157	Yes	Yes	Differential	Non-Uniform	Yes/P.S.
12B	Comb	E33 variation E33=77	Yes	Yes	Differential	Non-Uniform	Yes/P.S.
13A	Temp	Revised temperatures	Yes	Yes	Differential	Non-Uniform	Yes/Cl
13B	Temp	Insulated fork region	Yes	Yes	Differential	Non-Uniform	Yes/Cl

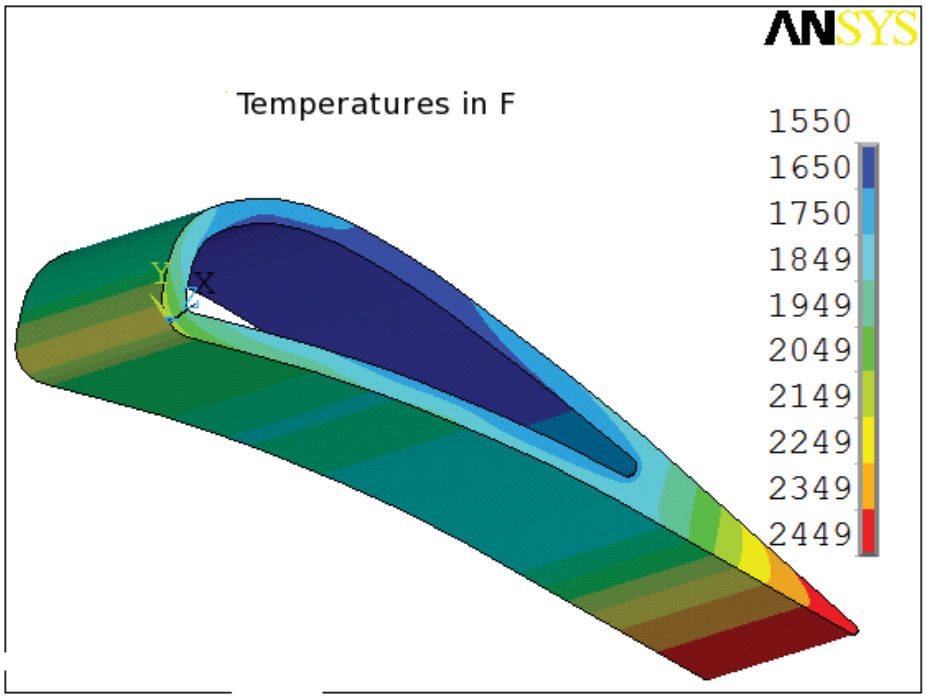

a) Baseline vane - no rib - no trailing edge ejection

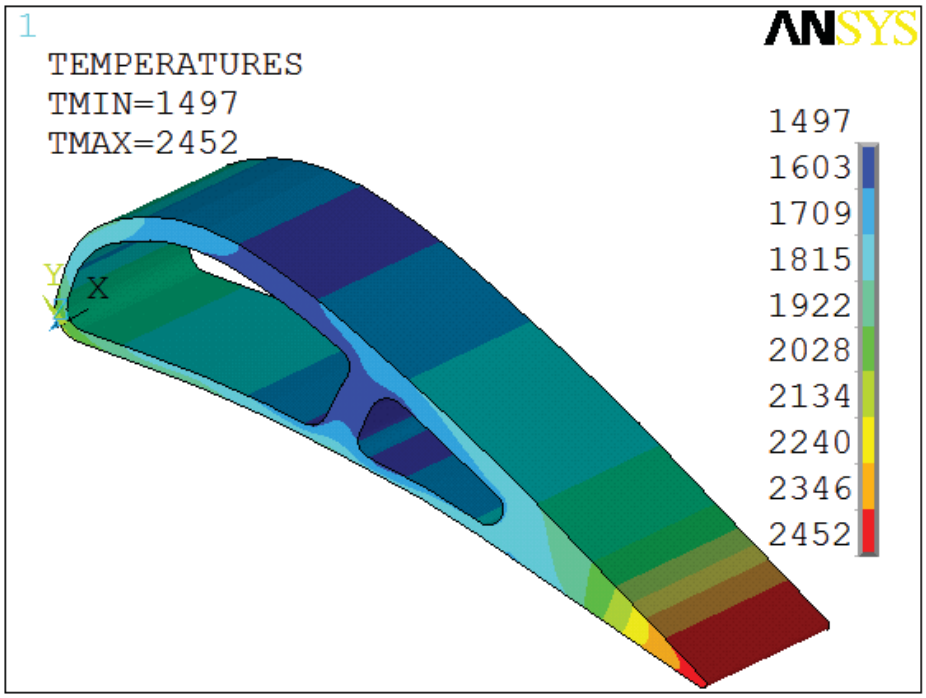

b) Differential wall thickness - no trailing edge ejection

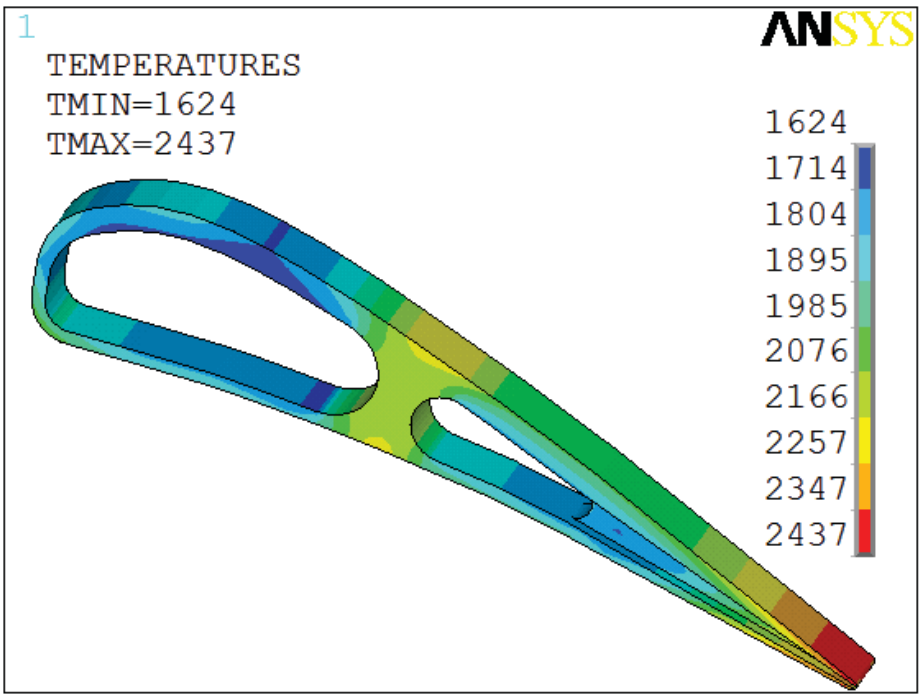

c) Centerline trailing edge ejection

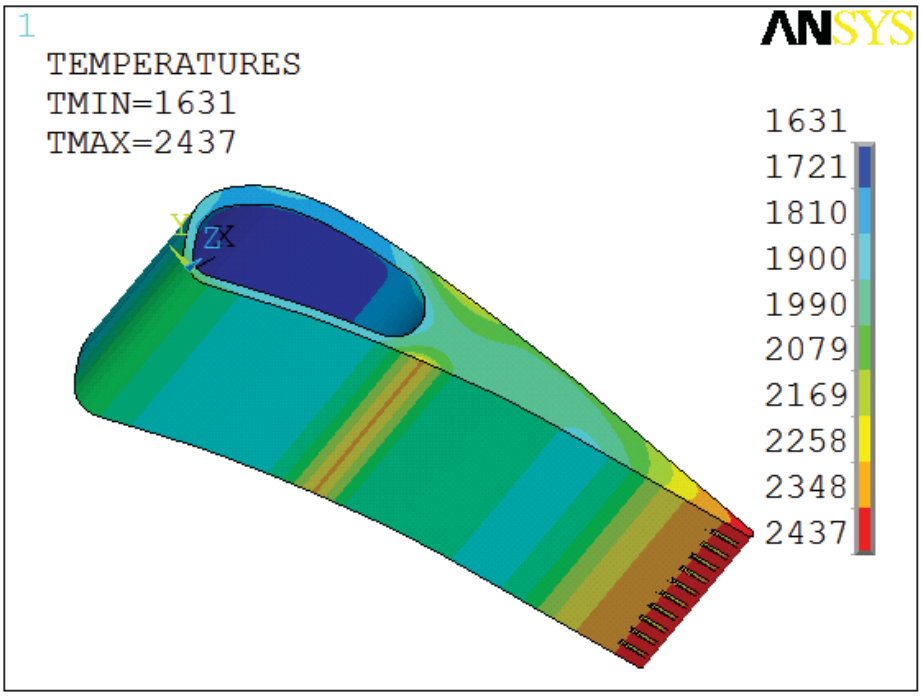

d) Pressure side trailing edge ejection

Fig. 5.0.3 Vane internal configurations

Table 5.0.2 - List of Comparisons

The four sections of Table 5.0.2 describe the comparisons made to illustrate the effects on midspan region stresses due to various internal configurations. The first section lists the comparisons made for configurations without trailing edge ejection. The second section lists comparisons for cases with trailing edge ejection. The third section lists comparisons that investigate the effects of CMC property configurations and boundary conditions. The fourth section lists comparisons that involved changes to the mesh used in the analysis. Also, included in this table are the pages in which the comparisons are discussed.

5.1 - No Trailing Edge Ejection Comparisons

There are ten comparisons for cases with no trailing edge. These are the cases listed in the first section of Table 5.0.2. Trailing edge ejection is commonly used to cool the portion of the vane suction surface aft of the throat. This is done to avoid large aerodynamic loss penalties associated with having film cooling rows aft of the vane throat. On the other hand it may be desirable to avoid trailing edge ejection tubes in CMC vanes. These tubes have a far greater length-to-hydraulic diameter ratio than are required for film cooling holes. If trailing edge ejection is not feasible in a particular application, suction surface film cooling rows downstream of the throat is an alternative. The reduction in vane cooling from using CMC vanes could still be achieved. However, the aerodynamic efficiency benefits of reduced coolant may be overwhelmed by the additional loss from having suction surface cooling rows downstream of the throat. Unless vane efficiency is severely degraded from aft suction surface film cooling rows, the benefits of reduced NOx would still be achieved.

In the following figures, which show stress contours, the vane orientation may be different in each part of the comparison. The different orientations arise because maximum stress locations are different for cash case. The vane in each figure was rotated to show the location of maximum stress.

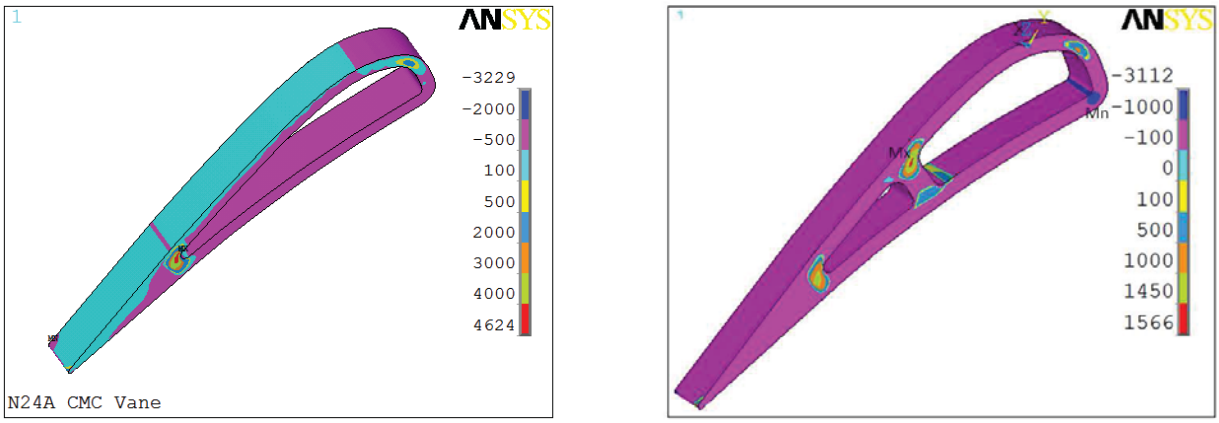

a) Through thickness stress, psi

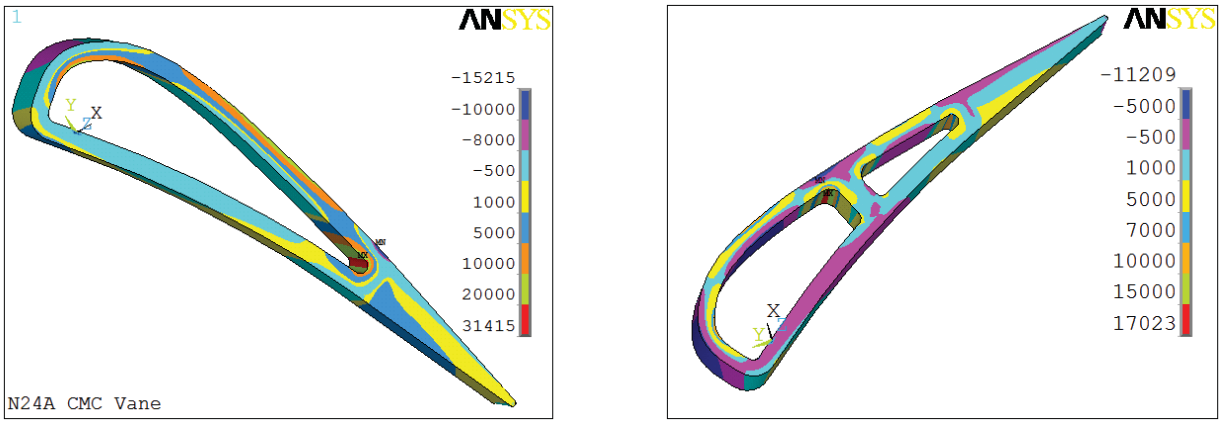

b) Hoop stress, psi

No rib - case 1A Rib - case 2A

Fig. 5.1.1.1 - Effect of rib - Pressure load only

5.1.1 - Effect of Rib. Figures 5.1.1.1 through 5.1.1.3 illustrate the effects of using a rib to connect the suction and pressure surfaces of the vane. Without a rib there is a single hole for an impingement tube, and with a rib two impingement tubes are needed. Comparisons are made for just pressure loads, cases 1A and 2A, just thermal loads, cases 1C and 2B, and when the pressure and thermal loads are simultaneously applied, cases 1D and 2C.

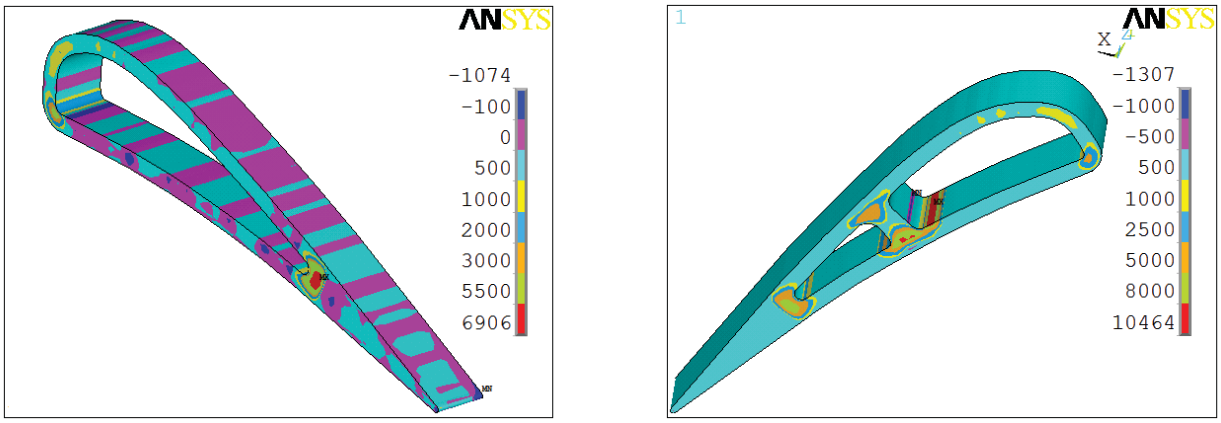

a) Through thickness stress, psi

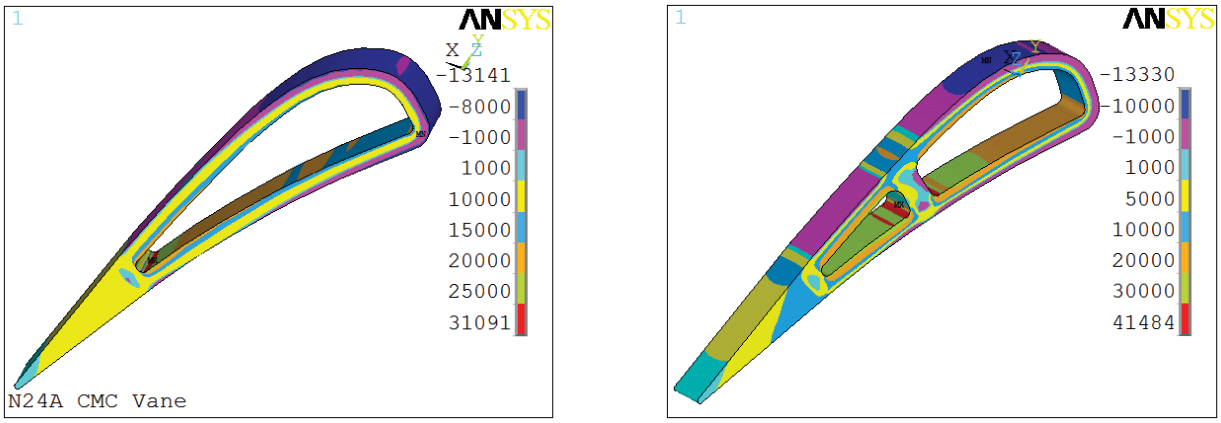

b) Hoop stress, psi

No rib - case 1C Rib - case 2B

Fig. 5.1.1.2 - Effect of rib - Thermal load only

Figure 5.1.1.1 shows through thickness and hoop stresses in the vane midspan region due only to pressure loads for the baseline cases without a rib(1A), and a case with a rib(2A). The presence of a rib is very effective in reducing maximum stresses. Without a rib the maximum tensile stress occurs in the fork region, where the suction and pressure surfaces join together. With a rib the maximum through thickness and pressure stresses occurs in the rib region, and are much lower than the maximum through thickness and hoop stresses for the case without a rib. Although not shown, for each of the six cases the maximum spanwise or radial stresses in the midspan region were lower than the maximum hoop stress for pressure, thermal, and combined loads.

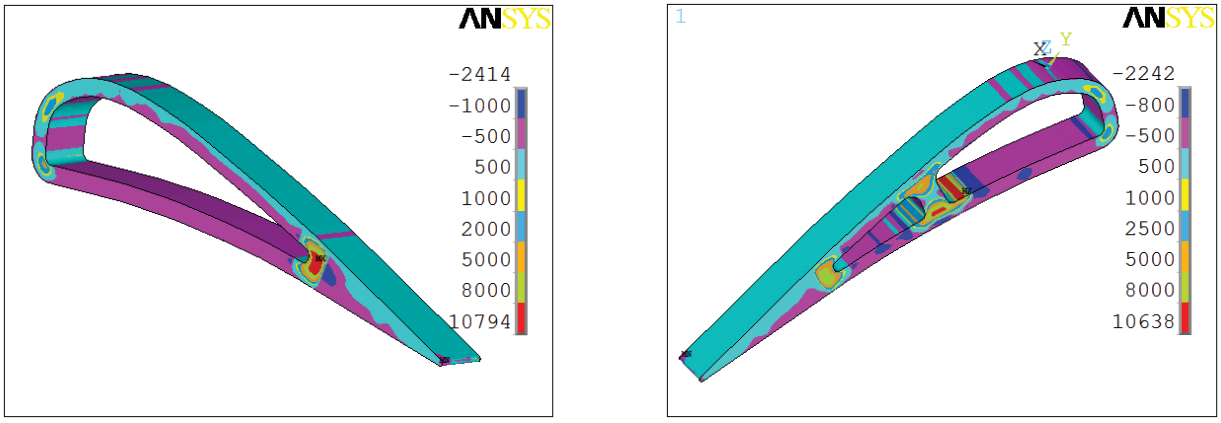

a) Through thickness stress, psi

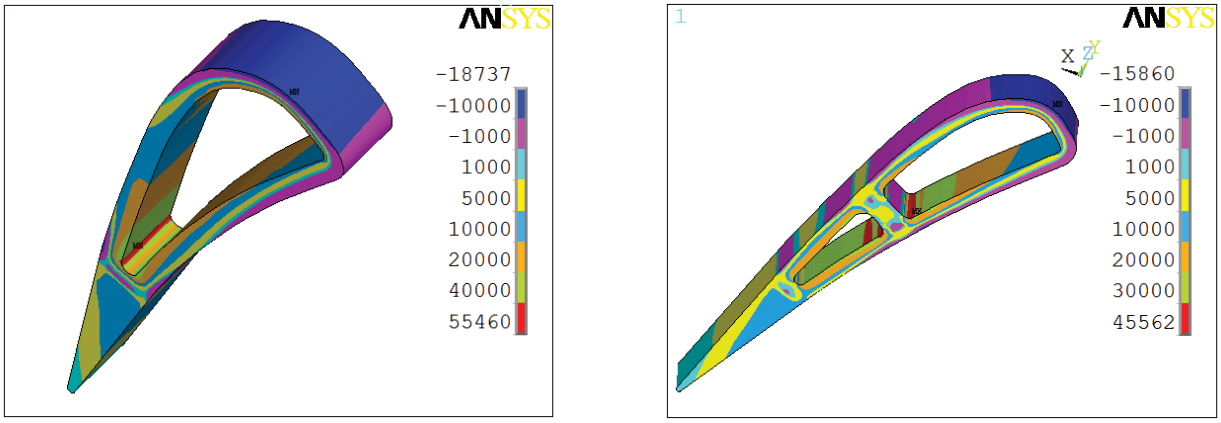

b) Hoop stress, psi

No rib - case 1D Rib - case 2C

Fig. 5.1.1.3 - Effect of rib - Combined pressure and thermal loads

Figure 5.1.1.2 shows stresses due to non-uniform thermal loads. With a rib maximum through thickness and hoop stresses are higher, and occur in the rib region. The thermal stresses in the fork region do not significantly change due to the presence of a rib. In the through thickness direction thermal load stresses are significantly greater than pressure load stresses. When a rib is used the maximum through thickness stress due to thermal loads is nearly seven times the maximum through thickness stress due to pressure loads. When a rib is used the maximum hoop stress due to thermal loads is over twice the maximum hoop stress due to pressure loads

Figure 5.1.1.3 shows stresses due to combined pressure and thermal loads. When no rib is present high stresses occur in the fork region for both pressure and thermal loads. Consequently, the maximum stress due to combining loads approaches adding the stress for both types of loads. The results are different when a rib is present. Even though the maximum hoop stress due to pressure loads is 17ksi(117MPa) the maximum stress due to combined loads is only 4ksi(28MPa) greater than the maximum hoop stress due to thermal loads.

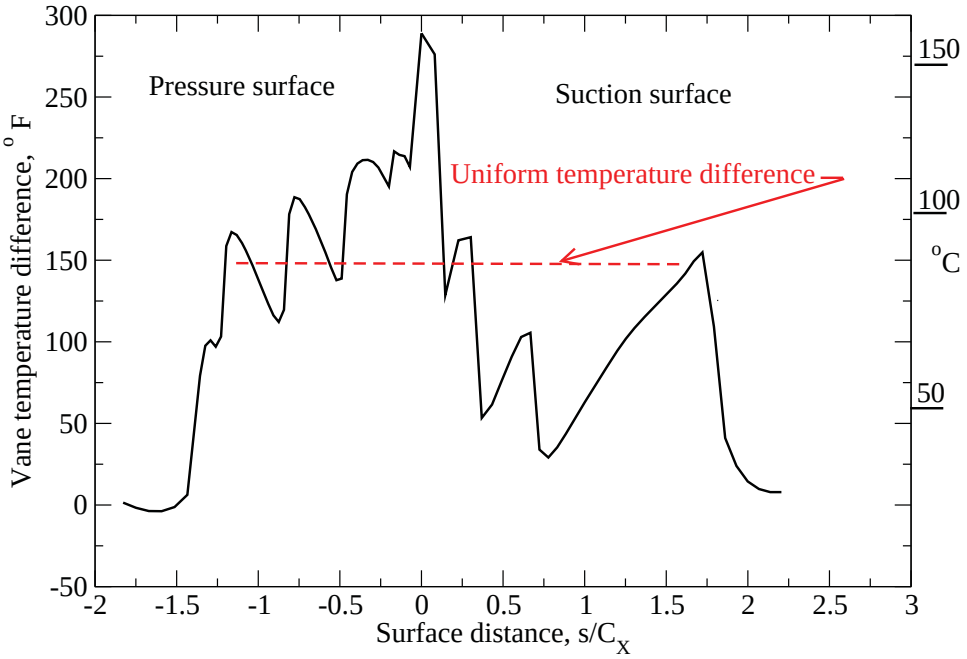

Fig. 5.1.2.1 Temperature difference across CMC vane walls

5.1.2 - Effect of Non-Uniform Temperature Gradient. Since thermal stresses are greater than pressure stresses, the effect of a uniform temperature gradient across the walls of the vane were determined. This was done for the case without a rib. Figure 5.1.2.1 shows the temperature difference across the vane walls. This figure shows the unwrapped vane midspan temperature difference. Local minimums occur just downstream of rows of cooling holes. (The presence of cooling hole rows was not included in the stress analysis.) The temperature difference shown in figure 5.1.2.1 results in the stress distribution previously shown in figure 5.1.1.4. Through thickness and hoop stresses for the uniform and non-uniform temperature difference cases are shown in figure 5.1.2.2. The uniform temperature difference across the CMC vane was $83.3°C(150°F)$. This figure shows that a non-uniform temperature difference increases both maximum through thickness and maximum hoop stress stress by over 50%.

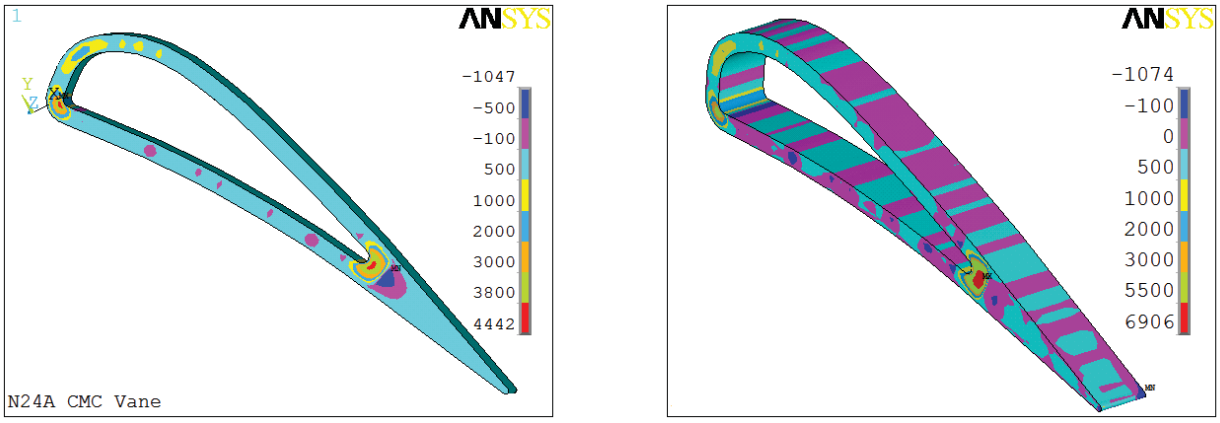

a) Through thickness stress, psi

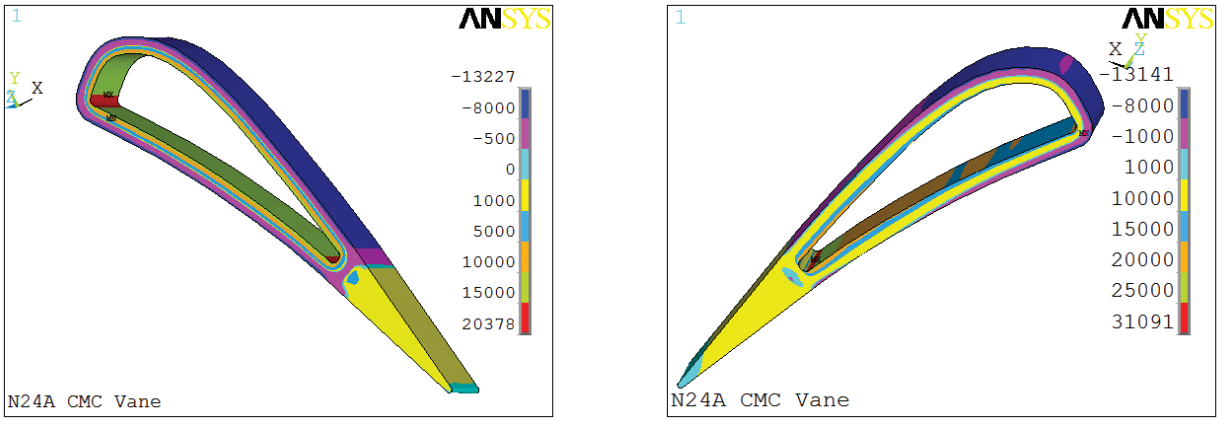

b) Hoop stress, psi

Uniform ΔT - case 1B Non-uniform ΔT - case 1C

Fig. 5.1.2.2 Effect of Non-uniform temperature gradient - Thermal load

Calculations were done where the uniform temperature gradient across the vane wall was halved. As expected, halving the gradient halves the thermal load stresses. Previous results for cases 2A and 2B showed that thermal stress generally exceed thermal stresses. While this comparison is for uniform differential temperatures, later comparisons for a case where the CMC thermal conductivity was increased show similar stress reductions due to reduced CMC vane thermal gradients.

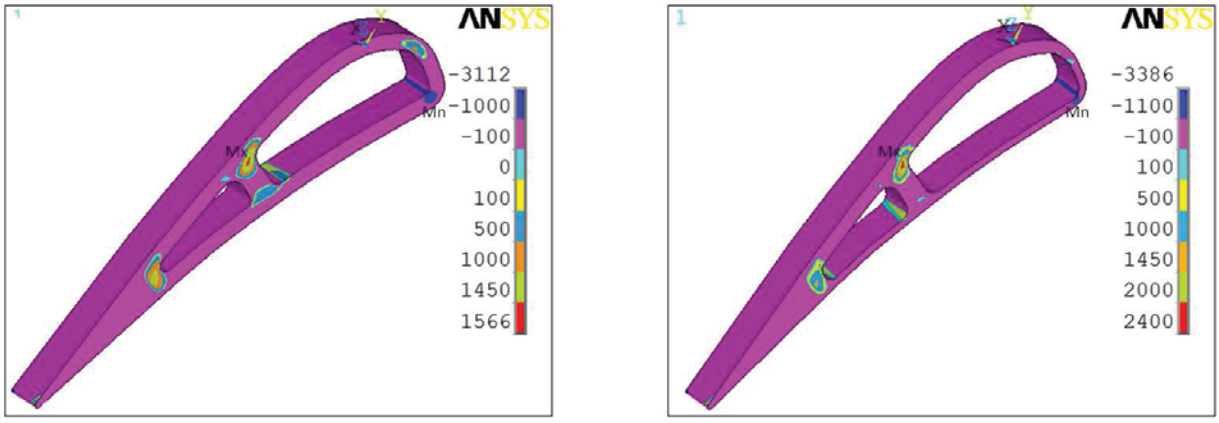

a) Through thickness stress, psi

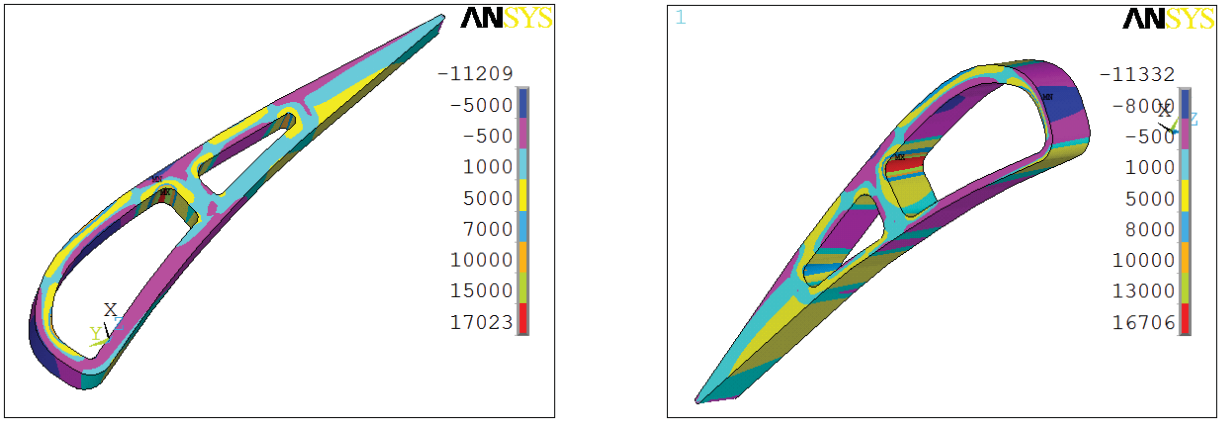

b) Hoop stress, psi

Uniform wall thickness - case 2A Differential wall thickness - case 3A

Fig. 5.1.3.1 Effect of Non-uniform wall thickness - Pressure load

5.1.3 - Effect of Differential Wall Thickness. In an effort to reduce the thermal gradient across the CMC vane wall a case was analyzed where the wall thickness along the pressure surface and in leading edge region was halved. Reducing the wall thickness from $2mm(80mil)$ to $1mm(40mil)$ reduced thermal gradients across the pressure surface. It was not practical to reduce the suction surface wall thickness below $2mm(80mil)$, since suction surface stresses rose very rapidly as the suction surface wall thickness was reduced. Figure 5.1.3.1 shows that the maximum through thickness stress due to pressure loads is higher for the thinner pressure surface wall. Fortunately, figure 5.1.3.2 shows that maximum through thickness stress due to thermal loads is lower by nearly 20% for the thinner pressure surface wall case.

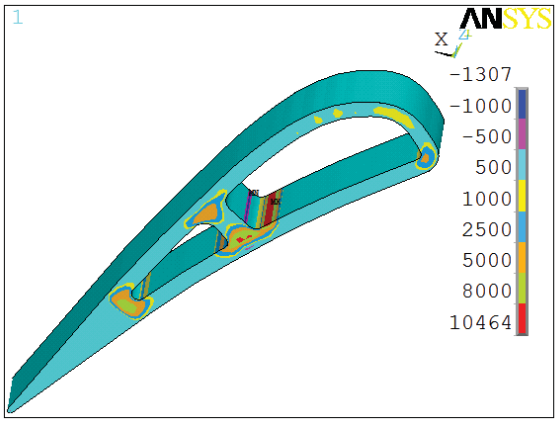

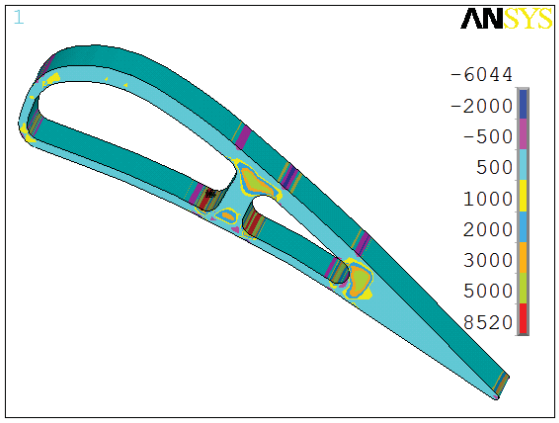

a) Through thickness stress, psi

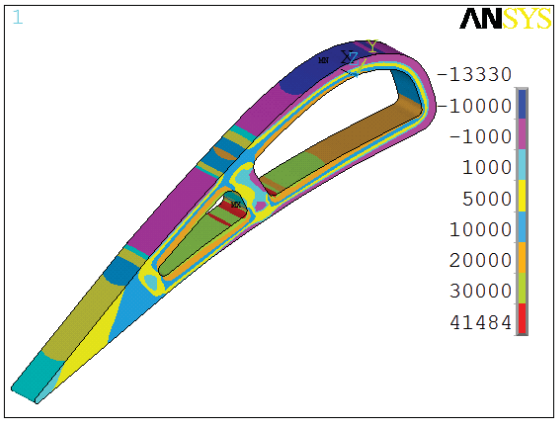

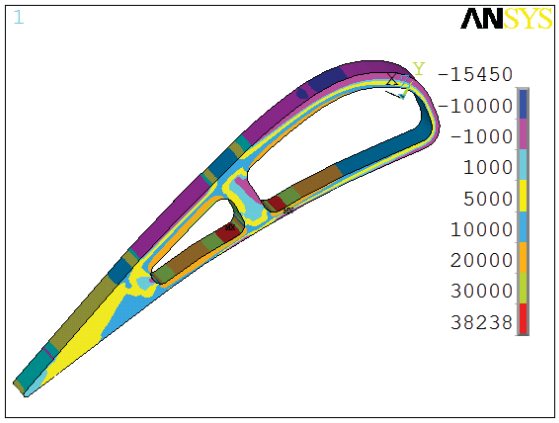

b) Hoop stress, psi

Uniform wall thickness - case 2B Differential wall thickness - case 3B

Fig. 5.1.3.2 Effect of Non-uniform wall thickness - Thermal load

The maximum hoop stress is lowered when the pressure surface is thinner than the suction surface. While the reduction in maximum hoop stress is only a few percent, stresses for both pressure and thermal loads are reduced.

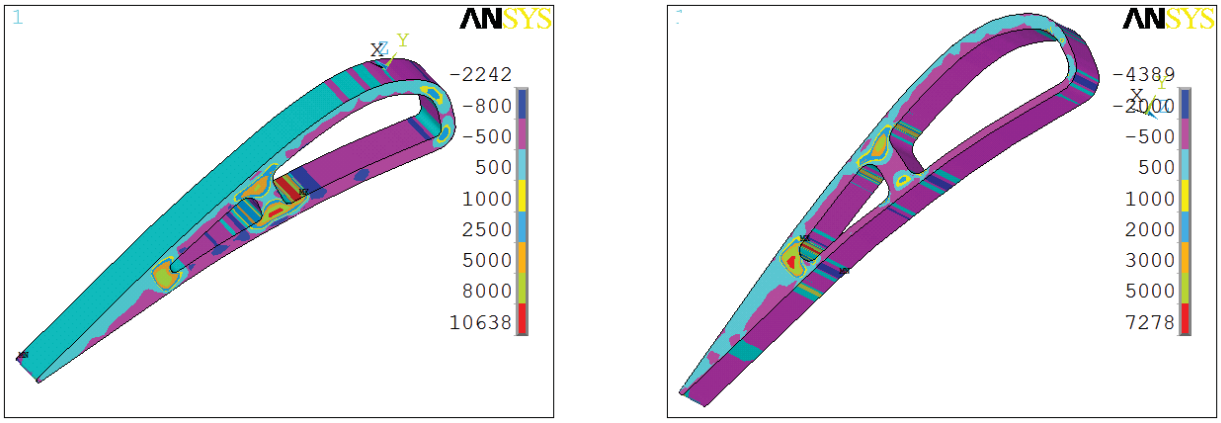

a) Through thickness stress, psi

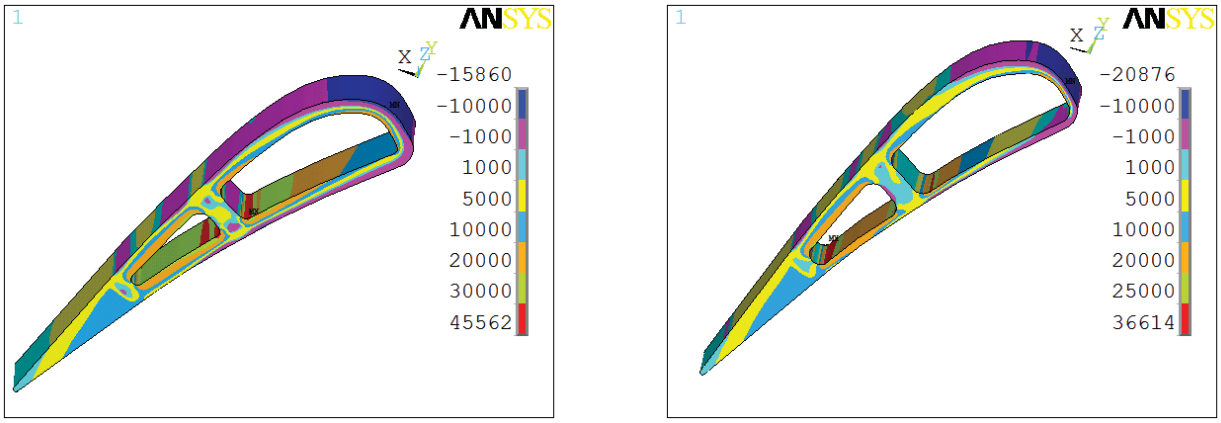

a) Through thickness stress, psi

Uniform wall thickness - case 2C Differential wall thickness - case 3D

Fig. 5.1.3.3 Effect of Non-uniform wall thickness - Combined pressure and thermal loads

5.1.4 - Effect of Combined Pressure and Thermal Loads. Figures 5.1.1.1 through 5.1.1.3 illustrated the effects of combining pressure and temperature loads on stresses for uniform wall thickness cases. Figures 5.1.3.1 through 5.1.3.3 illustrate the same effects for the differential wall thickness case. These two sets of comparisons show behavior typical of all cases examined. Also, the results are similar for either through thickness or hoop stresses. The maximum stress for combined loads is significantly lower than the algebraic sum of the maximum pressure load stress and the maximum thermal load stress. However, at the location of the maximum tensile stress from one load, which is generally a thermal load, there is a positive stress from the other load. The maximum stress from combined loads is slightly greater than the maximum stress from either a pressure or thermal load.

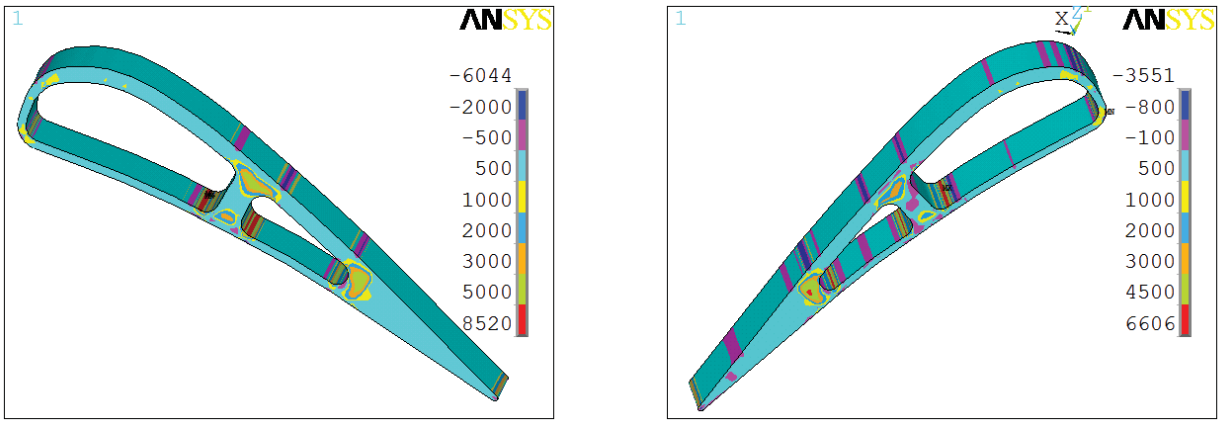

a) Through thickness stress, psi

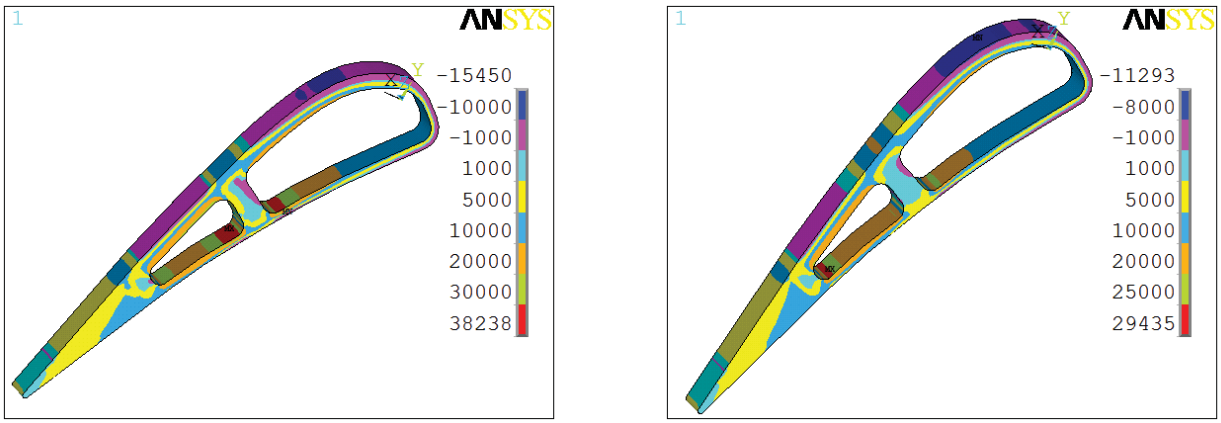

b) Hoop stress, psi

Cooled rib - case 3B Insulated rib - case 3C

Fig. 5.1.5.1 Effect of insulating connecting rib - Thermal load

5.1.5 - Effect of Insulating Connecting Rib. The effect of insulating the rib connecting the vane pressure and suction surfaces is to reduce maximum stresses due to thermal loads. Figures 5.1.5.1 shows that insulating the rib reduces peak through thickness stress by nearly 20%. Both the magnitude and location of the maximum hoop stress is affected by insulating the rib. With a cooled rib the maximum hoop stress occurs in the rib region, while for the insulated rib the maximum hoop stress is in the fork region. The maximum hoop stress is reduced by over 20% when the rib is insulated. For both cases internal cooling was assumed to be done using an impingement insert. For an uncooled or insulated rib there would be no impingement holes facing the rib. Since there are several pressure surface film cooling rows, cross flows passing over the rib from the internal pressure surface to the internal suction surface can be avoided.

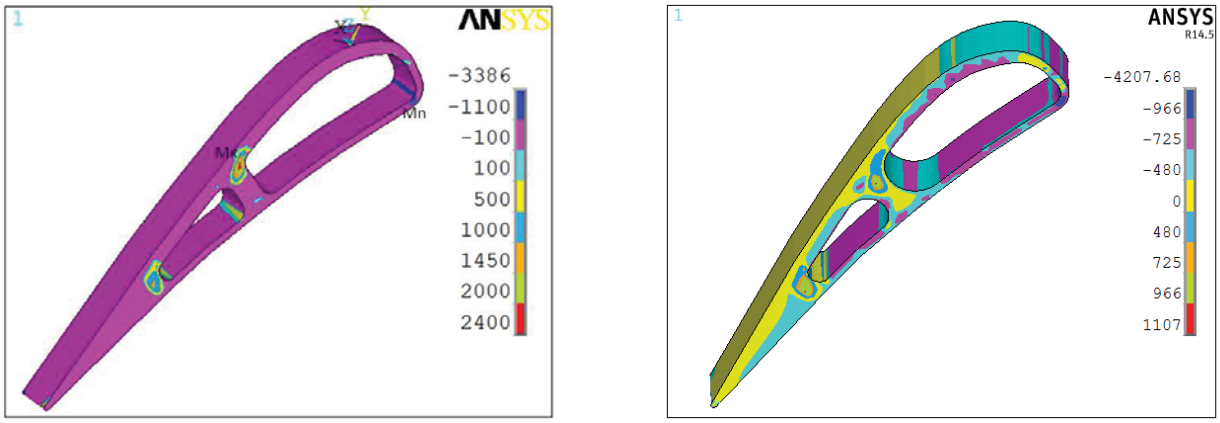

a) Through thickness stress, psi

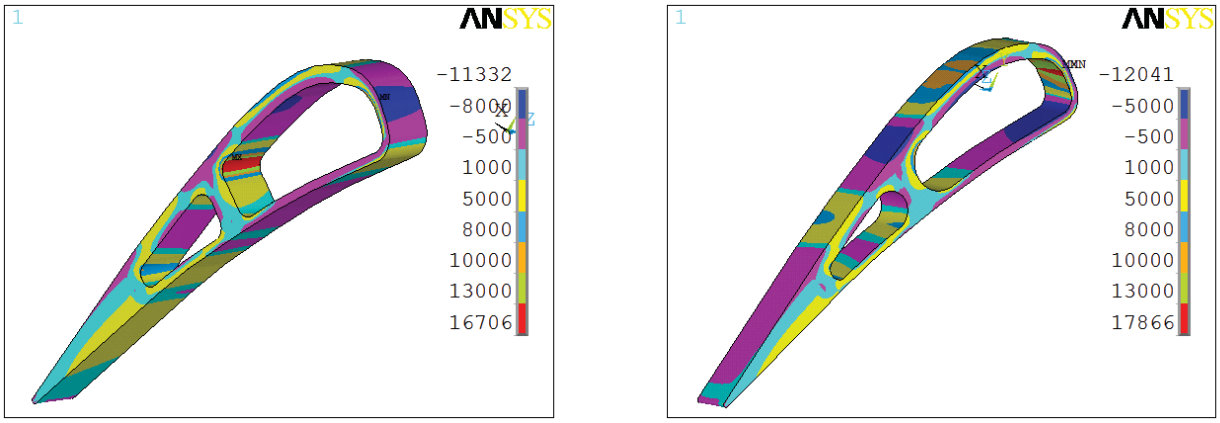

b) Hoop stress, psi

Small rib radii - case 3A Semi-circular rib radii - case 5D

Fig. 5.1.6.1 Effect of Rib shape - Pressure load

5.1.6 - Effect of Modifying Rib Shape. Figure 5.1.6.1 shows stresses caused by pressure loads for the reference rib geometry and a semi-circular rib geometry. In the semi-circular rib case each rib surface used to form the front and rear impingement cavities has a single radius of curvature. The rib in the other case has four corners with small radii are only 2.3% of the axial chord, C_X. The effect of larger rib radii is to reduce maximum through thickness stress due to pressure loads by more than half. The semi-circular rib increased the maximum hoop stress, and changed the location where the maximum hoop stress occurred. The maximum hoop stress increased by nearly 7%, and moved from the rib-suction surface region to the inner surface, near the leading edge. The minimum hoop stress for the semi-circular rib occurred on the exterior surface of the vane. Unfortunately, this rib configuration is unlikely to significantly affect thermal stresses.

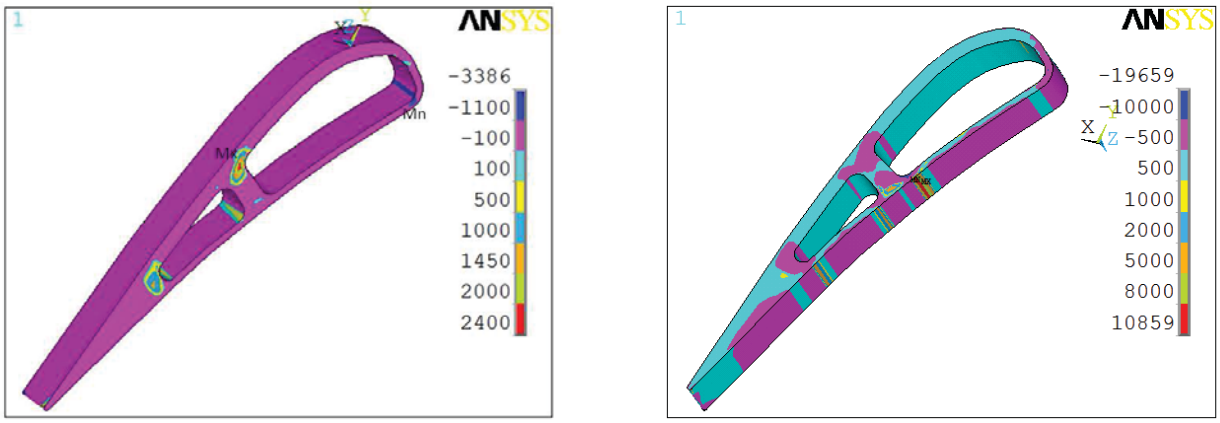

a) Through thickness stress, psi

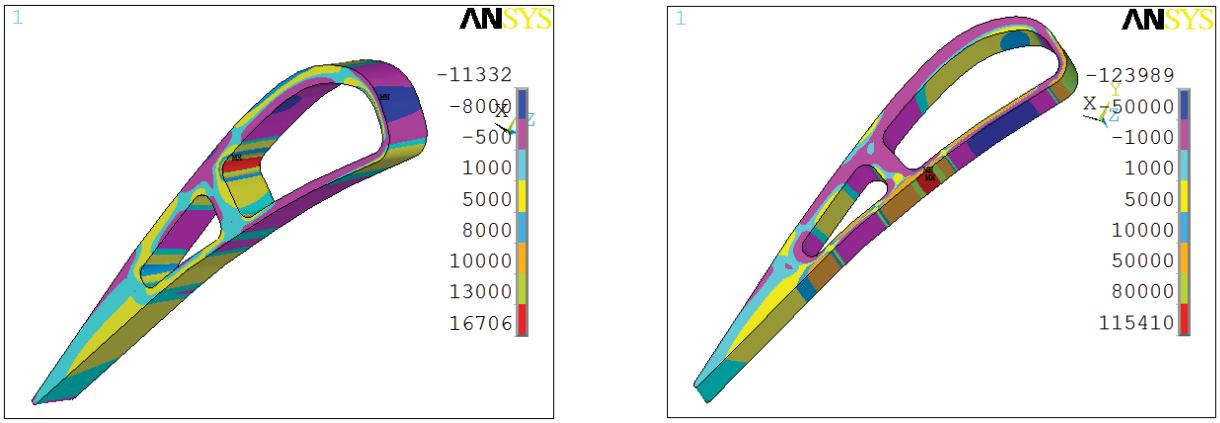

b) Hoop stress, psi

Internal pressure - case 3A No internal pressure - case 3A2

Fig. 5.1.7.1 Effect of no internal pressure - Pressure load only

5.1.7 - Effect of No Internal Pressure If the vane is uncooled, which may be the case for a HPT second stage CMC vane, there need not be an internal pressure causing a ballooning stress. When there is no internal pressure there is still a bending load on the vane, because the average external pressure surface pressure is higher than the average suction surface external pressure. While a second stage vane has a much lower inlet total pressure than the 50 atm. total pressure assumed for the first stage vane, the normalized external pressure ratio, $P/P_{\mathrm{T-IN}}$, distribution is expected to be similar to that for the first stage vane. Calculations showed that pressure load stresses are proportional to the inlet total pressure, $P_{\mathrm{T-IN}}$, when the normalized pressure distribution, $P/P_{\mathrm{T-IN}}$, is constant. For comparative purposes the analysis was done assuming the same inlet total pressure of 50 atm. as for the other cases. Figure 5.1.7.1 shows that pressure load stresses for a case with no internal pressure are much higher than those where the internal pressure is 50 atm. Both through thickness and hoop stresses are much higher for the case with no internal pressure. There were no thermal loads present for the case with no internal pressure, and previous cases showed that thermal stresses generally exceeded pressure stresses. With no internal pressure the maximum through thickness stress shown in figure 5.1.7.1a nearly equals the

maximum through thickness combined load stress for any case previously shown. Similarly, the maximum hoop stress shown in figure 5.1.7.1b exceeds the maximum hoop combined load stress for any of the previous cases. These results indicate that the stresses for an uncooled first stage HPT vane may exceed those for a cooled first stage vane. Even for an uncooled second stage HPT vane, stresses may be as high as for a cooled first stage vane, if the thermal gradients in the first stage vane are moderate.

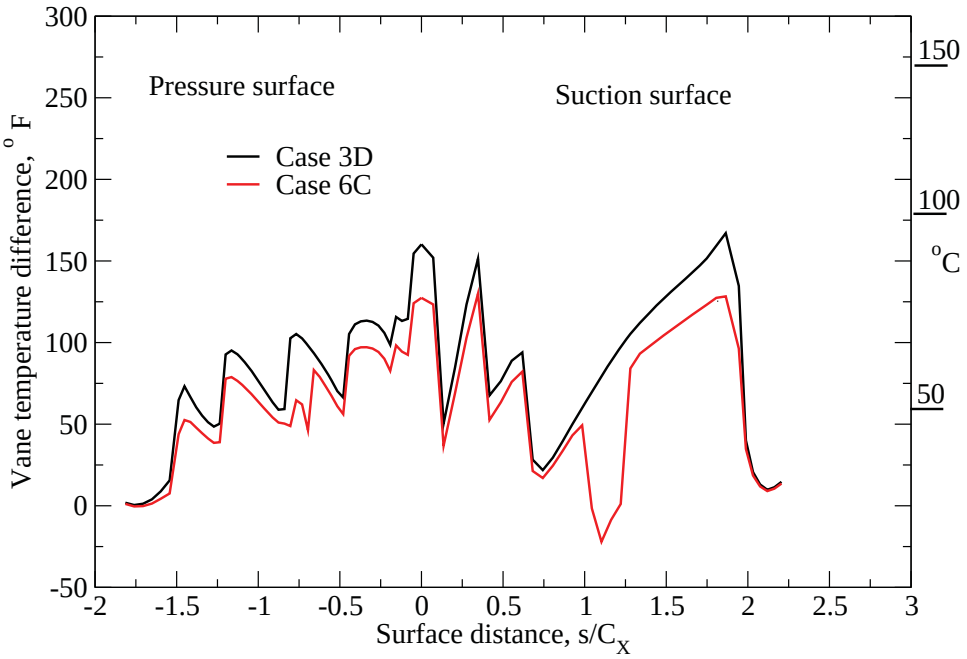

Fig. 5.1.8.1 Two temperature differences across CMC vane walls

5.1.8 - Effect of Revised Temperature Distribution The arrangement of film cooling rows can affect the CMC temperatures to some degree without affecting the amount of required film cooling. Figure 5.1.8.1 shows two temperature differences across the CMC vane. Case 6C has lower temperature differences across much of the vane surface. On the other hand, case 6C has higher streamwise temperature gradients on the suction surface between $s/C_X = 1$ and $s/C_X = 1.4$. The surface distance, s, is approximately twice the axial chord, C_X.

Figure 5.1.8.2 gives the through thickness and hoop stresses for the temperature differences shown in figure 5.1.8.1. Stresses are given for combined loads.. The results are somewhat unexpected, in that the lower temperature difference results in higher maximum through thickness stress. The increase in maximum through thickness stress is not large, being less than 8%, but is associated with a smaller temperature difference. Overall through thickness stresses, though not the maximum stress, are reduced with a lower temperature difference. This is most evidenced in the fork region where case 3D has stresses in excess of 5000 psi(34474 MPa), and the reduced temperature difference case, 6C, has no stresses in excess of 4500 psi(31027 MPa).

Both maximum and local hoop stresses are reduced with lower temperature difference. The reduction in maximum is only 4%. However, figure 5.1.8.2 shows large regions of the pressure surface with lower hoop stresses when the temperature difference across the CMC vane walls is lower.

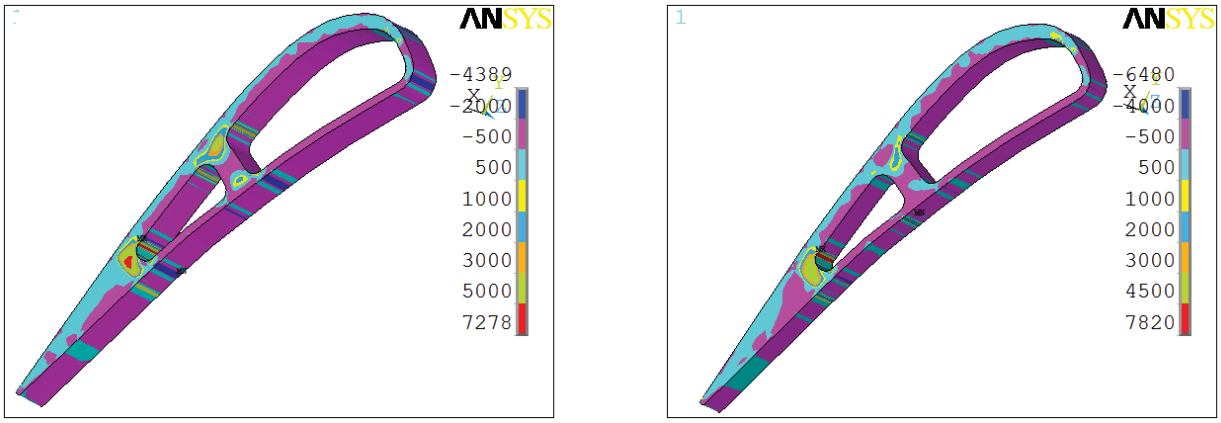

a) Through thickness stress, psi

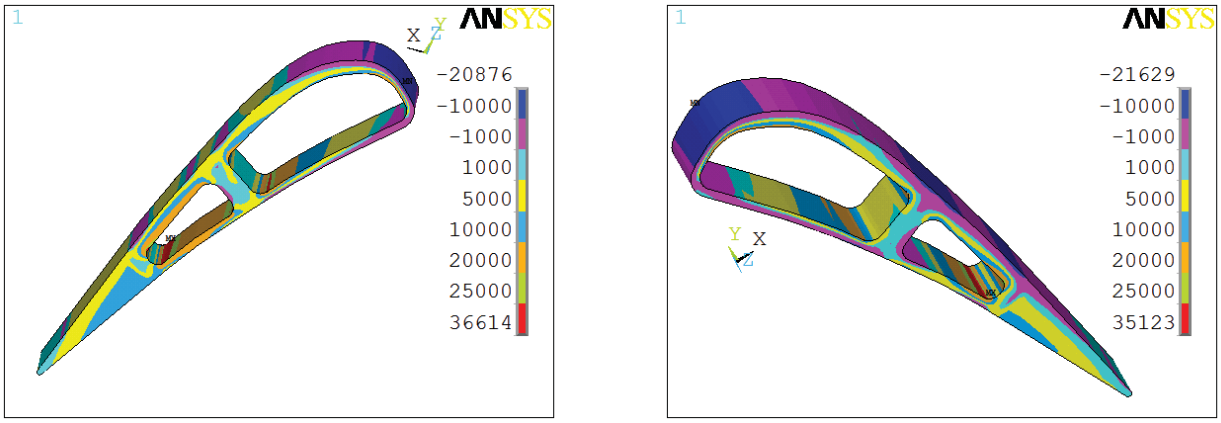

b) Hoop stress, psi

Original temp. dist. - case 3D Revised temp. dist. - case 6C

Fig. 5.1.8.2 Effect of revised temperature distribution - Combined loads

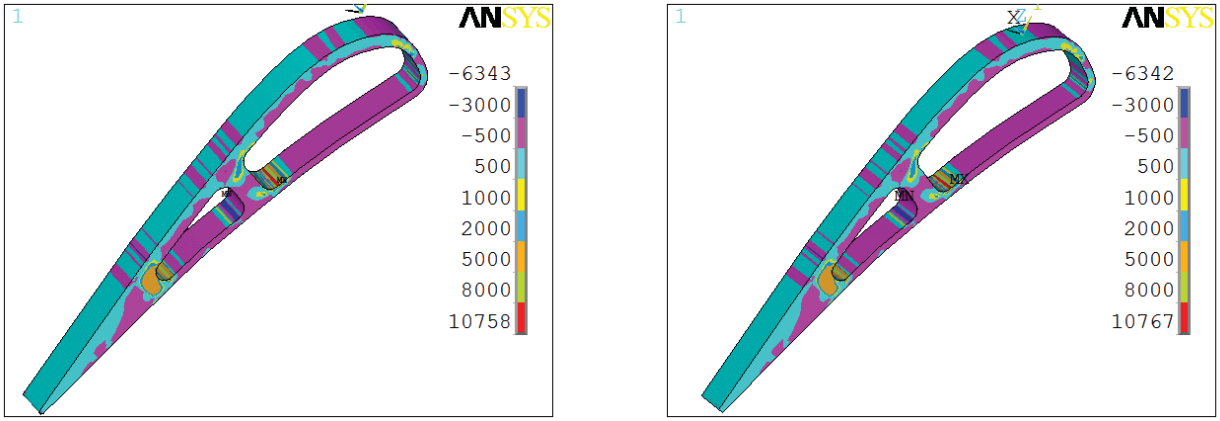

a) Through thickness stress, psi

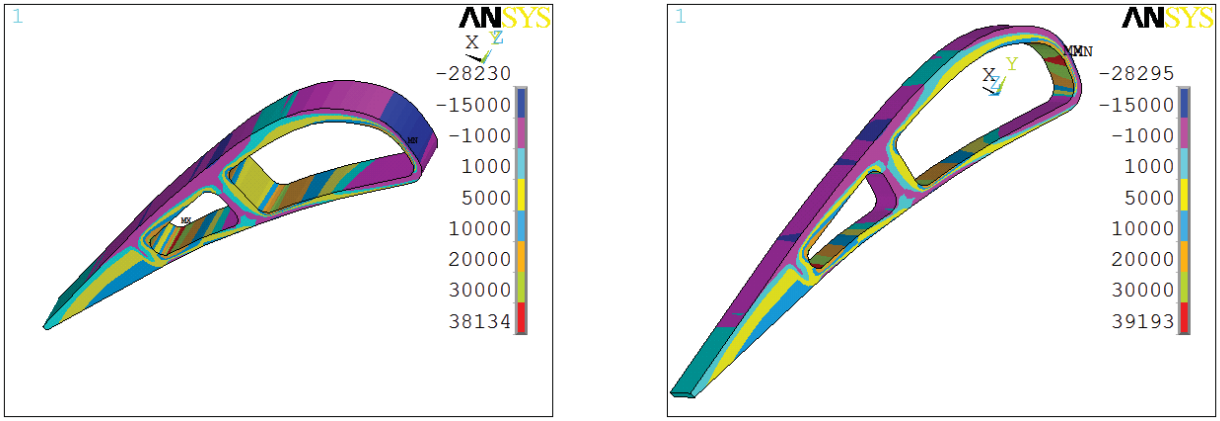

b) Hoop stress, psi

Circular trailing edge - case 7B Square trailing edge - case 7D

Fig. 5.1.9.1 Effect of modified trailing edge shape - Combined loads

5.1.9 - Effect of Trailing Edge Shape Figure 5.1.9.1 shows that the effect of changing the shape of the trailing edge from a semi-circle to a squared-off trailing edge is small. This analysis was done to determine if this geometric modification, which required a different grid topology, would result in a significantly changed stress distribution near the vane trailing edge. For the case with a semi-circular trailing edge, 7B, both through thickness and hoop stresses are low in the trailing edge region, relative to the rest of the vane.

5.2 - Trailing Edge Ejection

Typical metallic HPT first stage vane have some form of trailing edge ejection, whether along the vane centerline or at the rear of the pressure surface. From a fabrication point alone it would be convenient if trailing edge ejection could be avoided for CMC vanes. However, analysis showed that to maintain the suction surface of the vane either film cooling rows had to be placed downstream of the vane throat, or substantially more cooling air was required. Placing film cooling rows downstream of the vane throat, which is close to the midpoint of the vane surface, causes a substantial vane efficiency penalty. To cool the aft portion of the suction surface without trailing edge ejection requires high film effectiveness at a relatively long distance from the last cooling row. To achieve the high film effectiveness substantially more cooling air is required, since film effectiveness decreases with downstream distance from the location of the film row, but increases with increased amounts of film cooling. Trailing edge ejection is an effective cooling approach because there is a relatively small thermal resistance between the outer vane surface and the trailing edge ejection tube. In effect, trailing edge ejection redirects film cooling air from the last one or two rows of pressure side cooling holes, and uses this air in a conventional duct cooling approach before ejecting the air at the vane trailing edge.

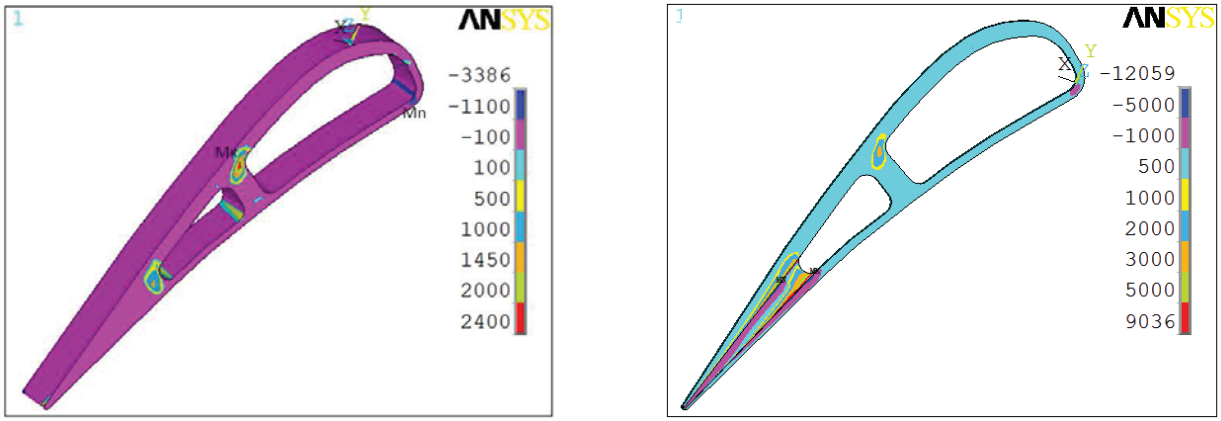

a) Through thickness stress, psi

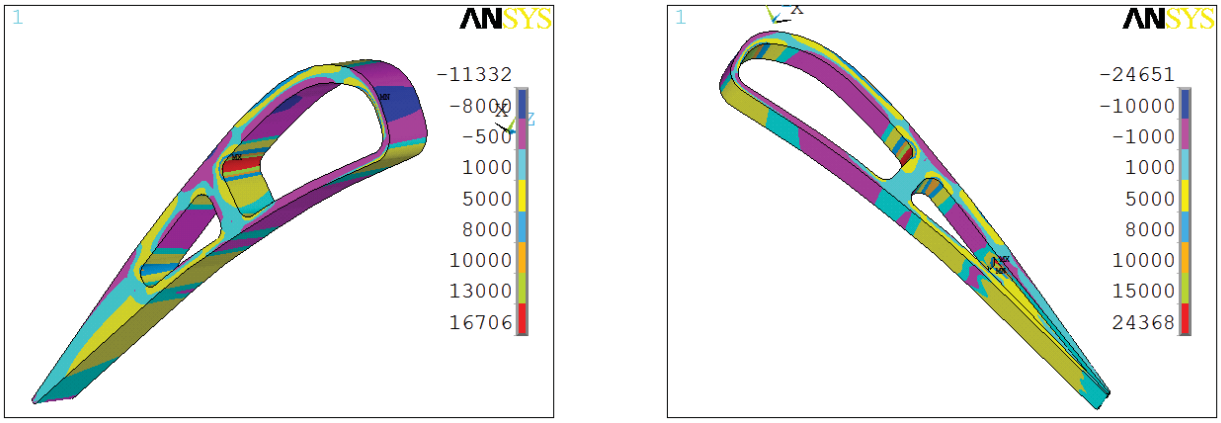

b) Hoop stress, psi

No trailing edge ejection - case 3A Centerline trailing edge ejection - case 4A

Fig. 5.2.1.1 Effect of centerline trailing edge ejection - Pressure load

5.2.1 - Effect of Centerline Trailing Edge Ejection From a thermal standpoint centerline trailing edge ejection is desirable because the distances between the trailing edge ejection tube and the vane walls are minimized. Figures 5.2.1.1 through 5.1.1.3 show through thickness and hoop stress when there are pressure, thermal, and combined loads. In the trailing edge ejection case the trailing edge ejection tube is a converging duct with a uniform height in the spanwise or radial direction. For all three loading conditions there are substantial increased in maximum through thickness or hoop stress when there is a tube connecting the aft cavity and the vane trailing edge. For pressure loads the maximum through thickness stress increased by nearly a factor of four, while the maximum hoop stress increase by nearly a factor of 1.5. For thermal loads the maximum through thickness stress increased by a factor of 3.5. The increase in maximum hoop stress was less, being only 20%. As in previous cases combined load stresses were heavily influenced by thermal load stresses. The maximum combined load through thickness stress with trailing edge ejection was over a factor of three greater than the maximum stress without trailing edge ejection. For hoop stresses the increase in maximum stress was nearly 30%.

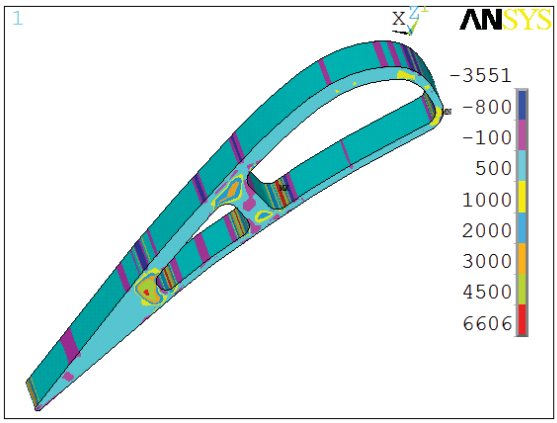

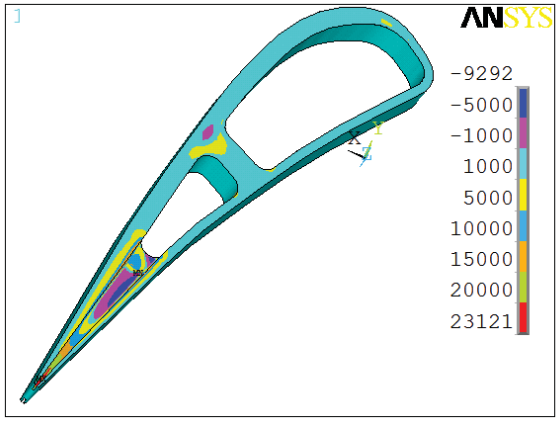

a) Through thickness stress, psi

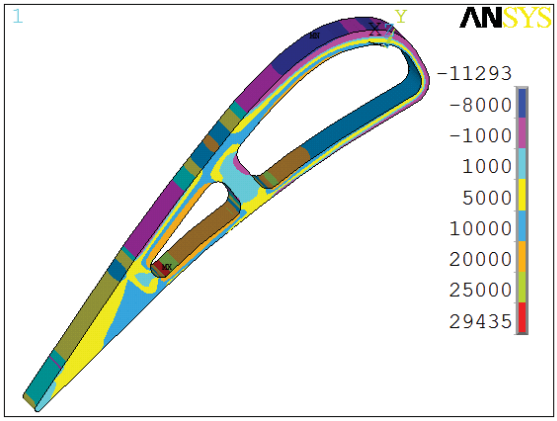

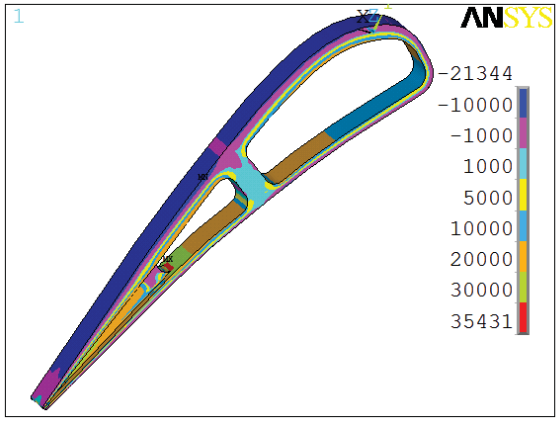

b) Hoop stress, psi

No trailing edge ejection - case 3C Centerline trailing edge ejection - case 4B

Fig. 5.2.1.2 Effect of centerline trailing edge ejection - Thermal load

While the maximum stresses are very high with trailing edge ejection, the high stresses are confined to very small regions. For pressure load and combined load through thickness stresses the maximum and minimum stresses are located near each other, and the maximum thermal load stress is located near the tube exit, while the minimum through thickness stress is on the inner pressure surface wall, close to the tube entrance. It may seem somewhat surprising that the location for the maximum through thickness stress changes between the thermal and combined load cases. The highly localized nature of the maximum stress obscures the fact that there was a high, but not the highest, stress at the same location as the maximum combined load stress.

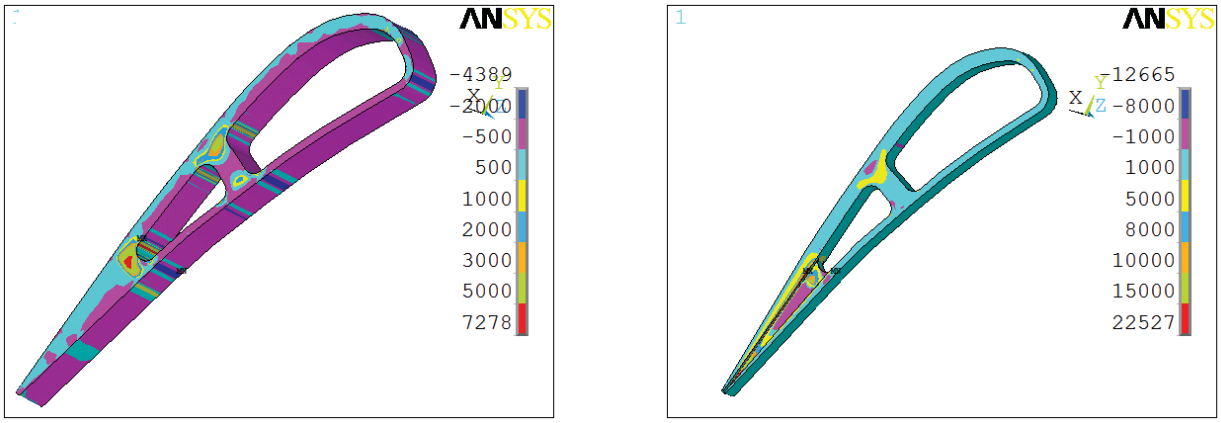

a) Through thickness stress, psi

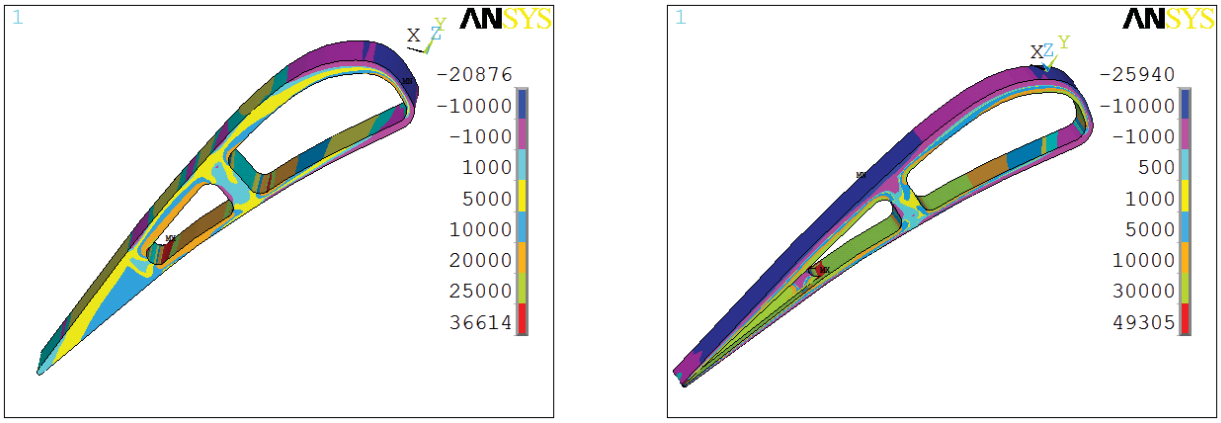

b) Hoop stress, psi

No trailing edge ejection - case 3D Centerline trailing edge ejection - case 4C

Fig. 5.2.1.3 Effect of centerline trailing edge ejection - Combined loads

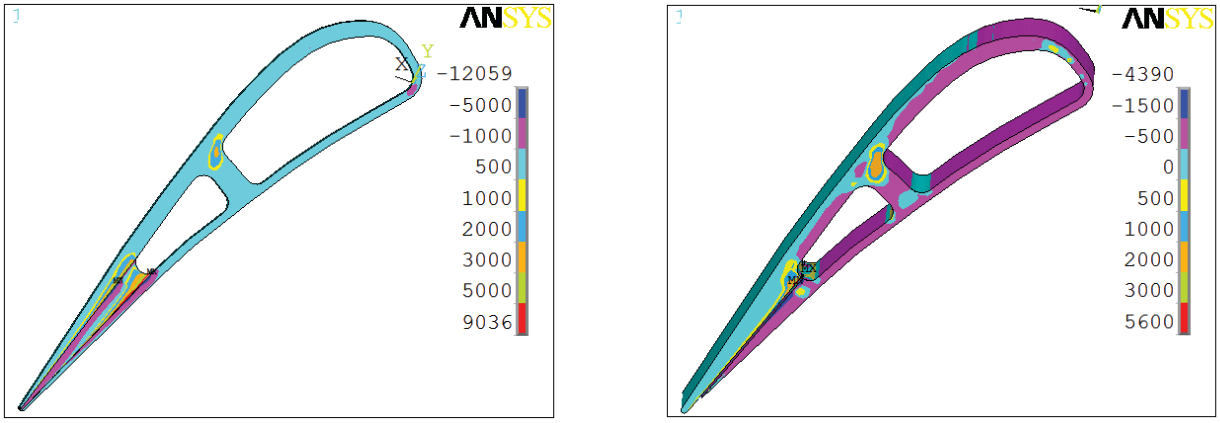

a) Through thickness stress, psi

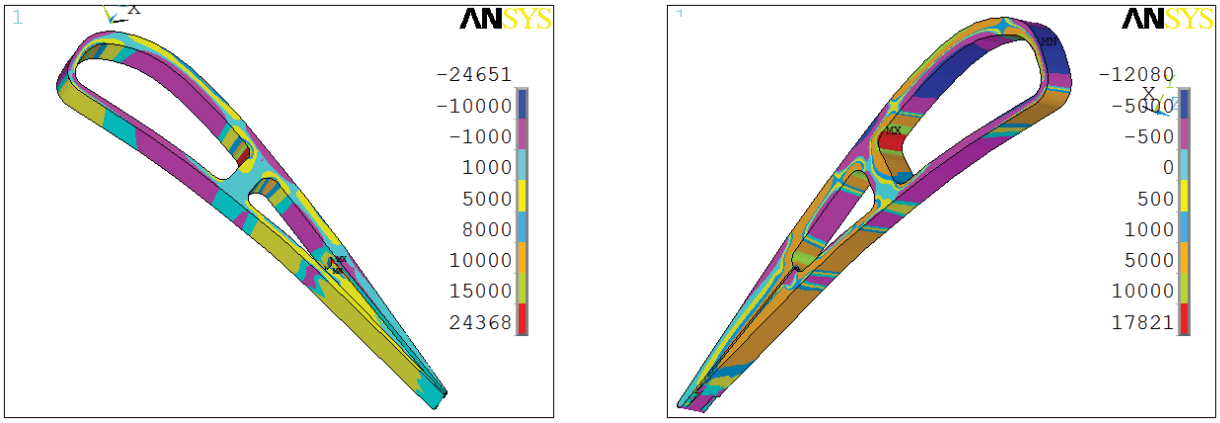

b) Hoop stress, psi

Centerline trailing edge ejection - case 4A Pressure side trailing edge ejection - case 5F

Fig. 5.2.2.1 Effect of pressure side trailing edge ejection - Pressure load

5.2.2 - Effect of Pressure Side Trailing Edge Ejection Because using a centerline trailing edge ejection tube resulted in high maximum stresses, changing the location of the trailing edge ejection tube was investigated. In this trailing edge configuration the tube exited the vane on the its pressure side, The shape of the tube was also changed, to be easier to fabricate. The pressure side trailing edge ejection tube had a constant rectangular cross section, and was 0.86 mm(34 mil) high, and 0.25 mm(10 mil) wide.

Figures 5.2.2.1 and 5.2.2.2 show stresses for the centerline and pressure side trailing edge ejection cases. While maximum through thickness stresses are still high, there was a substantial reduction in maximum stresses when pressure side trailing edge ejection is substituted for centerline trailing edge trailing edge ejection. The maximum through thickness stress is reduced by approximately 25% for both the pressure load and combined load cases. While the maximum hoop stress is also reduced by nearly 25% for the pressure load case, the maximum hoop stress is nearly the same for centerline and pressure side ejection for the combined load case.

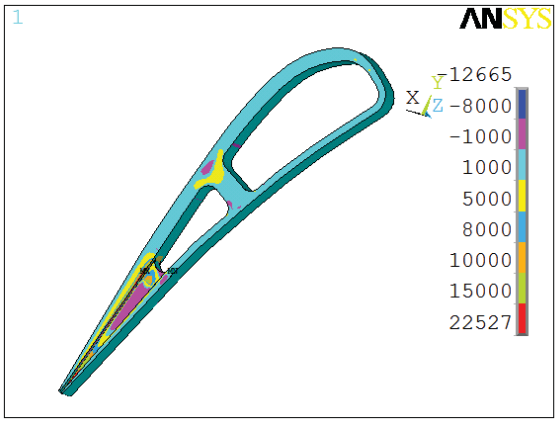

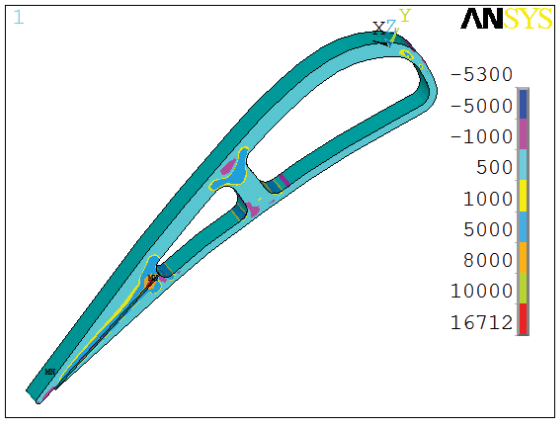

a) Through thickness stress, psi

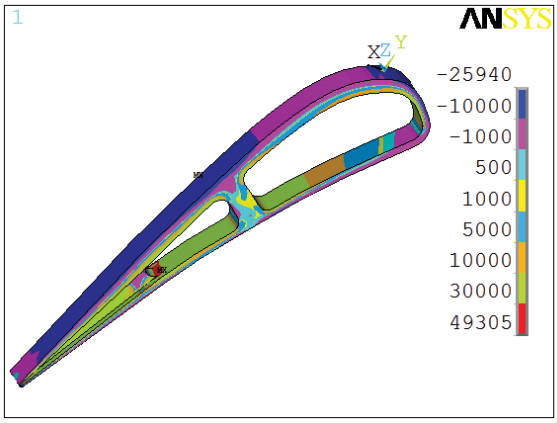

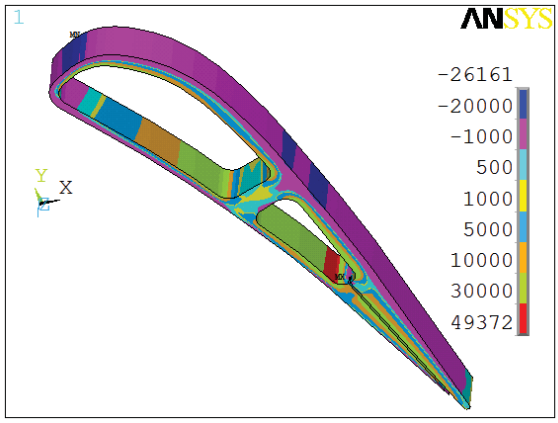

b) Hoop stress, psi

Centerline trailing edge ejection - case 4C Pressure side trailing edge ejection - case 5C

Fig. 5.2.2.2 Effect of pressure side trailing edge ejection - Combined loads

The locations of maximum and minimum through thickness stresses are approximately the same for pressure side and centerline trailing edge ejection. For combined loads the location of maximum through thickness stress is unchanged between centerline and pressure side trailing edge ejection. For the combined load case the location of minimum through thickness stress is near the tube entrance for centerline ejection, and near the tube exit for pressure side ejection. The location for maximum hoop stress due to pressure loads moves away from the tube when there is pressure side ejection. The hoop stress in the rib region reaches almost the same level for both forms of trailing edge ejection. For combined loads the location of maximum hoop stress is the same for both forms of trailing edge ejection.

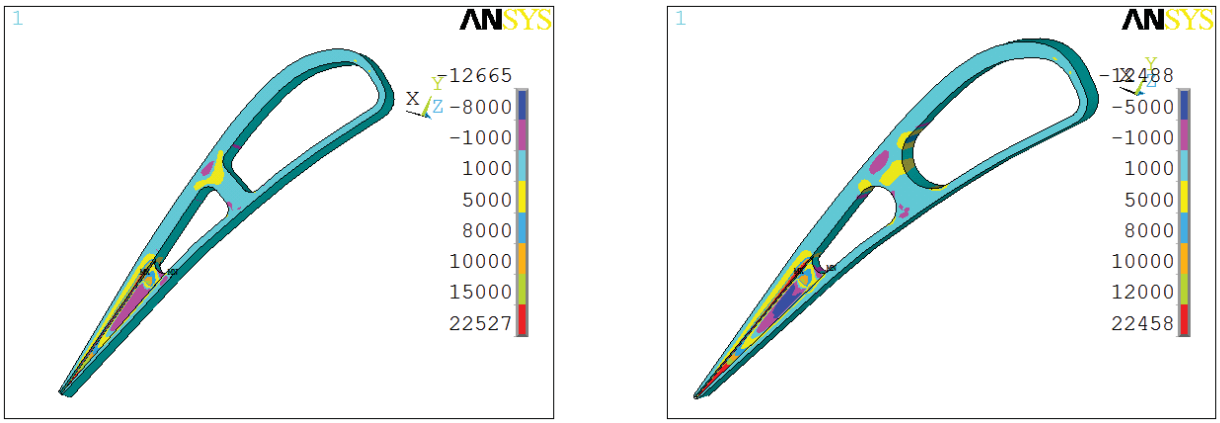

a) Through thickness stress, psi

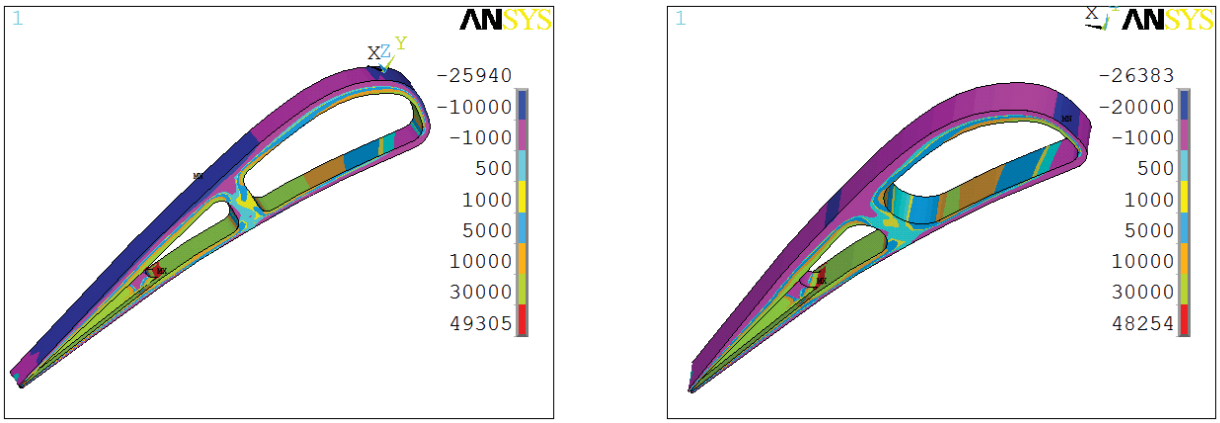

b) Hoop stress, psi

Small rib corner radii - case 4C Semi-circular rib - case 5A

Fig. 5.2.3.1 Effect of semi-circular rib with trailing edge ejection - Combined loads

5.2.3 - Effect of Modifying Rib Shape It was hoped that modifying the rib shape would reduce maximum stresses, even if they occur away from the rib region. Figure 5.1.6.1 showed that a semi-circular rib was beneficial for cases without trailing edge ejection. Figure 5.2.3.1 shows stresses for cases with centerline trailing edge ejection and two rib geometries. The rib geometries are the same as those shown in figure 5.1.6.1. One is a rib with four small radii where the rib joins the pressure and suction surfaces. The other geometry has the rib sides formed by constant radius arcs. The radius of the rib side facing the aft cavity is smaller than the radius of the rib side facing the forward cavity.

Because maximum through thickness and hoop stresses occur in the tube region, the rib shape had no significant effect on maximum stresses. In the rib region the results for combined pressure and thermal loads shown in figure 5.2.3.1 are different from the results shown in figure 5.1.6.1 for just pressure loads. For combined loads the semi-circular rib sides show higher through thickness stresses with a semi-circular rib, but for pressure loads the stresses are lower for a semi-circular rib. For combined loads the semi-circular rib shows lower hoop stresses, especially where the rib joins the vane pressure surface forming the forward cavity. For pressure loads figure 5.1.6.1 shows only a small decrease in stresses in the rib region for the semi-circular rib geometry.

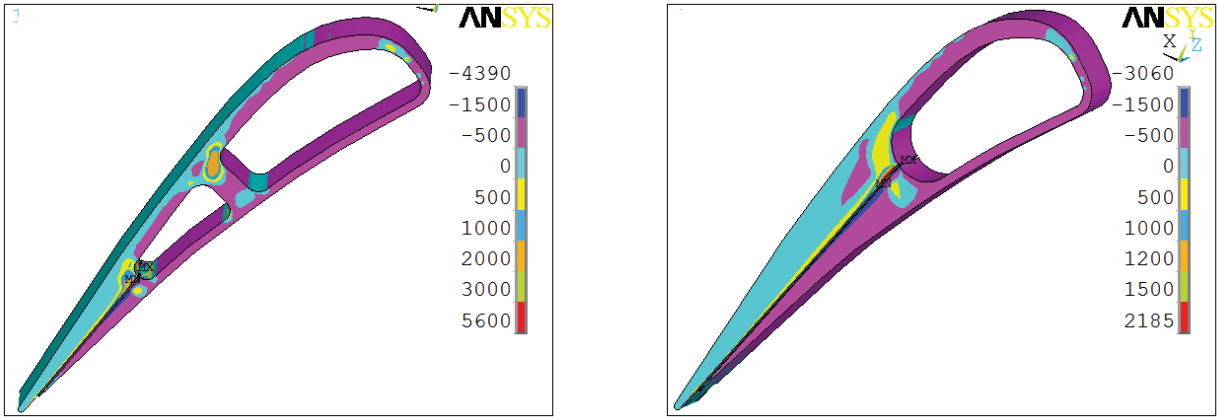

a) Through thickness stress, psi

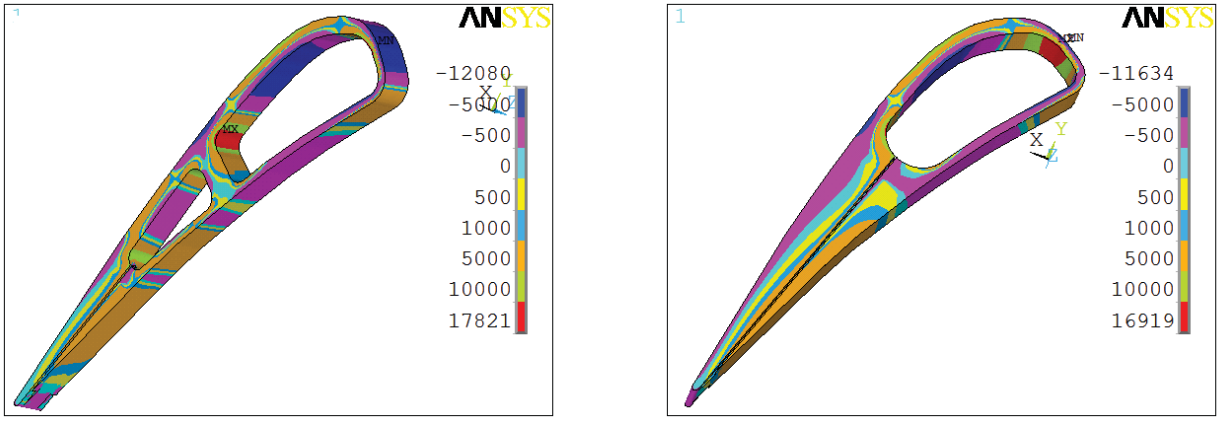

b) Hoop stress, psi

Two impingement cavities - case 5F Single impingement cavity - case 5E

Fig. 5.2.4.1 Effect of single impingement cavity - Pressure load

5.2.4 - Effect of Single Impingement Cavity Since semi-circular ribs were generally preferable to ribs with four small radii corners, a case was analyzed where the radius near the trailing edge ejection tube was maximized. This resulted in a single cavity configuration. Figure 5.2.4.1 and 5.2.4.2 shows result for two cavity and single cavity configurations. Both cases have pressure side trailing edge ejection tubes. Figure 5.2.4.1 shows results for pressure loads, and figure 5.2.4.2 shows results for combined loads. The single cavity configuration reduces maximum through thickness stress by over 60% for pressure load cases, and by over 25% for the combined load cases. For maximum hoop stresses the single cavity configuration was reduced by nearly 25% for the combined load case, but only by 5% for the pressure load only case. Other than a lower maximum through thickness stress, which is definitely beneficial, the through thickness stress distribution within the trailing edge ejection tube is similar for the single and two cavity cases. The location of maximum hoop stress moves away from the entrance to the trailing edge ejection tube for the single cavity cases. For the pressure load case the location of maximum hoop stress moved from the suction side of the rib to the leading edge region.

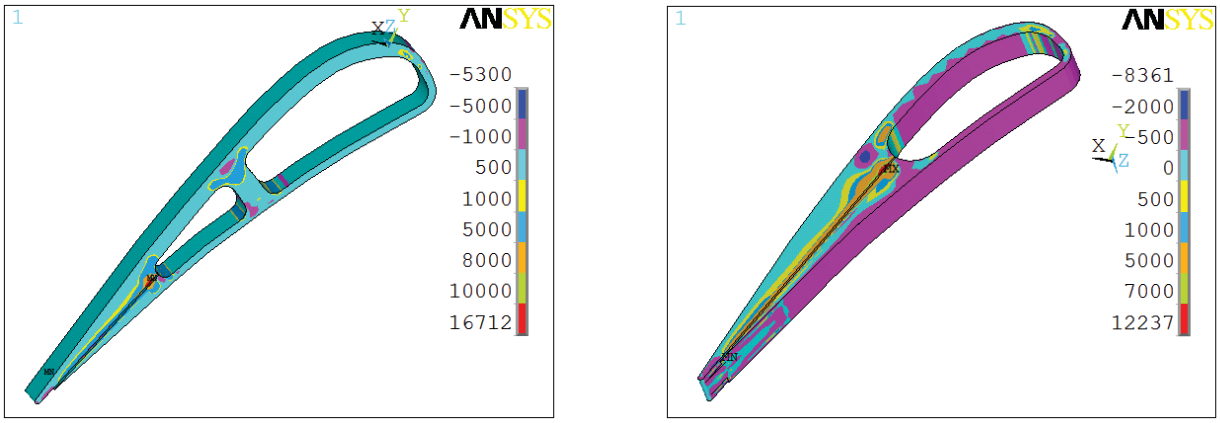

a) Through thickness stress, psi

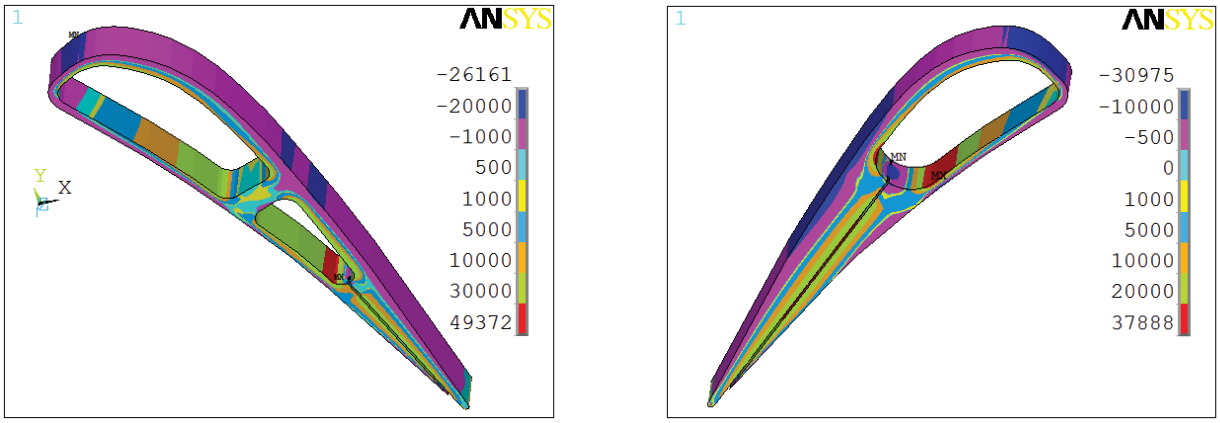

b) Hoop stress, psi

Two impingement cavities - case 5C Single impingement cavity - case 5G

Fig. 5.2.4.2 Effect of single impingement cavity - Combined loads

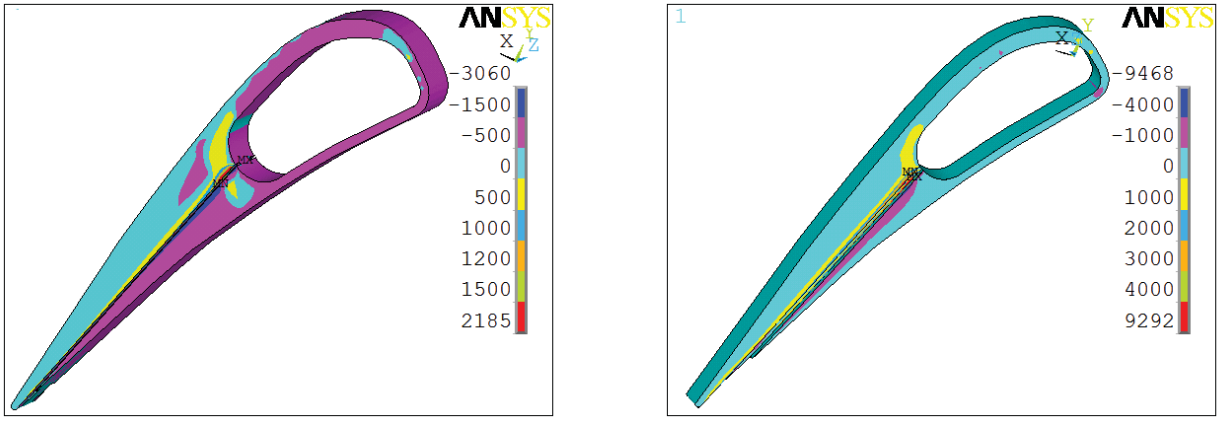

a) Through thickness stress, psi

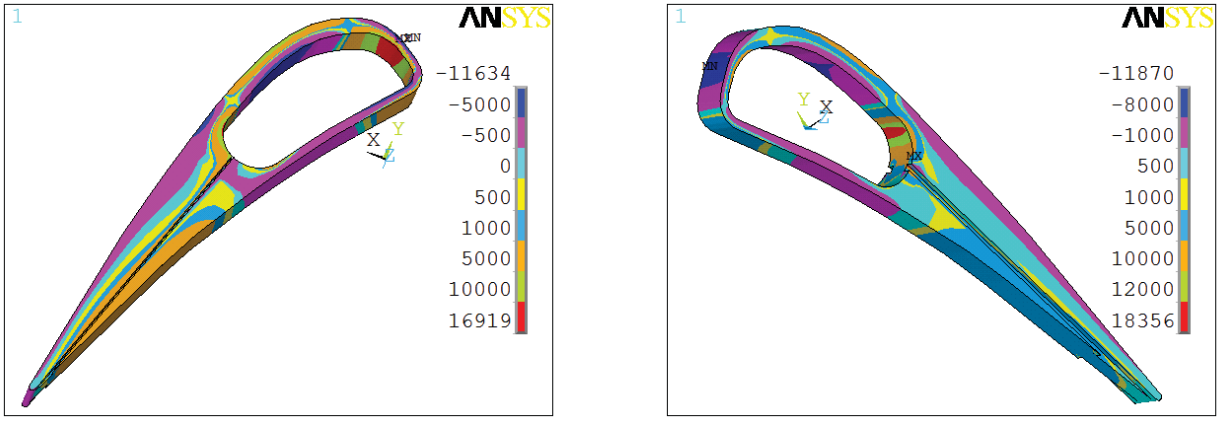

b) Hoop stress, psi

Rectangular tube - case 5E Square tube - case 11A

Fig. 5.2.5.1 Effect of trailing edge ejection tube geometry - Pressure load

5.2.5 - Effect of Rectangular & Square Ejection Tube Geometry The effect of the tube geometry was found to significantly affect stresses. The maximum through thickness stress increased by more than a factor of four when the tube geometry was changed from a 0.86mm X 0.25 mm(34 mil X 10mil) rectangle to a 0.76mm(30mil) square. Figure 5.2.5.1 for pressure loads shows that the maximum through thickness stress increases by more than a factor of four when the rectangular tube is replaced by a square tube. The maximum hoop stress increases by less than 9%, but the location of maximum hoop stress moves from the leading edge region to the entrance of the square tube.

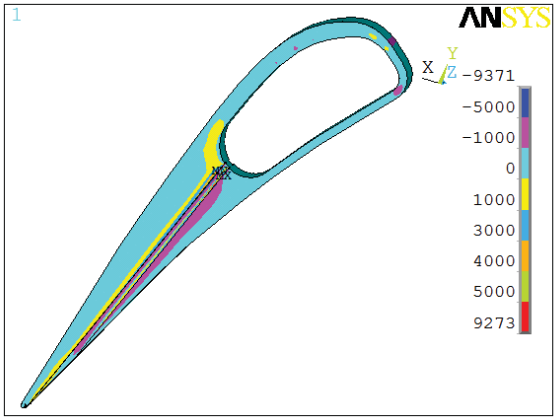

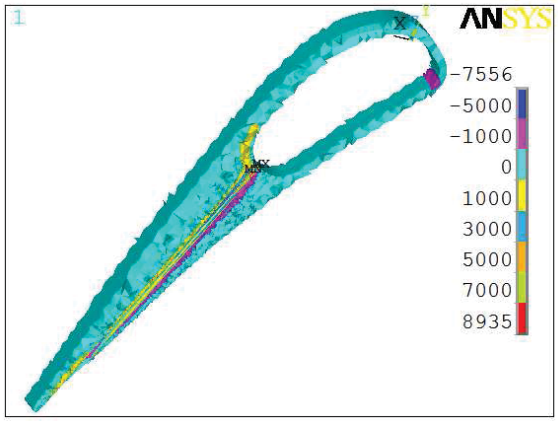

a) Through thickness stress, psi

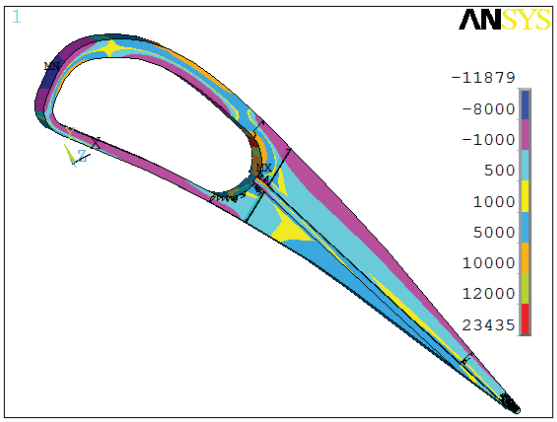

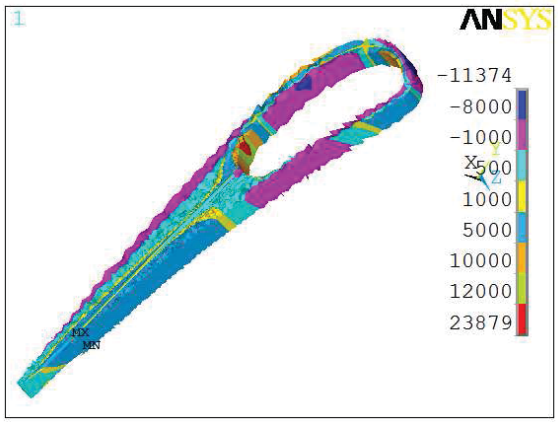

b) Hoop stress, psi

Square tube - case 11B Circular tube - case 11C

Fig. 5.2.6.1 Comparison of square and circular tube geometries - Pressure load

5.2.6 - Effect of Square & Circular Tube Geometry Figures 5.2.6.1 through 5.2.6.3 shows stresses for square and circular trailing edge ejection tube with pressure, thermal, and combined loads. The diameter of the circular tube, 0.76mm(30mil), is the same as the width of the square tube. Both have the same hydraulic diameter, but the cross sectional area of the square tube is greater by just over 20%. The difference in maximum stresses in either the through thickness or hoop directions between the square and circular trailing edge ejection tubes is small. While the maximum through thickness stress is higher for the circular tube for thermal loads, the maximum stress is lower for pressure or combined loads. The maximum hoop stress is higher for the circular tube for pressure loads, but the maximum hoop stress is lower for thermal or combined loads.

Comparing these results with those in figure 5.2.4.2 shows that for combined loads the maximum through thickness or hoop stress is nearly the same for all three trailing edge tube geometries. On the other hand figure 5.2.4.1 shows that for pressure loads the rectangular tube geometry has a much lower maximum through thickness stress, and also a reduced maximum hoop stress.

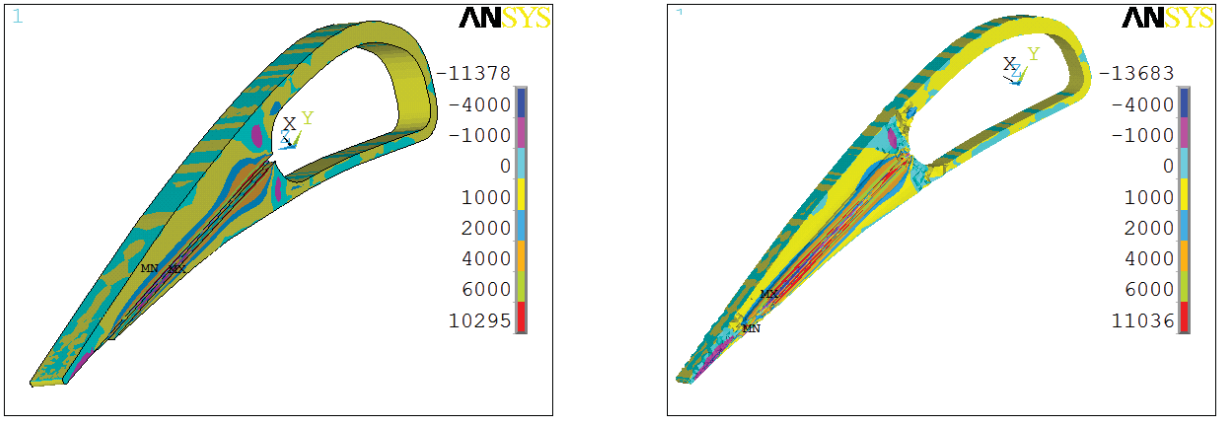

a) Through thickness stress, psi

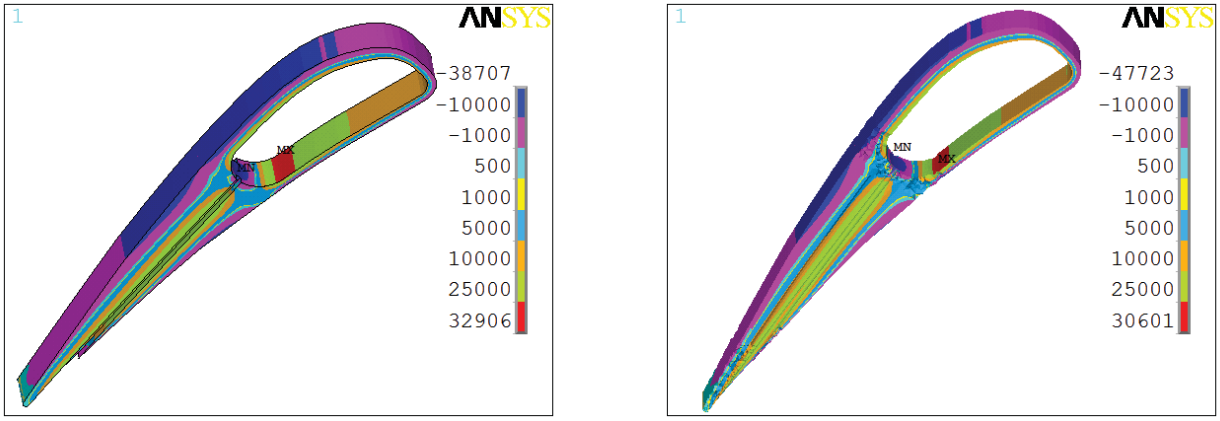

b) Hoop stress, psi

Square tube - case 11G1 Circular tube - case 11F1

Fig. 5.2.6.2 Comparison of square and circular tube geometries - Thernal load

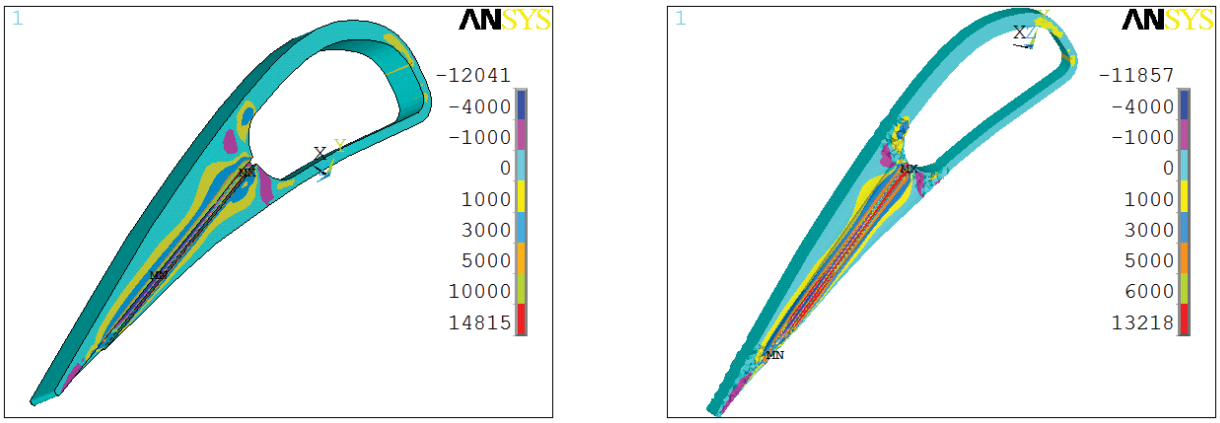

a) Through thickness stress, psi

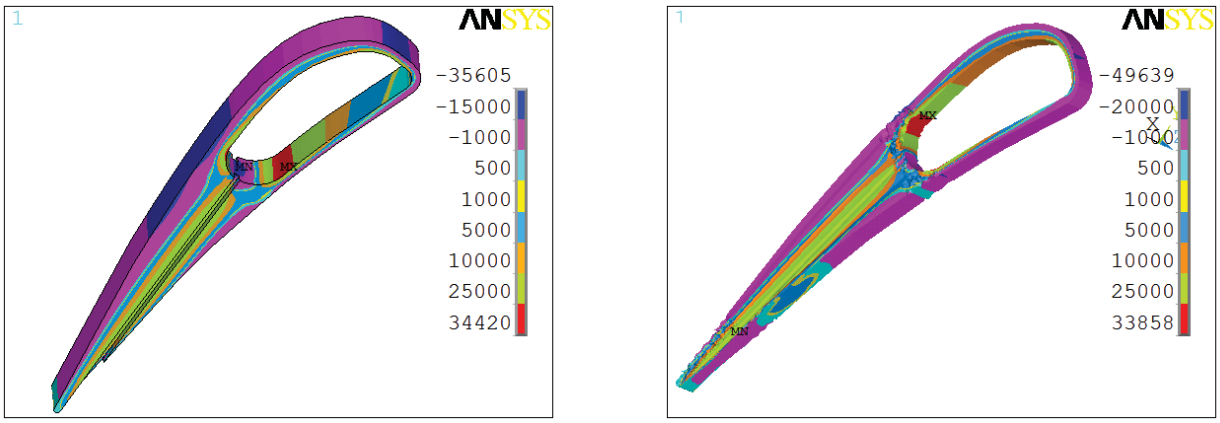

b) Hoop stress, psi

Square tube - case 11G2 Circular tube - case 11F2

Fig. 5.2.6.3 Effect of trailing edge ejection tube geometry - Thermal load

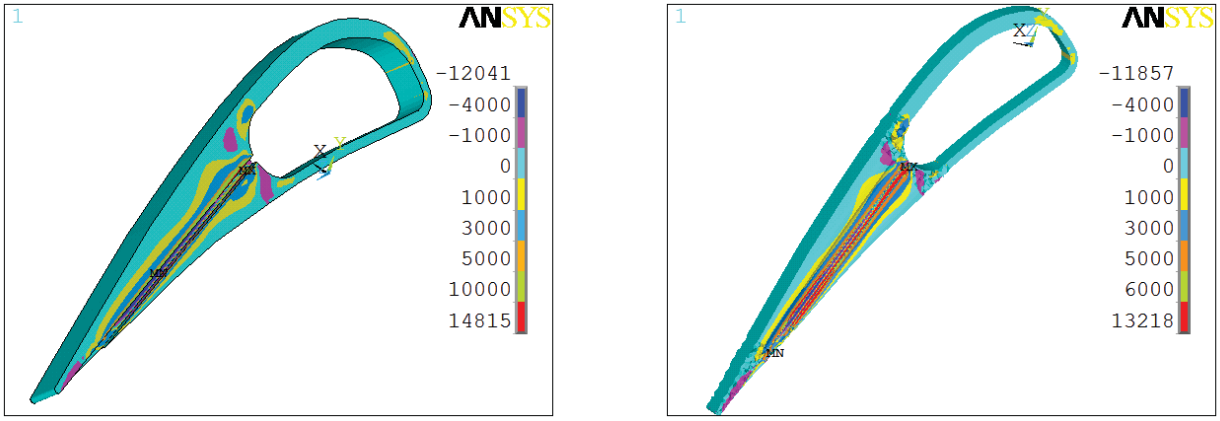

a) Through thickness stress, psi

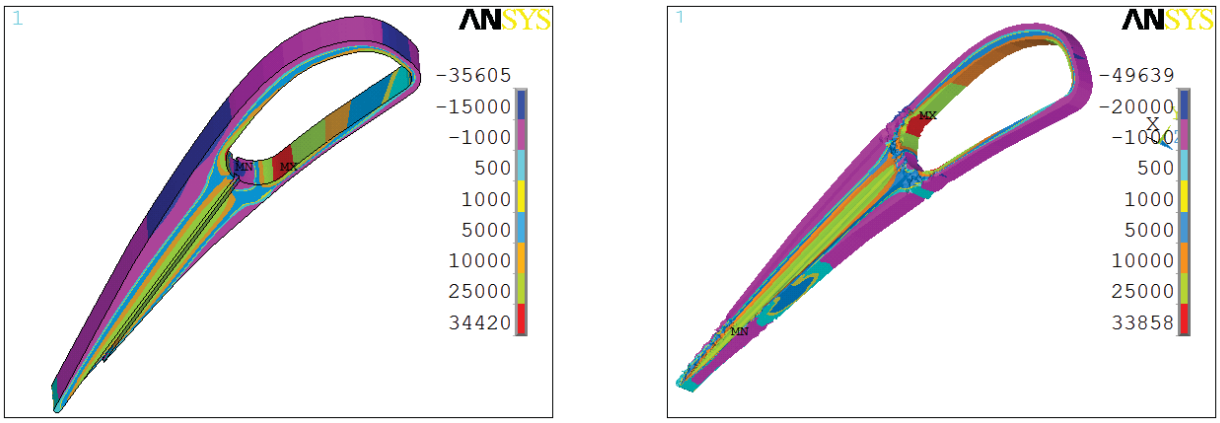

b) Hoop stress, psi

Square tube - case 11G2 Circular tube - case 11F2

Fig. 5.2.6.3 Effect of trailing edge ejection tube geometry - Combined loads

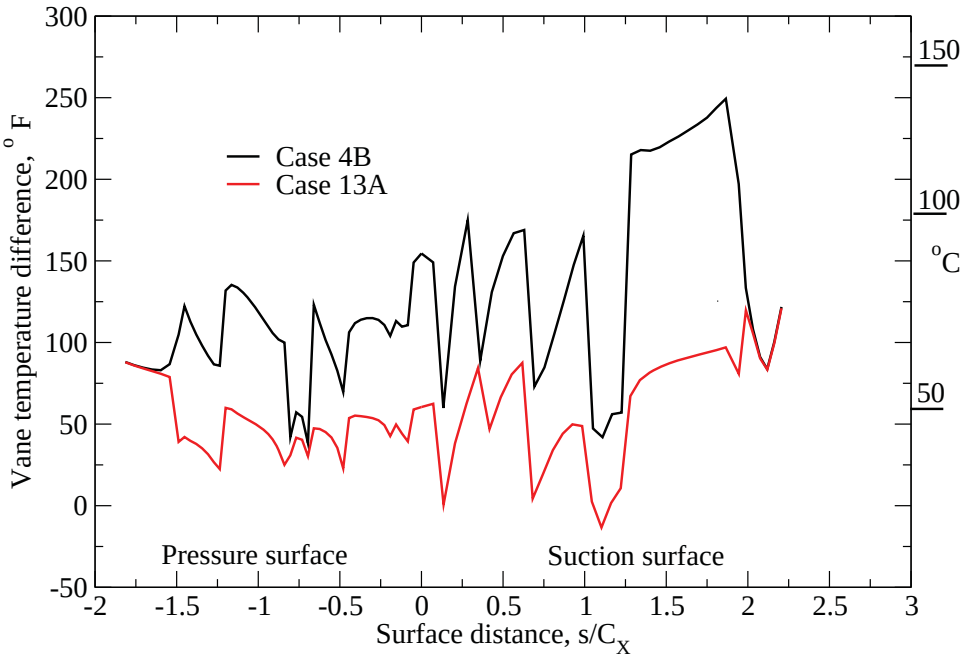

Fig. 5.2.7.1 Temperature difference across CMC vane walls

5.2.7 - Effect of Revised CMC Temperature Gradients Figure 5.2.7.1 shows two temperature difference distributions for the vane. Case 13A has a much lower average temperature difference across the CMC vane than does case 4B. To achieve the lower temperature difference case 13A required addition vane cooling. While the multiple film cooling row cause large variations in the temperature difference for both cases, case 13A has an average temperature difference only about half of the average temperature difference for case 4B.

Figure 5.2.7.2 shows stresses for both cases due to thermal loads. Surprisingly, the lower average temperature difference case, 13A, resulted in higher maximum through thickness stress. In the rib region the lower average temperature case, 13A, shows lower through thickness stresses. Near where the maximum through thickness stress occurs, the streamwise temperature gradient on the pressure surface are of opposite sign. Between $s/C_X = -1.4$ and -1.6 on the pressure surface case 4B has a negative streamwise pressure gradient, and case 13A has a positive streamwise pressure gradient. For case 13A temperatures are increasing with pressure surface distance, and for case 4B temperatures are decreasing with pressure surface distance. These results imply that streamwise temperature gradients, as well as temperature gradients across the vane significantly affect thermal stresses.

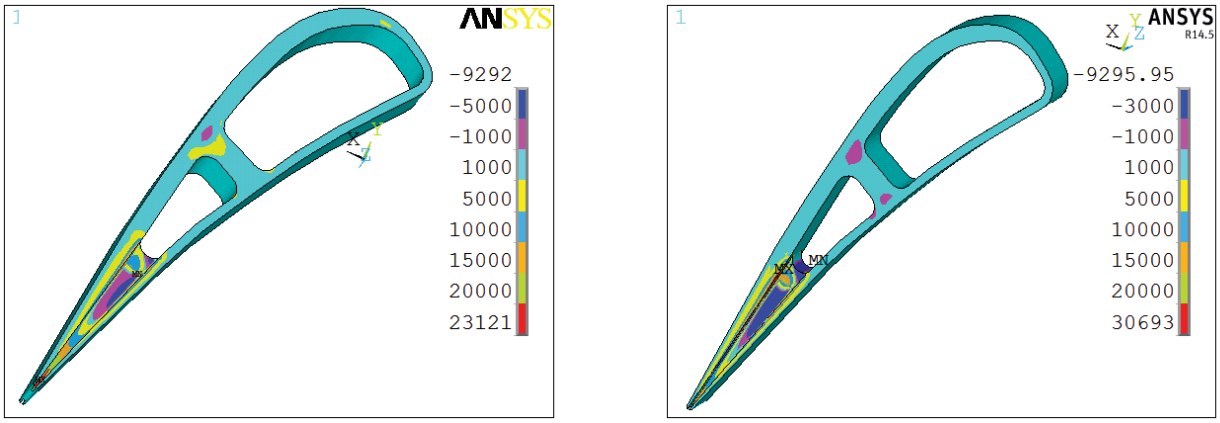

a) Through thickness stress, psi

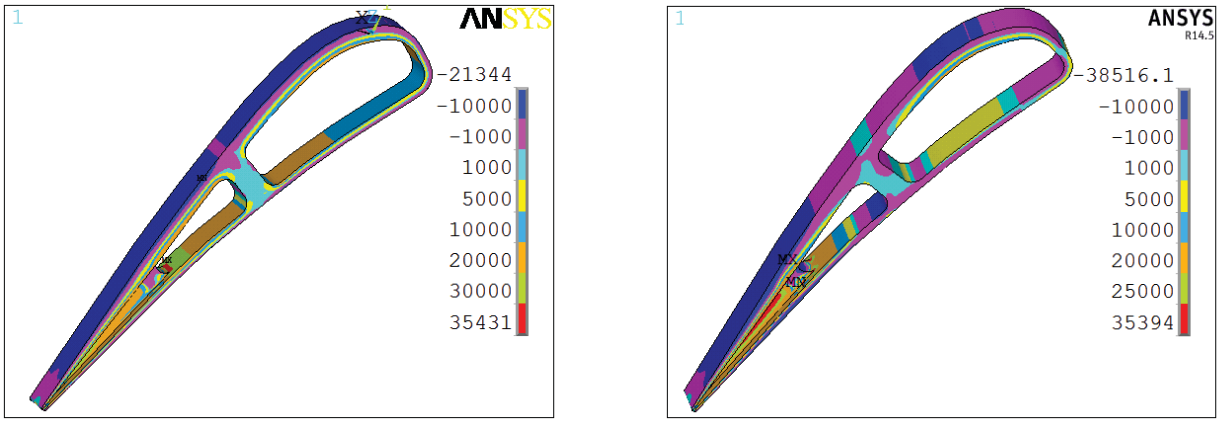

b) Hoop stress, psi

Reference case temperature gradients - case 4B Lowered CMC temperature gradients - case 13A

Fig. 5.2.7.1 Effect of changing CMC temperature gradient - Thermal load

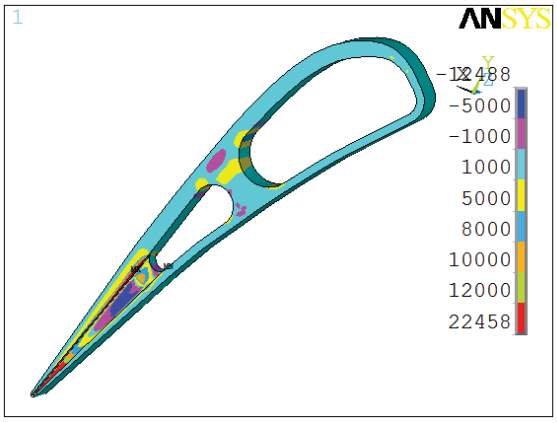

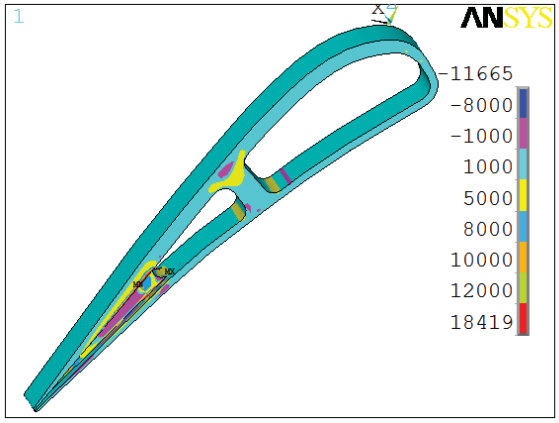

a) Through thickness stress, psi

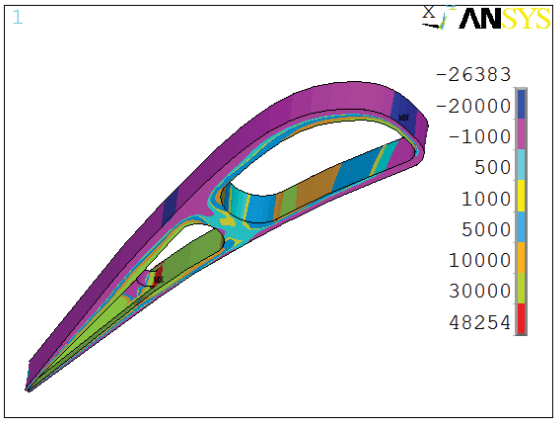

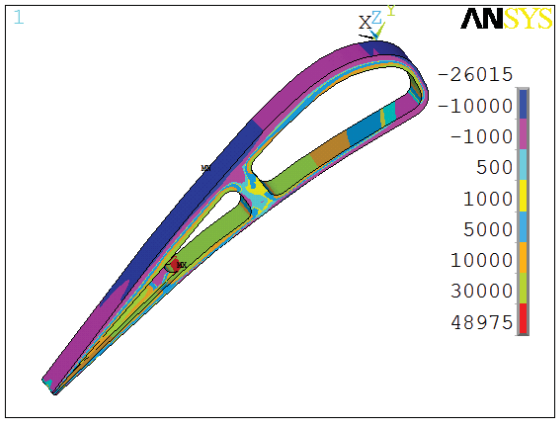

b) Hoop stress, psi

$h_{\text{TUBE}} = 8000 W/m -^{\circ} K$ - case 5A $h_{\text{TUBE}} = 4000 W/m -^{\circ} K$ - case 5B

Fig. 5.2.8.1 Effect of varying ejection tube heat transfer coefficient - Thermal load

5.2.8 - Effect of Reduced Tube Heat Transfer Coefficient The heat transfer coefficient(s) within the ejection tube can be varied in a number of ways. Reducing the amount of trailing edge ejection coolant reduces the average tube heat transfer coefficient, and the reduction in tube flow rate could be balanced by an increase in film cooling. Increasing the tube cross sectional area for the same flow rate would also reduce the average tube heat transfer coefficient. An analysis was done to determine the effects of halving the ejection tube heat transfer coefficient. Figure 5.2.8.1 shows the results of this analysis. Maximum through thickness stresses are reduced by 18% when the tube heat transfer coefficient is halved. The location of maximum through thickness stress is unchanged. Hoop stresses are not affected by reducing the average heat transfer coefficient.

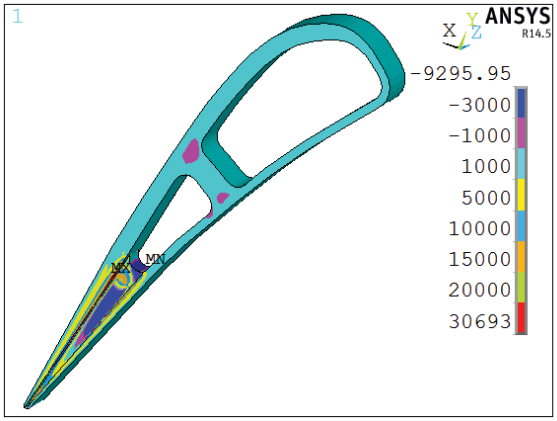

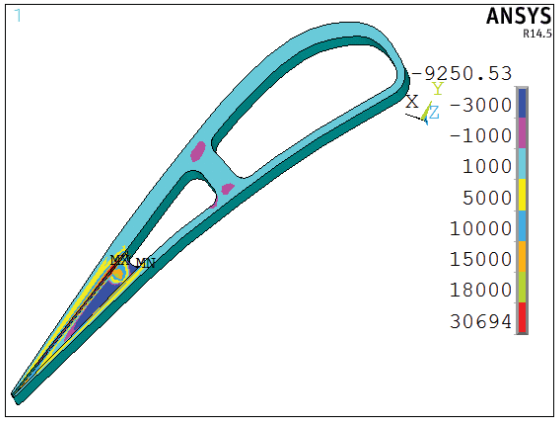

a) Through thickness stress, psi

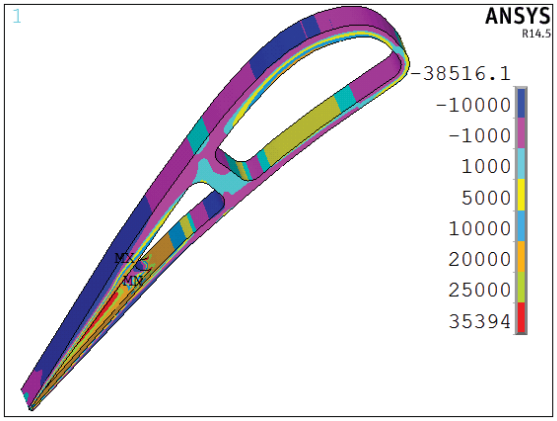

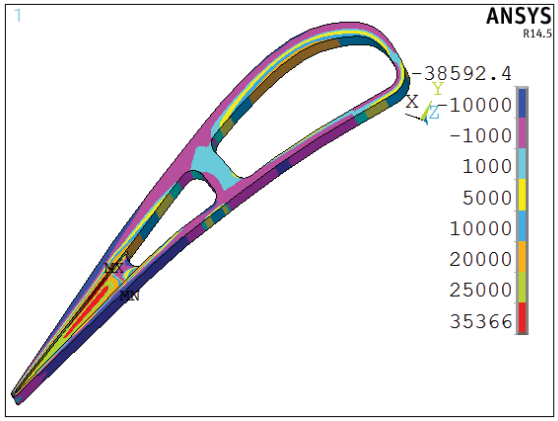

b) Hoop stress, psi

Uninsulated fork region - case 13A Insulated fork region - case 13B

Fig. 5.2.9.1 Effect of insulating fork region - Thermal load

5.2.9 - Effect of Insulating Fork Region Because high stresses were often seen at the entrance of the trailing edge ejection tube, an analysis was done to determine if these stresses would be less if the fork region at the entrance to the trailing edge ejection tube was insulated. Figure 5.2.9.1 shows the results of this analysis for a case with thermal loads. The thermal boundary condition on the cavity surface in the fork region had no noticeable effect on either through thickness or hoop stresses.

5.3 -CMC Material Property and Boundary Condition Effects

In this section four comparisons are examined. The first comparison is for the effects of varying the through thickness stiffness modulus, E_{33}, This parameter is expected to experience significant variations due to even small changes in material composition. The second comparison is for variations in thermal conductivity. It is desirable to increase CMC thermal conductivity, since this decreases the thermal gradients across the vane walls. The third comparison examines the effects of changing the stiffness of the two vane end plates. This was done by halving the thickness of each end plate. This comparison helps to answer the question of whether increasing the rigidity lowers stresses in the midspan region. The fourth comparison examines the effects of changing the boundary conditions on midspan stresses. The boundary conditions are applied to the edges of each end plate.

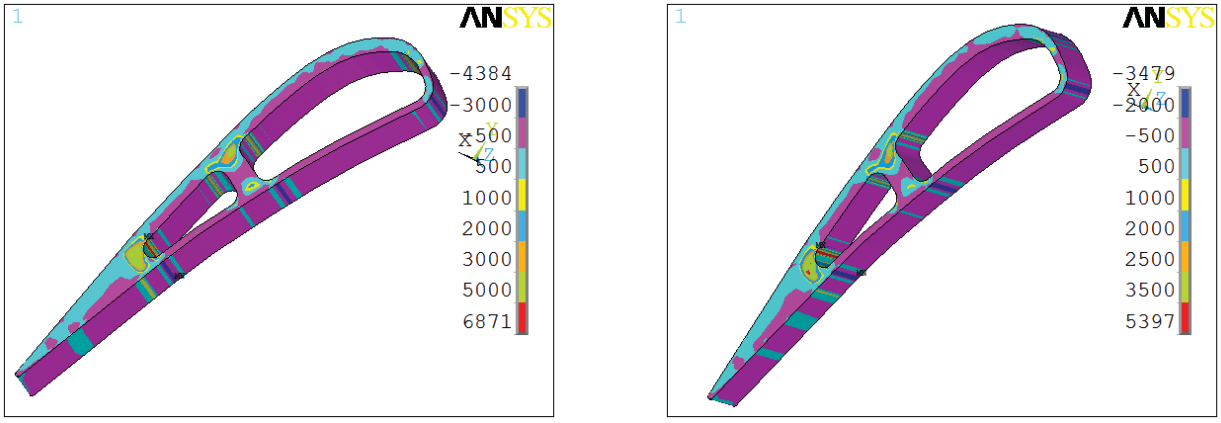

a) Through thickness stress, psi

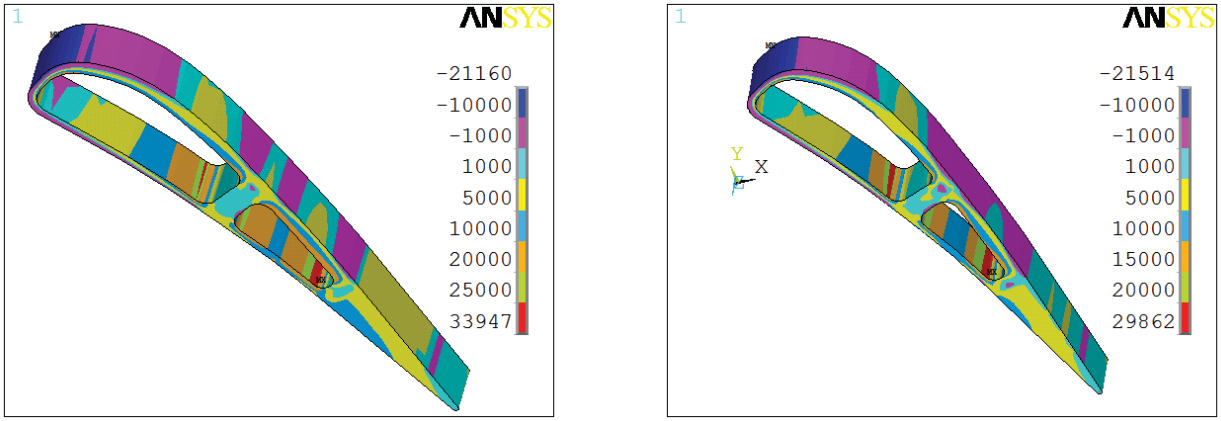

b) Hoop stress, psi

E_{33} = 157 GPa(22.8 M psi) - case 6A E_{33} = 77 GPa(11.2 M psi) - case 6B

Fig. 5.3.1.1 Effect of through thickness stiffness- Combined loads

5.3.1 - Effect of Through Thickness Stiffness Modulus The through thickness stiffness modulus, E_{33}, was varied to determine the sensitivity of stresses to changes in this parameter. When E_{33} was varied Poisson's ratio was held constant at 0.17 for the through thickness direction properties. Figure 5.3.1.1 and 5.3.1.2 show stresses for two values of E_{33} for pressure and thermal loads combined. Figure 5.3.1.1 compares cases without trailing edge ejection, and figure 5.3.1.2 compares cases with pressure side trailing edge ejection through a rectangular ejection tube. Stresses are reduced as E_{33} is reduced, but by less than proportionately. For cases without trailing edge ejection, and when E_{33} is nearly halved the maximum through thickness stress is reduced by only about 20%. Nearly halving E_{33} reduces the maximum hoop stress by 12%. Figure 5.3.1.2 shows similar results for trailing edge ejection cases. Nearly halving E_{33} reduces the maximum through thickness stress by 28%, and reduces the maximum hoop stress by 11%.

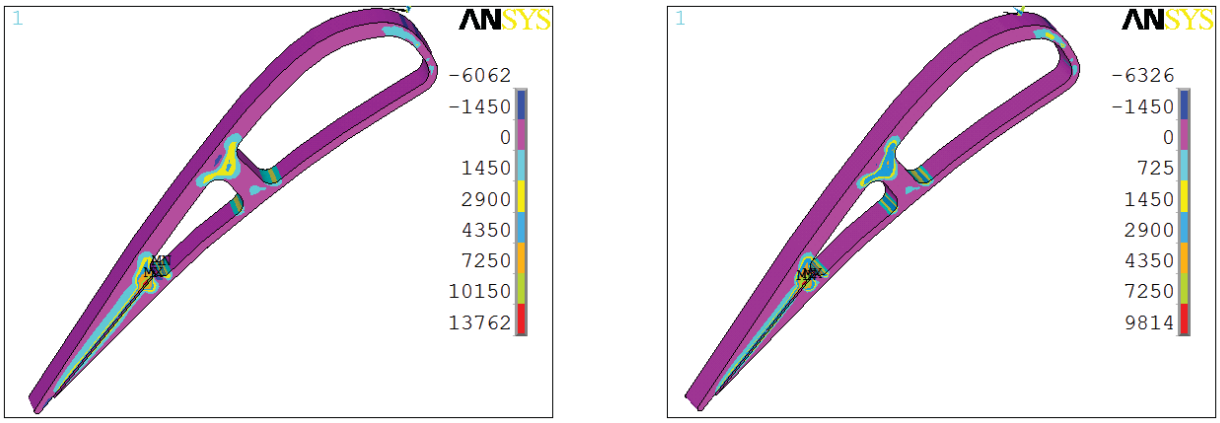

a) Through thickness stress, psi

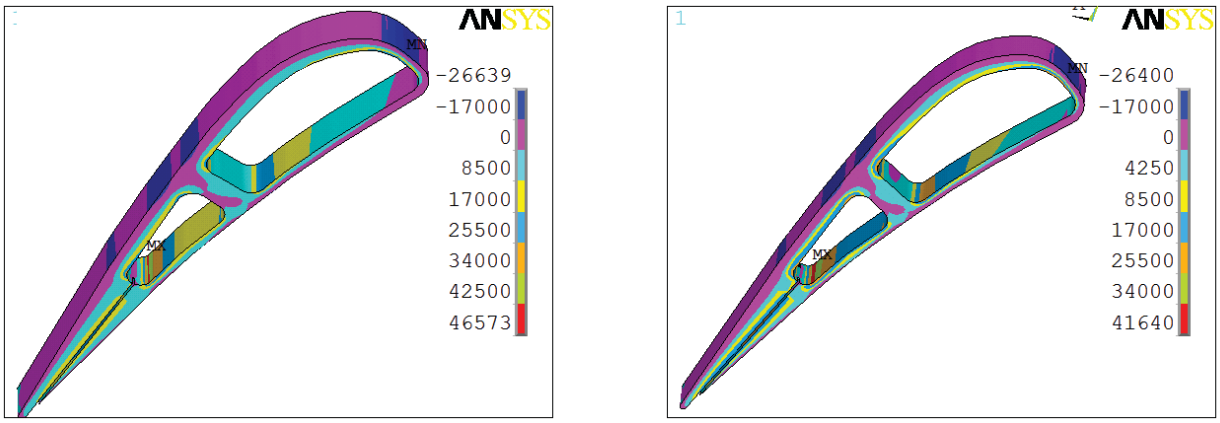

b) Hoop stress, psi

E_{33} = 157 GPa(22.8 M psi) - case 12A E_{33} = 77 GPa(11.2 M psi) - case 12B

Fig. 5.3.1.2 Effect of through thickness stiffness- Combined loads

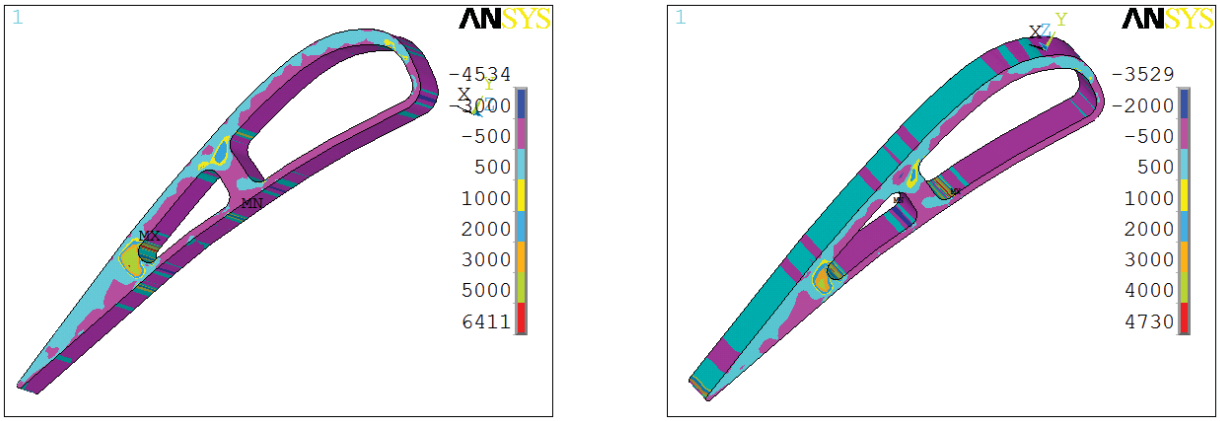

a) Through thickness stress, psi

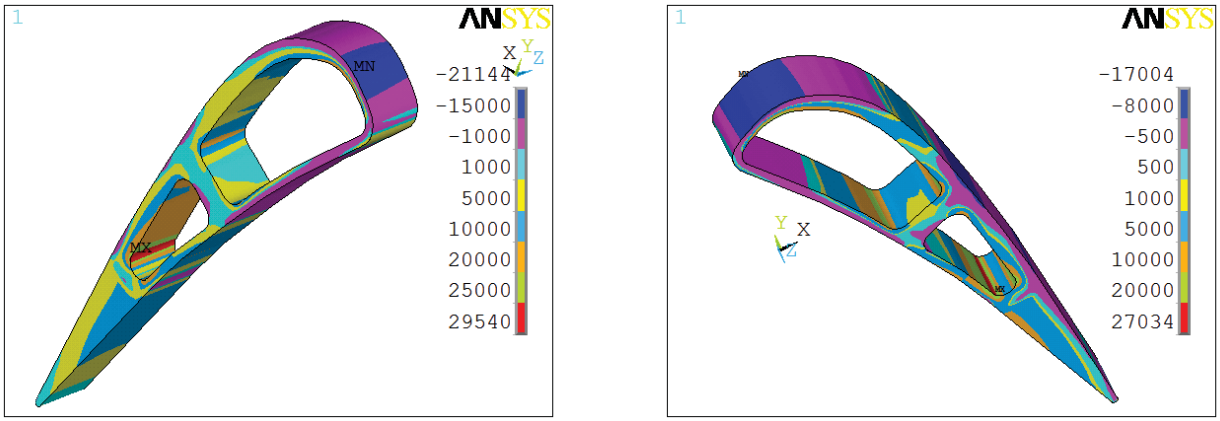

b) Hoop stress, psi

$k_{\text{CMC}} = 20$ W/m-K - case 6G $k_{\text{CMC}} = 40$ W/m-K - case 8A

Fig. 5.3.2.1 Effect of doubling CMC thermal conductivity - Combined loads

5.3.2 - Effect of Doubling Thermal Conductivity Increasing the CMC thermal conductivity decreases the temperature difference across the CMC vane. The difference is not proportional to the increase in thermal conductivity. The overall thermal resistance is determined by the internal and external heat transfer coefficients, the thermal resistance of the EBC protective layer, as well as the thermal resistance of the vane itself. When the CMC thermal conductivity is increased less vane coolant is required, so that the temperature differences across the vane also change. Under these circumstances the chief benefit for stress reductions may be reductions in streamwise temperature gradients. Since the analysis was done with less cooling for the higher thermal conductivity case, there is also a cycle benefit to higher CMC conductivity.

Figure 5.3.2.1 shows a comparison for cases with combined loads and no trailing edge ejection. Maximum through thickness stress is reduced by more than 25% when the CMC thermal conductivity is doubled from $20 W/m - ^{\circ} K$. Maximum hoop stress is reduced by less than 9%. The location of maximum stress changed when the CMC conductivity was doubled. When the CMC thermal conductivity doubled, the location of the maximum through

thickness stress moved from the suction side of the fork region to forward of the rib on the pressure surface. The location of maximum hoop stress remained in the fork region, but shifted from the suction side to the pressure side as the conductivity doubled.

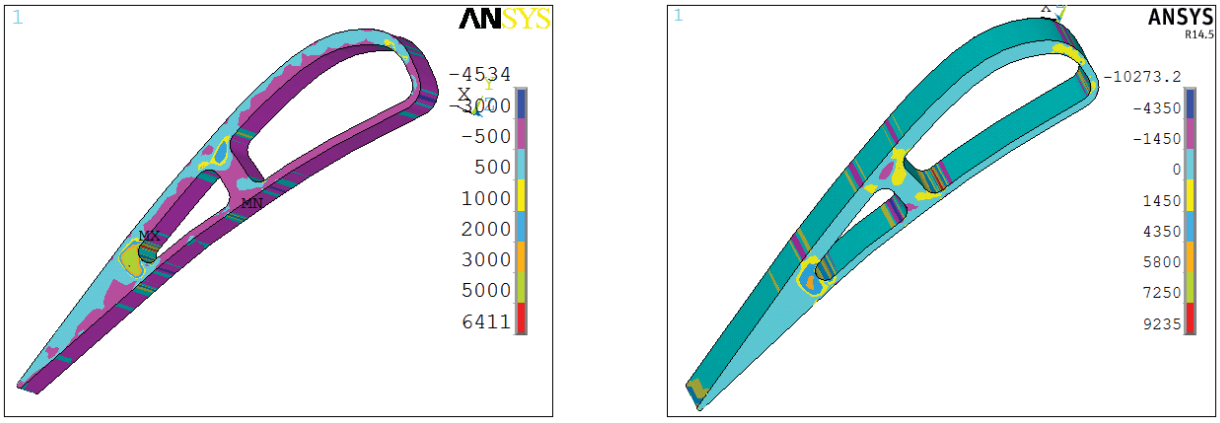

a) Through thickness stress, psi

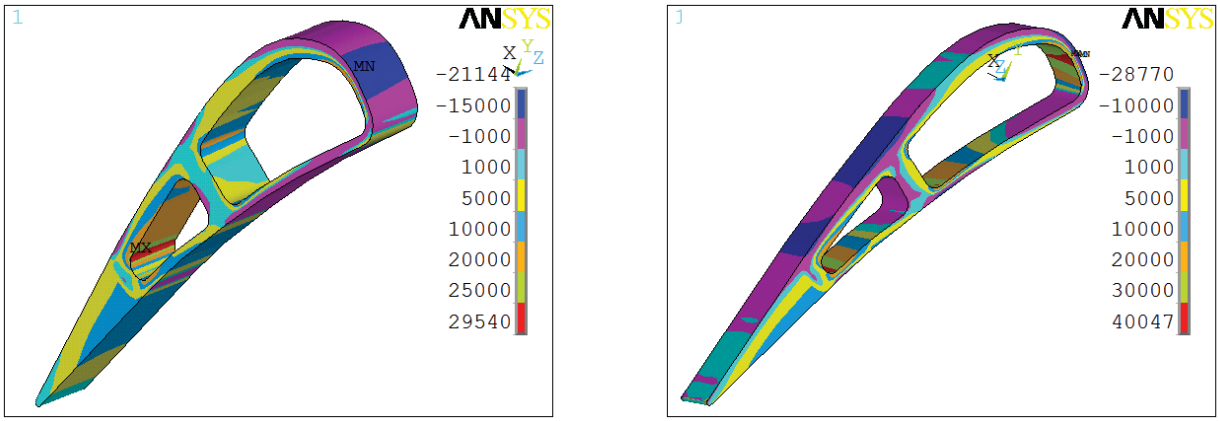

b) Hoop stress, psi

Original end plate thickness- case 6G End plate thickness halved - case 7A

Fig. 5.3.3.1 Effect of reducing end plate thickness - Combined loads

5.3.3 - Effect of Reducing End Plate Stiffness The stiffness of the end plate has a significant effect on vane stresses, even in the midspan region, away from the end plate. Previous results were calculated where the two end plates were 4mm(160 mil) thick, and had the same material properties as the CMC vane. Figure 5.3.3.1 shows stresses when the thickness of both end plates is halved. Results are shown for combined loads and cases where there is no trailing edge ejection. This allows greater vane deflections, especially in the midspan region. The maximum through thickness stress increased by nearly 45% when thickness of both end plates was halved, and the maximum hoop stress increased by 36%. The location of maximum stresses also changed. The maximum through thickness stress moved from the suction side of the fork to just forward of the rib on the pressure surface when the end plate thicknesses were halved. The maximum hoop stress moved from the suction side of the fork to the leading edge region when the end plate thicknesses were halved. These results show the desirability of using stiff end plates with CMC vanes.

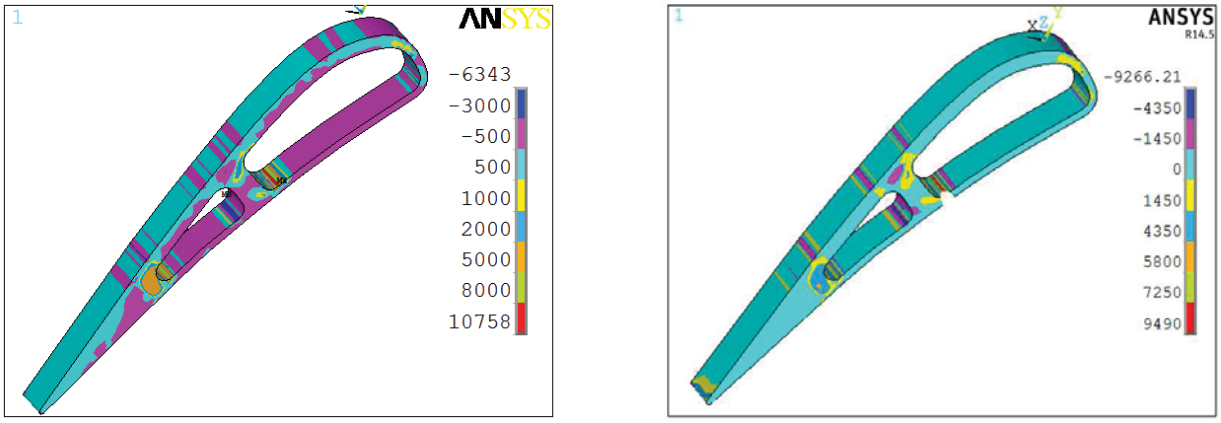

a) Through thickness stress, psi

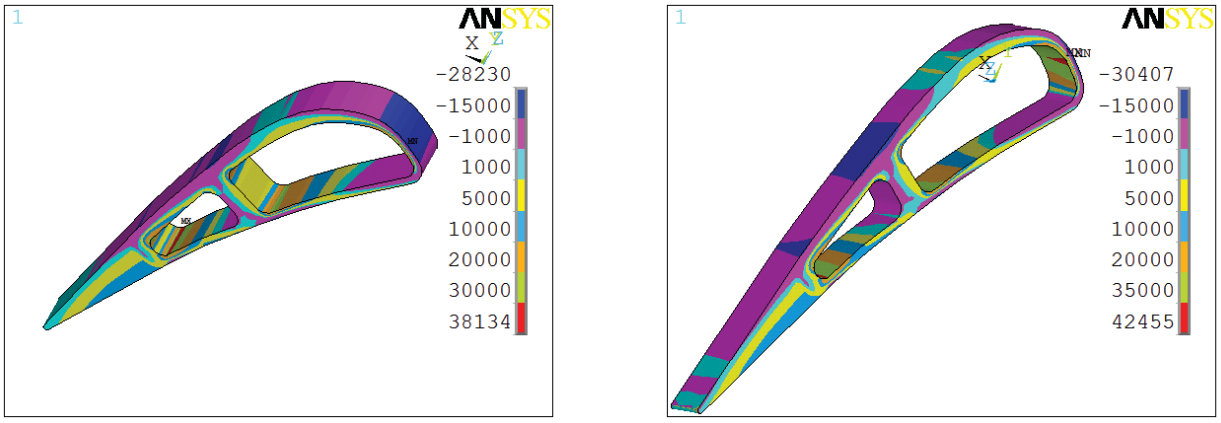

b) Hoop stress, psi

Original boundary condition- case 7B Modified boundary condition - case 7C

Fig. 5.3.4.1 Effect of modifying plate boundary condition - Combined loads

5.3.4 - Effect of Boundary Condition Variation The effect of changing the end plate boundary conditions was examined. Figure 5.3.4.1 shows results for two cases with different end plate boundary conditions. Case 7B has the standard boundary conditions, and case 7C has the modified boundary conditions. For the standard boundary conditions the hub end plate is held in the axial and spanwise directions, and along its leading edge in the pitchwise direction. The other end plate is free to move in all directions. For case 7C there is an additional constraint along the edge of the hub end plate. The hub end plate is fixed at the pressure side corner, where the axial and pitchwise edges meet. When the additional constraint was added to the end plate, the maximum through thickness stresses decreased by 12%, and the location of maximum stress remained the same. The maximum hoop stresses increased by 12%, and the maximum hoop stress location moved from the pressure side of the fork to the leading edge region.

5.4 - Mesh Refinement Studies

This section gives the results of four comparisons for results with different computational meshes. The first comparison examines the effects on midspan region stresses due to a variation in the mesh density used for each end plate. The second comparison examines the effects of changing the mesh density in the leading edge region. The last two comparisons examine the effects on stresses for changes in the mesh used around the trailing edge ejection tube. One case is for a square trailing edge ejection tube and the other is for a circular tube.

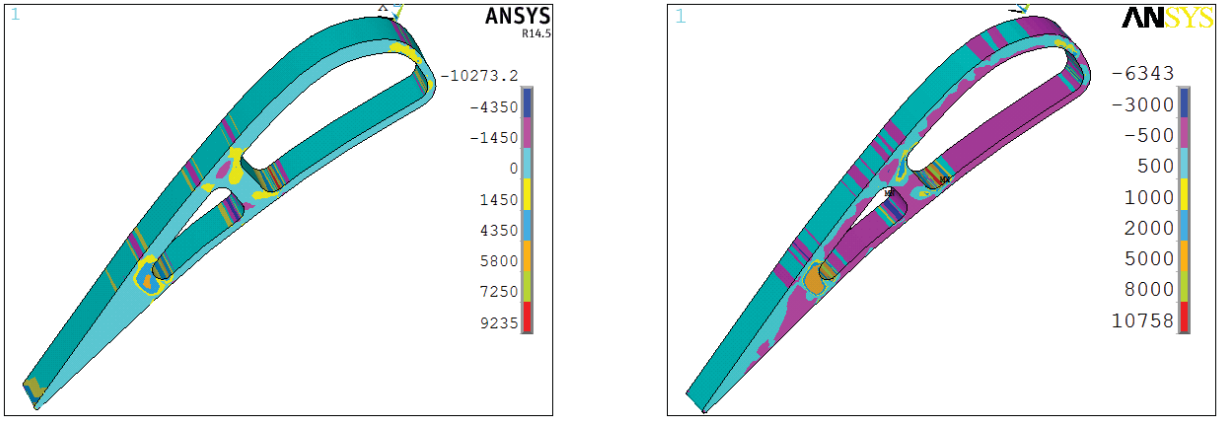

a) Through thickness stress, psi

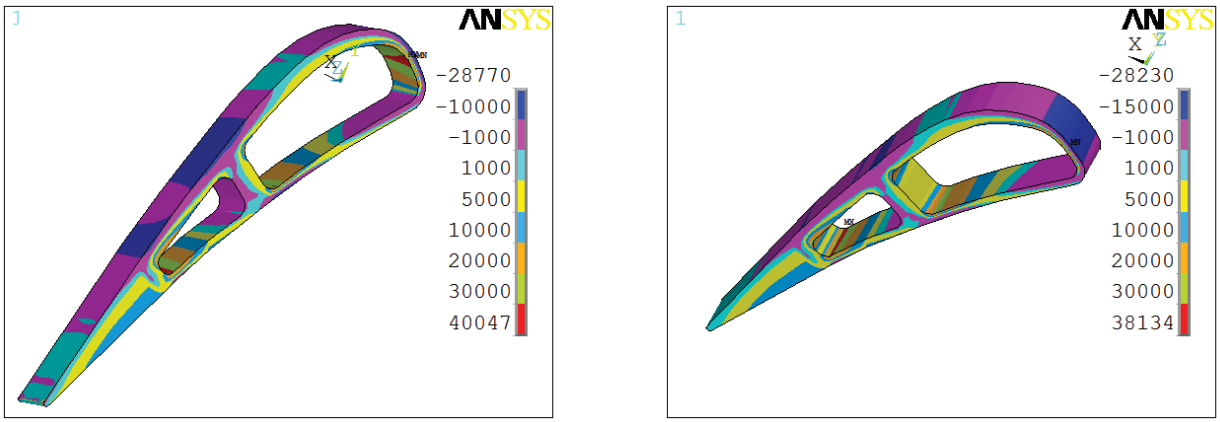

b) Hoop stress, psi

"Coarse" mesh - case 7A Finer mesh - case 7B

Fig. 5.4.1.1 Effect of increasing end plate mesh density - Combined loads

5.4.1 - Effect of Vane and End Plate Mesh Density Figure 5.4.1.1 shows stresses for two cases with different mesh density. Comparisons are for combined thermal and pressure loads. This comparison is for thinner end plates of 2mm(80mil) thickness, and not the standard end plate thickness of 4mm(160mil). Case 7A has typical mesh of 30000 total elements for cases without trailing edge ejection. Case 7B has a more dense mesh of 50000 total elements. When the number of end plate elements increased, there was also an increase in the number of vane elements. Only in the region of maximum stress does increasing the number of elements have an effect. It is not unexpected that an increase in the number of elements would increase the maximum stress. Since maximum stresses are so highly localized, the magnitude of the stress gradient is very high at the location of maximum stress. Increasing the number of elements positions nodes closer to the theoretical location of maximum stress, and a higher maximum stress is expected as the mesh density increases. Figure 5.1.1,1a shows that the maximum through thickness stress increased by 17%. As expected the location of maximum through thickness stress did not change. Somewhat unexpectedly figure 5.4.1.1b shows that the maximum hoop stress decreased by 5% as the total number of elements increased. The response of the maximum hoop stress to the increase in the number of elements occurred because the location of maximum hoop stress changed as the number of elements increased. The maximum hoop stress moved from leading edge to the pressure side of the fork region.

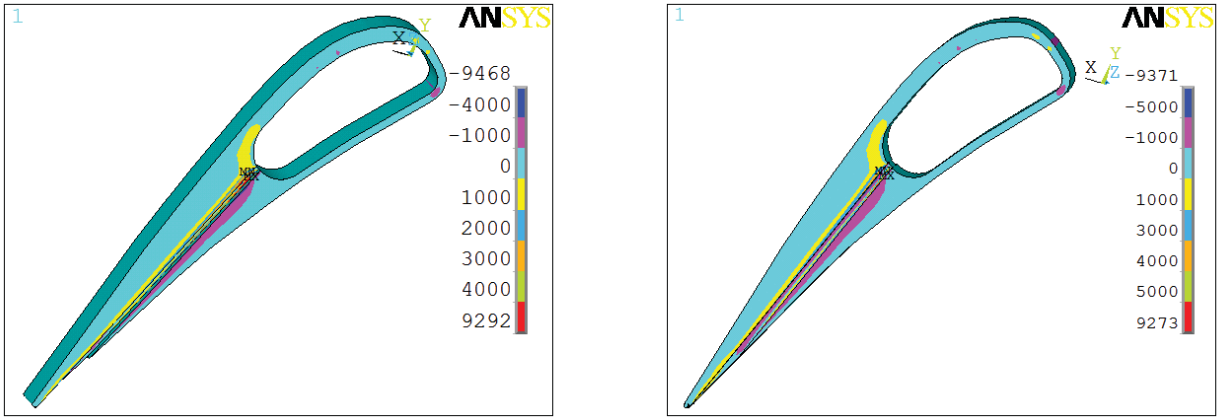

a) Through thickness stress, psi

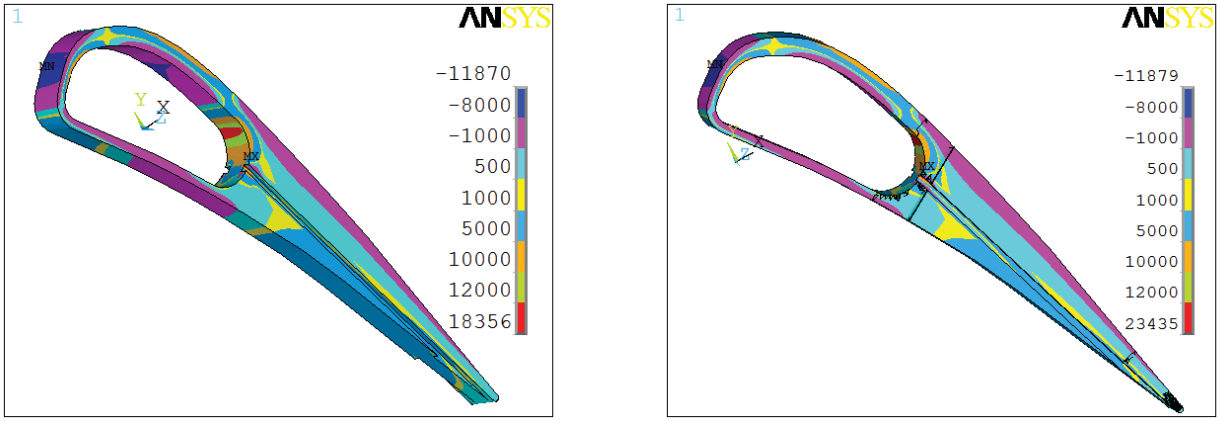

b) Hoop stress, psi

Hexagonal mesh elements - case 11A Hexagonnal & tetrahedral elements - case 11B

Fig. 5.4.2.1 Effect of varying mesh type for square tube - Pressure load

5.4.2 - Effect of Mesh Shape for Square Ejection Tube Figure 5.4.2.1 shows the effects of mesh element shape for squared tube cases. For case 11A a hexahedral mesh was used 11A with 130,000 elements. Typically, hexahedral elements were used for the ANSYS analysis. The number of elements was significantly increased when trailing edge ejection was used because a mesh was needed for each of the ten trailing edge ejection tubes. Case 11B used a combination of hexahedral and tetrahedral mesh elements. Transitional pyramid elements were used in the fork and trailing edge regions. Case 11B had 230,000 elements. Through thickness stresses are unaffected by the shape of the mesh elements. Only the magnitude of the maximum hoop stress is affected by the shape of the mesh elements. While the increase of 28% in maximum hoop stress is large, the increase is confined to a very small region. Part of the increase in maximum hoop stress may be due to a larger number of mesh elements. Also, hexahedral elements are preferred to tetrahedral elements for achieving accurate results, Brauer[31]. However, tetrahedral elements are required when the trailing edge ejection tube is circular.

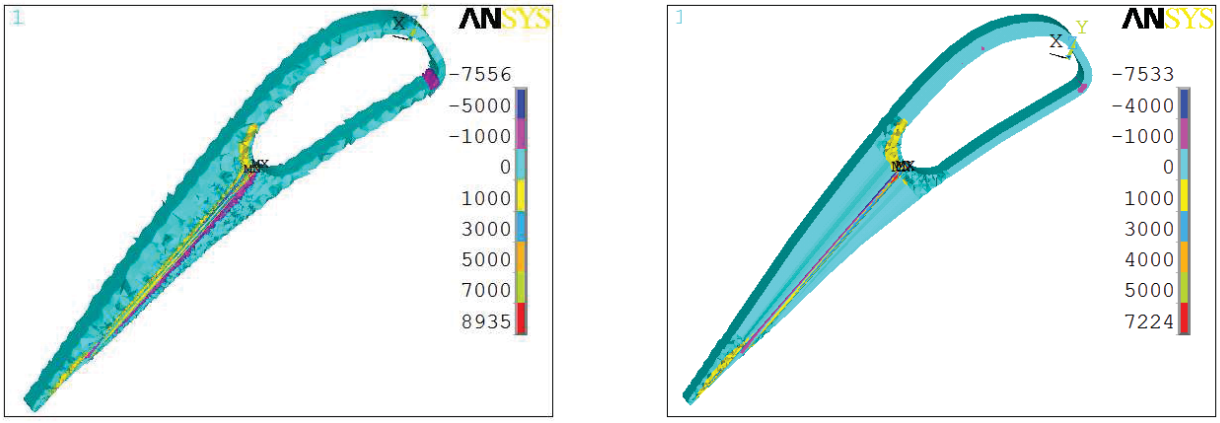

a) Through thickness stress, psi

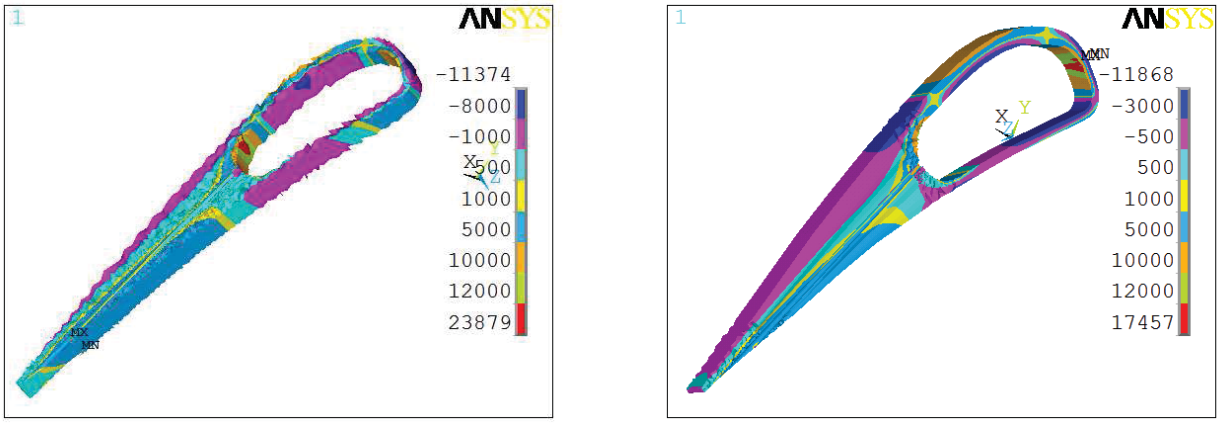

b) Hoop stress, psi

"Standard" mesh density case 11C Reduced mesh density - case 11E

Fig. 5.4.3.1 Effect of varying mesh density for circular tube - Pressure load

5.4.3 - Effect of Mesh for Circular Ejection Tube Due to complexity of circular ejection tube model, tetrahedral shaped elements were used in case 11C. This case had 720,000 elements. Case 11E had a combination of hexahedral and tetrahedral elements, Transitional pyramid elements were used in the fork and trailing edge regions. Case 11E had 350,000 elements. Figure 5.4.3.1 shows that the only effect of using fewer elements is a reduction in maximum stress. The maximum through thickness stress is reduced by 19%, but the location at the tube entrance is unchanged. The maximum hoop stress is reduced by 27%, and the location of maximum stress changed between the two cases. For case 11C the maximum hoop stress occurred more than half way down the ejection tube, and for case 11E the maximum hoop stress occurred in the leading edge region.

5.5 - Maximum Component Stresses

Even though maximum stresses are often confined to a very small region of the vane, comparisons of maximum stress in the three component directions is useful. These comparisons help to show a path to reduced stresses. by different vane internal geometries, and also the effects of modeling assumptions.. Tables IIa through IId show the maximum component stresses, and the location where these stresses occur. The maximum through thickness or interlaminar, the maximum hoop, and the maximum spanwise or radial stress is given for pairs of cases. Comparisons are given for pairs of cases to illustrate the change in maximum stresses for a specific effect. Table IIa shows results for cases without trailing edge ejection, and Table IIb shows results for cases with centerline and pressure side trailing edge ejection. Table IIIc shows results for property and boundary condition variations, while Table IId shows results of mesh sensitivity studies. While no figures were given for the spanwise stresses in the midspan region, these tables include the maximum spanwise stress in the midspan region, The location of the maximum spanwise stress is also given.

Table IIa shows that, except for one case, the maximum spanwise stress is lower than the maximum hoop stress. The assumed orientation of the reference material, N24A, was that the material properties in the hoop and span directions were the same. Since spanwise maximum stresses were almost always lower than the maximum stress in the hoop direction, hoop stresses were of greater interest. Table IIa shows that the location of maximum hoop stress was generally different from the location of maximum spanwise stress.

Table IIa shows that the case of no internal pressure, 5.1.7, results in very high maximum hoop and spanwise stresses. For this case the maximum through thickness stress is comparable to the maximum through thickness stress for cases with combined loads. Without an internal pressure no vane thermal stresses are expected to occur.

Maximum thermal stresses are generally higher than maximum pressure stresses. Table IIa shows that maximum thermal stresses are very sensitive to variations in temperature distributions. There was over a 50% increase in maximum thermal load stresses when a uniform CMC temperature differential was replaced by wall temperatures consistent with a film cooled vane. There was over a 20% reduction in maximum thermal load stresses when the rib connecting the pressure and suction surface was insulated. Table IIb shows similar results for cases with trailing edge ejection. Changing the CMC temperature gradients resulted in maximum through thickness and spanwise stresses increasing by more than 30%.

Table IIb shows that maximum stresses increase significantly when there is a trailing edge ejection tube. Pressure side, as differentiated from centerline, trailing edge ejection is sometimes favored for vane efficiency reasons, since it allows for a thinner trailing edge thickness. The results in Table IIb show that it is also preferable from a stress standpoint. For pressure loads and combined loads the reduction in maximum through thickness stress is over 25%. For combined loads the reduction in maximum spanwise stress is nearly 40%. Maximum hoop loads are less affected by going from centerline to pressure side ejection.

In contrast to the results without trailing edge ejection, maximum spanwise stresses for several cases exceed maximum hoop stresses. However, maximum spanwise stresses vary over a wide range. For the single impingement cavity case, which has the lowest combined load maximum through thickness stress, the maximum spanwise stress is within 15% of the maximum hoop stress. The 5.2.7 comparison shows that the maximum spanwise stress

decreased by over 10% when the trailing edge ejection tube was halved.

Table IIc shows that reducing the through thickness modulus of elasticity, E_{33}, or increasing the CMC thermal conductivity is effective in reducing maximum through thickness stresses. Using thinner end plates, which is desirable from a weight standpoint, results in higher maximum stresses in the midspan region of the vane. Halving the thickness of the end plates caused the maximum through stress to increase by more than 40%. The other maximum stresses also increased.

Table IId shows that maximum stresses are somewhat sensitive to the type of mesh used. Since all other comparisons were done with the same mesh type, the relative change between cases is expected to be accurate. The values in Table II are maximum values, and near the maximum values the component stresses change very rapidly. Therefore, it is not surprising that as the number of elements in the finite element analysis increase, maximum stresses also increase. The results for comparisons 5.4.1 and 5.4.3 show that more elements give higher maximums in regions of high gradients. Using a mixture of hexahedral and tetrahedral mesh element resulted in higher maximum hoop and spanwise stresses compared with just using hexahedral elements.

Table IIa. Comparisons for midspan region maximum calculated stress, ksi,(MPa)

5.1 - No Trailing Edge Ejection

Case	Load	Through thickness		Hoop		Span	
		Value	Location	Value	Location	Value	Location
5.1.1 - Effect of Rib							
1A	Press	4.62(31.9)	Fork	31.4(217)	Fork	13.3(92.0)	T.E.
2A	Press	1.57(10.8)	Rib	17.0(117)	Rib	13.3(92.0)	T.E.
% change		-66		-46		0	
1C	Temp	6.91(47.6)	Fork	31.1(214)	L.E.	28.5(197)	Fork
2B	Temp	10.5(72.4)	Rib	41.5(286)	Rib	34.3(236)	P-aft of rib
% change		+52		+33		+20	
1D	Comb	10.8(75.4)	Fork	55.5(383)	Fork	29.1(201)	Fork
2C	Comb	10.6(73.1)	Rib	45.6(314)	Rib	36.9(254)	P-aft of rib
% change		-2		-18		+27	
5.1.2 - Effect of Non-Uniform Temperature Gradient							
1B	Temp	4.44(30.6)	L.E.	20.4(141)	L.E.	17.7(122)	Fork
1C	Temp	6.91(47.6)	Fork	31.1(214)	L.E.	28.5(197)	Fork
% change		+56		+53		+61	
5.1.3 - Effect of Differential Wall Thickness							
2A	Pres	1.57(10.8)	Rib	17.0(117)	Rib	13.3(92.0)	T.E.
3A	Pres	2.40(16.5)	Rib	16.7(115)	Rib	13.8(94.8)	P-L.E.
% change		+53		-2		+4	
2B	Temp	10.5(72.4)	Rib	41.5(286)	Rib	34.3(236)	P-aft of rib
3B	Temp	8.52(58.7)	Rib	38.2(263)	Rib	31.2(215)	Fork
% change		-20		-8		-9	
5.1.4 - Effect of Combining Pressure and Temperature Loads							
3A	Pres	2.40(16.5)	Rib	16.7(115)	Rib	13.8(94.8)	P-L.E.
3C	Temp	6.61(45.6)	Rib	29.4(203)	Fork	26.3((182)	P-aft of rib
3D	Comb	7.28(50.2)	Fork	36.6(252)	Fork	27.2(188)	P-aft of rib
5.1.5 - Effect of Insulating Rib							
3B	Temp	8.52(58.7)	Rib	38.2(263)	Rib	31.2(215)	Fork
3C	Temp	6.61(45.6)	Rib	29.4(203)	Fork	26.3(182)	P-aft of rib
% change		-22		-23		-16	
5.1.6 - Effect of Modified Rib Shape							
3A	Pres	2.40(16.5)	Rib	16.7(115)	Rib	13.8(94.8)	P-L.E.
5D	Pres	1.11(7.65)	Rib	17.9(123)	L.E.	15.4(106)	P-for. of rib
% change		-54		+7		+12	
5.1.7 - Effect of No Internal Pressure							
3A	Pres	2.40(16.5)	Rib	16.7(115)	Rib	13.8(94.8)	P-L.E.
3A2	Pres	10.9(75.2)	Rib	115.(793)	Rib	59.8(412)	P-for. of rib
% change		+354		+589		+333	
5.1.8 - Effect of Revised Temperatures							
3D	Comb	7.28(50.2)	Fork	36.6(252)	Fork	27.2(188)	P-aft of rib
6C	Comb	7.82(53.9)	Fork	35.1(242)	Fork	40.2(277)	P-for. of rib
% change		+7		-4		+48	
5.1.9 - Effect of Trailing Edge Shape							
7B	Comb	10.8(74.2)	Rib	38.1(263)	Fork	38.4(264)	P-for. of rib
7D	Comb	10.8(74.2)	Rib	39.2(270)	L.E.	38.4(264)	R-for. of rib
% change		0		+3		0	

Table IIb. Comparisons for midspan region maximum calculated stress, ksi,(MPa)
5.2 - Trailing Edge Ejection

Case	Load	T.E.	Through thickness		Hoop		Span	
		Ejection	Value	Location	Value	Location	Value	Location
5.2.1 - Effect of Centerline Trailing Edge Ejection								
3A	Pres	No	2.40(16.5)	Fork	16.7(115)	Fork	11.1(76.5)	P-front
4A	Pres	Cl	9.04(62.3)	Tube	20.2(139)	Fork	16.5(114)	Fork
% change			+277		+21		+41	
3C	Temp	No	6.61(45.6)	Rib	29.4(203)	Fork	26.3(181)	P aft of rib
4B	Temp	Cl	23.1(159)	Tube	35.4(244)	Tube	74.4(513)	Tube
% change			+249		+20		+183	
3D	Comb	No	7.28(50.2)	Fork.	36.6(252)	Fork	27.2(178)	P aft of rib
4C	Comb	Cl	22.5(155)	Tube.	49.3(340)	Tube	83.4(575)	Tube
% change			+209		+35		+207	
5.2.2 - Effect of Pressure Side Trailing Edge Ejection								
4A	Pres	Cl	9.04(62.3)	Tube	20.2(139)	Fork	16.5(114)	Fork
5F	Pres	PS	5.60(38.6)	Tube	17.8(123)	Rib	17.1(118)	Fork
% change			-38		-12		+4	
4C	Comb	Cl	22.5(155)	Tube	49.3(340)	Tube	83.4(575)	Tube
5C	Comb	PS	16.7(115)	Tube	49.4(340)	Fork	51.2(353)	Fork
% change			-26		0		-39	
5.2.3 - Effect of Revised Rib Shape								
4C	Comb	Cl	22.5(155)	Tube	49.3(340)	Tube	83.4(575)	Tube
5A	Comb	PS	22.5(155)	Tube.	48.2(333)	Fork.	83.4(575)	Tube
% change			0		-2		0	
5.2.4 - Effect of Single Impingement Cavity								
5F	Pres	PS	5.60(38.6)	Tube	17.8(123)	Rib	17.1(118)	Fork
5E	Pres	PS	2.19(15.1)	Tube	16.9(117)	L.E.	15.8(109)	Pres. surf.
% change			-61		-5		-8	
5C	Comb	PS	16.7(115)	Tube	49.4(340)	Fork	51.2(353)	Fork
5G	Comb	PS	12.2(84.4)	Tube	37.9(261)	P.S.	43.5(300)	Tube
% change			-27		-23		-15	
5.2.5 - Effect of Trailing Edge Ejection Tube Geometry								
5E	Pres	PS	2.19(15.1)	Tube	16.9(117)	L.E.	15.8(109)	Pres. surf.
11A	Pres	PS	9.29(64.1)	Tube	18.4(127)	Fork	18.5(128)	Pres. surf.
% change			+324		+9		+17	
5.2.6 - Effect of Square & Circular Tube Geometry								
11A	Pres	PS	9.29(64.1)	Tube	18.4(127)	Fork	18.5(128)	Pres. surf.
11C	Pres	PS	8.94(61.6)	Tube	13.8(95)	L.E.	94.0(648)	Pres. surf.
% change			-3		-25		+408	
11G1	Temp	PS	10.3(71.0)	Tube	32.9(227)	P.S.	69.7(480)	Tube
11F1	Temp	PS	11.0(76.1)	Tube	30.6(211)	P.S.	74.2(512)	Tube
% change			+7		-7		+6	
11G2	Comb	PS	14.8(102)	Tube.	34.4(237)	P.S.	71.8(495)	Tube
11F2	Comb	PS	13.2(91.1)	Tube	33.9(233)	S.S.	75.5(521)	Tube
% change			-11		-1		+5	
5.2.7 - Effect of Revised CMC Temperature Gradients								
4B	Temp	Cl	23.1(159)	Tube	35.4(244)	Tube	74.4(513)	Tube
13A	Temp	Cl	30.7(212)	Tube	35.4(244)	Tube	102(701)	Tube
% change			+33		0		+37	
5.2.8 - Effect of Reduced Tube Heat Transfer Coefficient								
5A	Comb	PS	22.5(155)	Tube.	48.2(333)	Fork.	83.4(575)	Tube
5B	Comb	PS	18.4(127)	Tube.	49.0(338)	Fork.	74.2(512)	Tube
% change			-18		+2		-11	
5.2.9 - Effect of Insulating Fork Region								
13A	Temp	Cl	30.7(212)	Tube	35.4(244)	Tube	102(701)	Tube
13B	Temp	Cl	30.7(212)	Tube	34.4(244)	Tube	102(701)	Fork
% change			0		0		0	

Table IIc. Comparisons for midspan region maximum calculated stress, ksi,(MPa)

5.3 - Property and Boundary condition effects

Case	Load	T.E.	Through thickness		Hoop		Span	
		Ejection	Value	Location	Value	Location	Value	Location
5.3.1 - Effect of Through Thickness Stiffness Modulus								
6A- E_{33} = 157 GPa	Comb	No	6.87(47.4)	Fork	33.9(234)	Fork	24.4(167)	P-aft of fork
6B E_{33} = 77 GPa	Comb	No	5.40(37.2)	Fork	29.9(206)	Fork	24.5(169)	P-L.E.
% change			-22		-12		0	
12A - E_{33} = 157 GPa	Comb	PS	13.7(94.9)	Tube	46.6(321)	Fork	47.8(329)	Tube
12B - E_{33} = 77 GPa	Comb	PS	9.81(67.7)	Tube	41.6(287)	Fork	46.9(324)	Tube
% change			-29		-11		-2	
5.3.2 - Effect of CMC Thermal Conductivity								
6G	Comb	No	6.41(44.2)	Fork	29.5(204)	Fork	32.4(224)	P-aft of fork
8A	Comb	No	4.73(32.6)	Fork	27.0(186)	Fork	29.7(205)	P-for. of rib
% change			-26		-8		-8	
5.3.3 - Effect of End Plate Stiffness								
6G	Comb	No	6.41(44.2)	Fork	29.5(204)	Fork	32.4(224)	P-aft of fork
7A	Comb	No	9.24(63.7)	Fork	40.0(276)	L.E.	38.3(264)	P-for. of rib
% change			+44		+36		+18	
5.3.4 - Boundary Conditions								
7B	Comb	No	10.8(74.5)	Rib	38.1(263)	Fork	38.4(265)	P-for. of rib
7C	Comb	No	9.49(65.4)	Rib	42.5(293)	L.E.	38.8(268)	P-for. of rib
% change			-12		+12		+1	

Table IId. Comparisons for midspan region maximum calculated stress, ksi,(MPa)

5.4 - Mesh Refinement

Case	Load	T.E.	Through thickness		Hoop		Span	
		Ejection	Value	Location	Value	Location	Value	Location
5.4.1 - End Plate								
7A	Comb	No	9.24(63.7)	Fork	40.0(276)	L.E.	38.3(264)	P-front
7B	Comb	No	10.8(74.5)	Rib	38.1(263)	Fork	38.4(265)	P-front
% change			+17		-5		0	
5.4.2 - Square Trailing Edge Ejection Tube								
11A	Pres	PS	9.29(64.1)	Tube	18.4(127)	Fork	18.5(128)	Pres. surf.
11B	Pres	PS	9.27(64.0)	Tube	23.4(161)	Tube	20.3(140)	Pres. surf
% change			0		+27		+10	
5.4.3 - Circular Trailing Edge Ejection Tube								
11C	Pres	PS	8.94(61.6)	Tube	13.8(95)	L.E.	94.0(648)	Pres. surf.
11E	Pres	PS	7.22(50.0)	Tube	17.5(121)	L.E.	29.4(122)	Pres. surf.
% change			-19		+27		-69	

5.6 - Conclusions

The results of the stress analysis for the full size EEE vane showed that stresses from expected thermal loads are greater than stresses expected from pressure loads even though the inlet total pressure was 50 atm. All components of stress, through thickness, hoop, and spanwise, were higher due to thermal loads compared with pressure loads. Maximum stresses occurred either in the fork region, where the pressure and suction surfaces meet, or in the rib connecting these two surfaces. When there was trailing edge ejection, maximum stresses often occurred in the trailing edge ejection tube. These maximum stresses often occurred in the fork region near the tube entrance.

The reference material, N24A, was a two-dimensional woven material. The desired maximum stress in the trough thickness, or interlaminar, direction was 10.3 MPa(1.5 ksi). The desired maximum stress in the hoop and spanwise directions was 17ksi(117 MPa). Maximum calculated combined load through thickness stress was more than four times greater than the desired maximum through thickness stress. The maximum combined load hoop stress and the maximum spanwise stress were about double the desired stress for the better low stress cases examined. Maximum stresses were very localized. In many cases close to 98% of the vane cross section had stresses less than one half of the maximum component stress. Also, for cases with trailing edge ejection maximum and minimum stresses were located close to each other within the ejection tube. This suggests that a creep analysis of vane stresses, which is expected to be more applicable in the engine environment, may result in lower maximum component stresses. Kaufman[xx] showed a significant reduction in maximum stress for a metal vane when creep was taken into account.

The analysis was done for thermal loads, pressure loads, and thermal and pressure loads combined. Stresses due to thermal loads were greater than those due to pressure loads. The location of maximum pressure load stress was not coincident with the location of maximum thermal load stress. The maximum combined load component stress was generally only slightly greater than the the maximum thermal load component stress.

The stress analysis results indicate that not including stress augmentation due to rows of film cooling holes is not a short coming of the analysis. Hoop stresses are most affected by the presence of a row of film cooling holes, due to their relatively close spacing in the spanwise direction. Many cases showed large regions of the vane with low stresses, where rows of film cooling holes could be placed without exceeding desired maximum hoop stress. Stress augmentation in the spanwise direction due to rows of film cooling holes is much less than in the hoop direction due to the wider spacing between rows than between holes in a row.

6.0 - Radial Cooled Vane

Current cooling schemes rely on impingement and film cooling to achieve acceptable material temperatures. These schemes are well suited for commercial turbofan and military engine applications. Impingement cooling schemes rely on an insert to distribute the vane cooling air. For small size vanes, such as for use in turboshaft engine applications, impingement cooling may not be practical. Radial cooling has been proposed for small CMC vanes, such as would be found in turboshaft engine applications. With radial cooling the impingement scheme is replaced by using several cooling tubes, oriented in the spanwise or radial direction. No impingement insert is required, and the diameter of the radial cooling holes can be small, approaching the diameter of film cooling holes if necessary. Similar to film cooling, many small diameter radial tubes, as opposed to one or two maximum diameter tubes, facilitate heat removal from the radial tubes. However, pressure drop considerations favor somewhat larger diameter tubes, since radial cooling tubes are much longer than film cooling tubes. An additional reason for investigating the feasibility of radial cooling for turboshaft engine applications is that as the vane size decreases the thermal resistance within the vane material also decreases. Vane wall thickness decreases as the vane size decreases. The decrease in vane size is generally coupled with an increase in freestream and coolant side convective resistances. The convective resistances increase as the combustor outlet pressure decreases, and historically the combustor outlet pressure is lower for smaller size engines.

It is easier to fabricate CMC vanes with radial cooling tubes and no film cooling, than to fabricate CMC vanes with radial cooling tubes from which film cooling is extracted. On the other hand, the heat flux absorbed by the air flowing through the tubes is less when film cooling is used. Without film cooling, air flowing through the radial tubes absorbs the entire heat flux due to the gas-to-wall temperature difference. With film cooling, air is extracted from the tubes and is used to reduce the external heat flux by insulating the wall with a film of cooler air. For the same coolant amount, when film cooling air is extracted from the tubes the average tube heat transfer coefficient is lower than when no film cooling is used. Vane thermal analyses were done for vanes cooled only by radial cooling, and for vanes cooled by radial cooling coupled with film cooling. The configuration where trailing edge ejection is used in conjunction with radial cooling is also analyzed.

The thermal and aerodynamic performance was determined for two vane external configurations. One was a half scale version of the vane used for the full size vane structural analysis. The other was a vane shape specified by Dr. Jerry Lang at the NASA Glenn Research Center. Both vanes had acceptable aerodynamics. The calculated profile loss was similar for the two vanes.

The analysis showed that neither vane could be effectively cooled using only radial cooling. Film cooling or trailing edge ejection was required to be used in conjunction with radial cooling. With film and radial cooling the aggressive future engine goals of NASA's Large Civil Tilt Rotor(LCTR)[10] program could be achieved. These goals are a gas temperature of $1927°C(3500°F)$, and a coolant temperature of $594°C(1100°F)$. The gas temperature includes a pattern factor to account for temperature variations at the combustor outlet. The coolant temperature is significantly warmer than ambient due to a takeoff pressure of 30 atm. The thermal and aerodynamic analysis results were transmitted to Dr. Lang to be used in his structural analysis of the LCTR vane.

Thermal and aerodynamic results will be given for the half scale vane of Halila et al.[8] and for the NASA vane. For each vane results will be given with and without film cooling, and when trailing edge ejection is used in conjunction with film cooling. Current engines have lower combustor outlet temperatures, and the engine Overall Pressure Ratio(OPR) is also lower. Results will be given for engine gas temperatures of $1427°C(2600^{circ}F)$ and $1927°C(3500°F)$. For the lower gas temperature the analysis assumed a coolant temperature of $376°C(708°F)$, which is consistent with an engine OPR of 17.. For the gas temperature of $1927°C(3500°F)$ coolant temperature is $594°C(1100°F)$, and the engine OPR was 30. Heat transfer coefficients changed as the gas temperature changed, primarily due to changes in the vane inlet total pressure.

Figure 6.0.1 shows the two vane shapes. The half size vane is the vane given by Halila et al.[8] with the dimensions reduced by a factor of 2. This vane is designated as the half scale EEE vane. The vane shape designated as the NASA vane is the one specified by NASA personnel. The NASA vane has a longer axial chord, but its true chord-to-axial chord ratio is lower than the true chord-to-axial chord ratio for the half scale EEE vane. The true chord-to-axial chord ratio for the NASA vane is 1.727. Most of the gas turning for the NASA vane occurs in the last half of the vane, and this results in an aft loaded pressure distribution.

Figure 6.0.2 compares the pressure distributions for the two vanes. The pressure distributions were calculated for the same axial chord-to-pitch(solidity) ratio. Since the NASA vane has a longer chord than the half scale EEE vane, there would be fewer NASA vanes in an engine with the same vane inner and outer diameters. The aft vane loading tends to delay suction surface transition at low Reynolds numbers. The aft loading results in favorable pressure gradients for more of the suction surface, and this tends to reduce boundary layer growth.

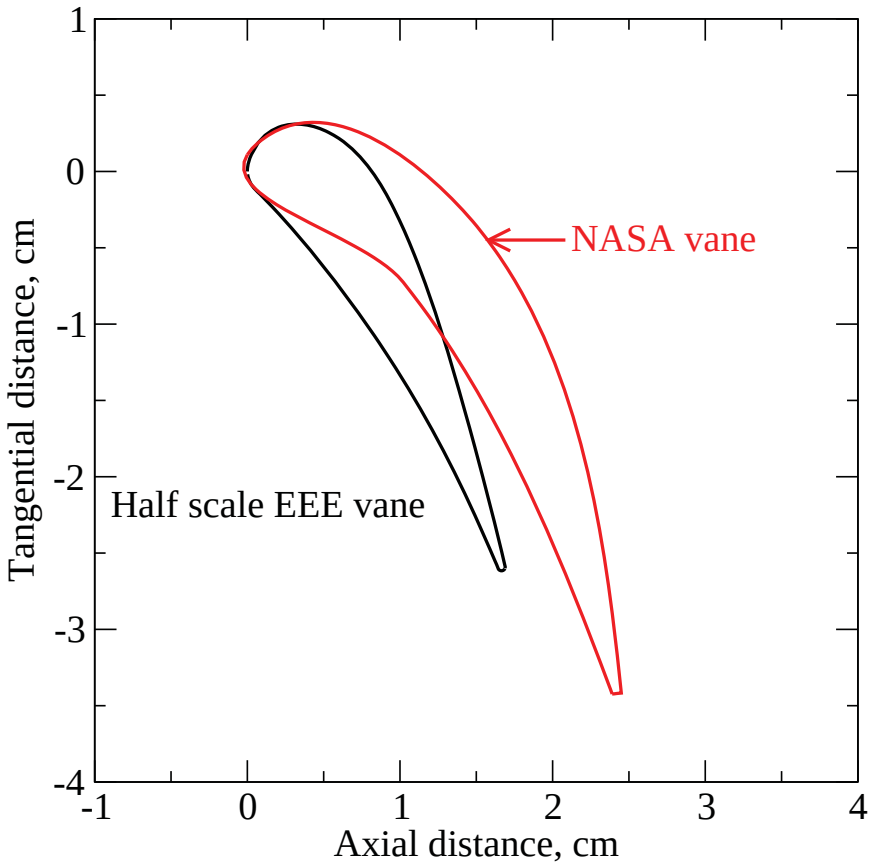

Fig. 6.0.1 Comparison of vane eometries

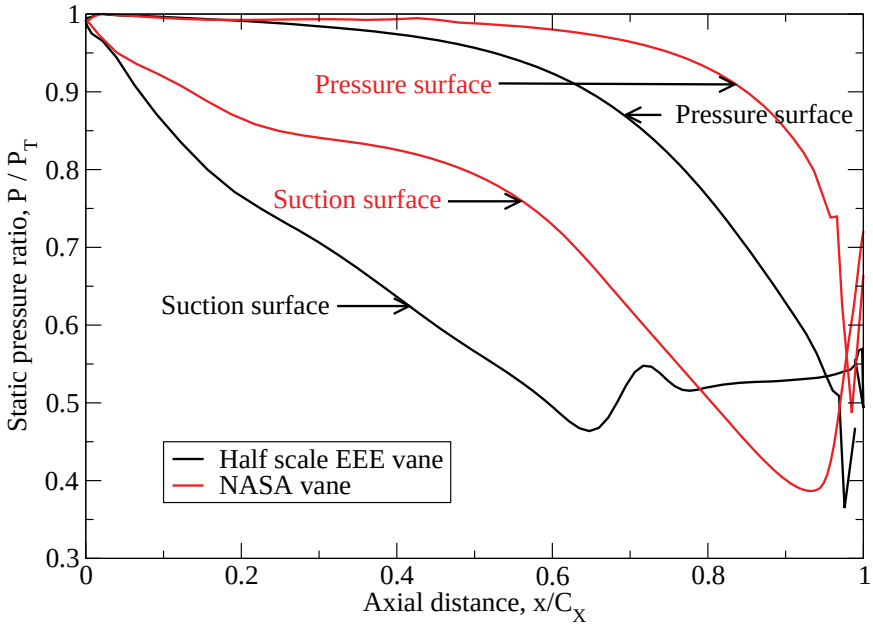

Fig. 6.0.2 Pressure distribution for both vanes

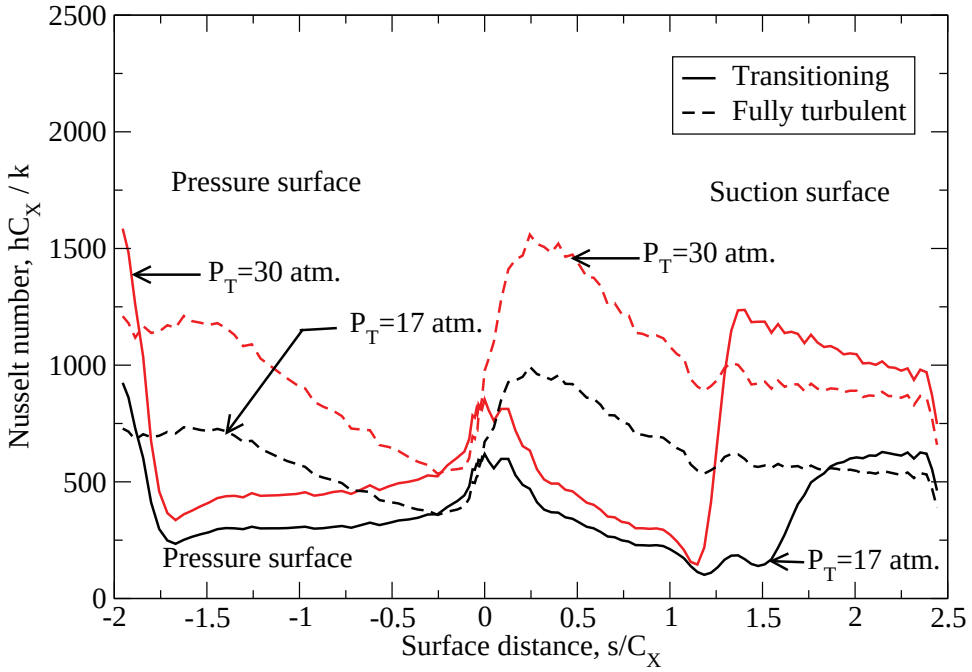

Fig. 6.1.0.1 Midspan Nusselt number distributions

6.1 - Half scale EEE vane

Figure 6.1.0.1 shows four Nusselt distributions for the half scale EEE vane. These distributions are shown for vane inlet total pressures of 17 and 30 atm., and for two transition modeling assumptions. If there is no vane film cooling, transition does not occur close to the leading edge at these low Reynolds numbers. The Reynolds number is almost proportional to the inlet pressure and surface distance. Both of these quantities are lower in turboshaft engine applications than in commercial engines in the CF6 size class. The transition analysis accounted for an inlet turbulence of 10%. Prior to the flow becoming fully turbulent, the effective viscosity included a freestream turbulence effect. This effect is the reason that the transitioning Nusselt numbers are higher than the fully turbulent Nusselt numbers along the forward portion of the pressure surface. Where the suction surface heat transfer approaches zero, at s/C_X near 1.0, the boundary layer is nearly separated. This corresponds to the adverse pressure gradient region seen in figure 6.0.2. Figure 6.1.0.1 shows that when the flow is assumed fully turbulent, there is a heat transfer decrease in this region, but the boundary layer does not approach separation. Data, such as Arts[32], show that flows downstream of film cooling rows are turbulent, even at low Reynolds numbers.

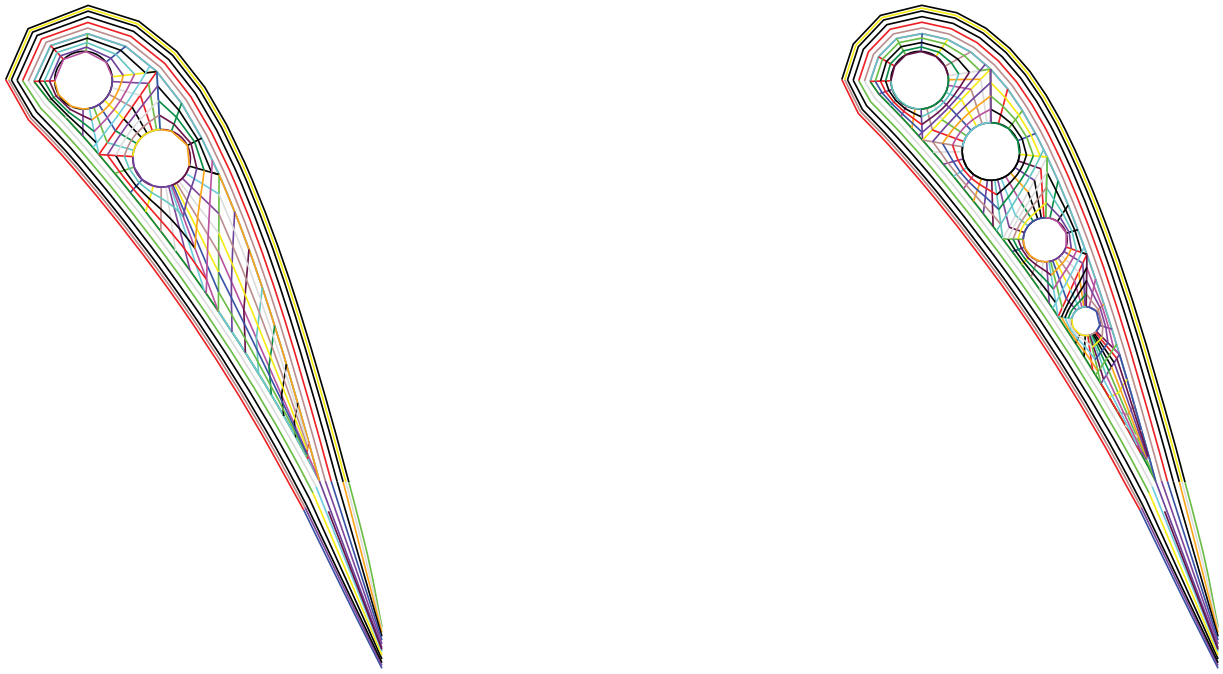

2 radial holes 4 radial holes

Fig. 6.1.1.1 Two radial cooling hole configurations.

6.1.1 - Radial cooling tubes - no film cooling. Figure 6.1.1.1 shows the half scale EEE vane with two and four cooling tubes. The two tube configuration has two 2.54mm(100mil) diameter cooling tubes. In the four tube configuration the two forward tubes are also 2.54mm(100mil) in diameter, and the third and fourth tubes have a smaller diameter in order to fit within the CMC shell. The third tube is 2.0mm(78mil) in diameter, and the fourth tube is 1,27mm(50mil) in diameter. The shell for the half scale vane was assumed to be 1mm(40mil) thick, and that the EBC protective layer was 0.127mm(5mil) thick. The thermal analysis assumed that the space inside the CMC shell was filled with a CMC material having the same $20 W/m -^{\circ} C$ thermal conductivity as the CMC shell.

Figure 6.1.1.2 through 6.1.1.5 show outer surface temperatures for both the CMC layer and the EBC layer. Figures 6.1.1.2 and 6.1.1.3 show the effects of having four instead of two radial cooling holes. These results are for a gas temperature, T_{G}, of $2600^{\circ}F(1700^{\circ}K)$, and a total pressure of 17 atm. Even though this relatively low gas temperature is below the desired maximum EBC temperature, CMC temperatures exceed the maximum desired CMC temperature of $2400^{\circ}F(1589^{\circ}K)$. The four tube configuration has less of the vane seeing excessive CMC temperatures than does the two tube configuration. Aft of where there is insufficient space for a cooling tube, heat can not be effectively removed, and CMC temperatures are excessive.

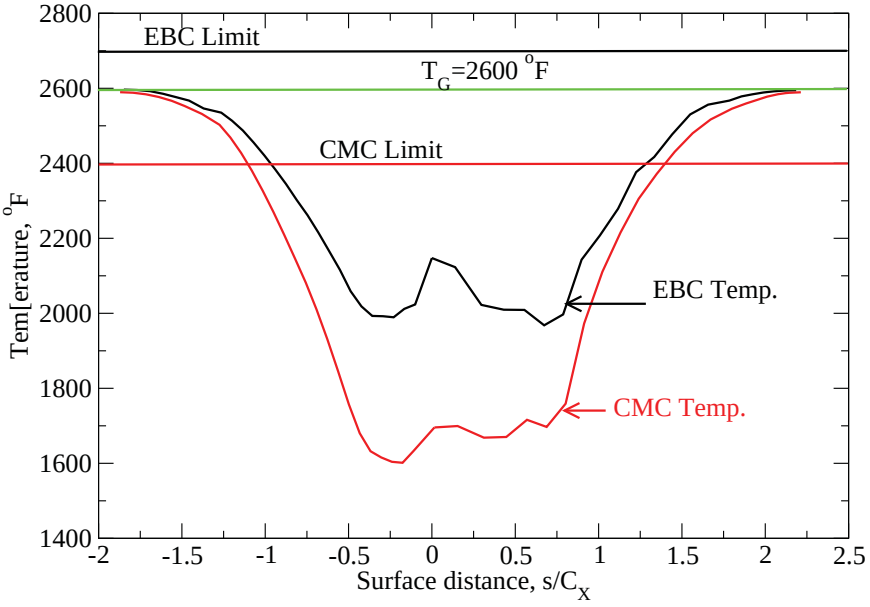

Fig. 6.1.1.2 CMC and EBC temperatures - two tubes - P=17 atm. - $T_G = 2600°F$ - no film cooling

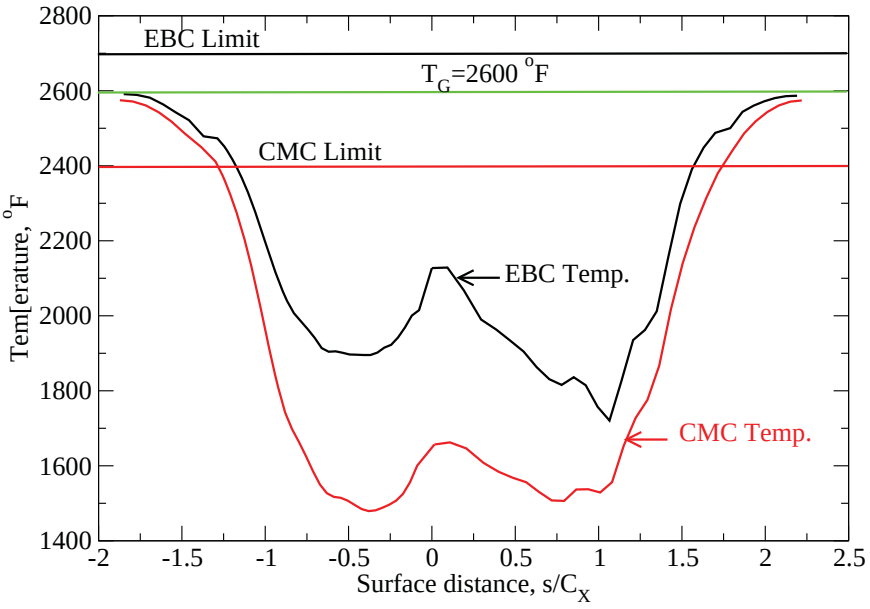

Fig. 6.1.1.3 CMC and EBC temperatures - four tubes - P=17 atm. - $T_G = 2600°F$ - no film cooling

Figures 6.1.1.4 and 6.1.1.5 show temperatures for cases similar to that shown in figure 6.1.1.3, except that the gas temperature was increased to $3500°F(2200°K)$, and the total pressure was increased to 30 atm. Increasing the total pressure increases both the coolant temperature, and the internal and external heat transfer coefficients. For comparison purposes the internal heat transfer coefficient, h_I, was set to $5000W/m^2 -° K$ in figure 6.1.1.4. This is the same value as was used for the lower total pressure cases. Figure 6.1.1.5 shows results where the internal heat transfer coefficient is increased to $8000W/m^2 -° K$.

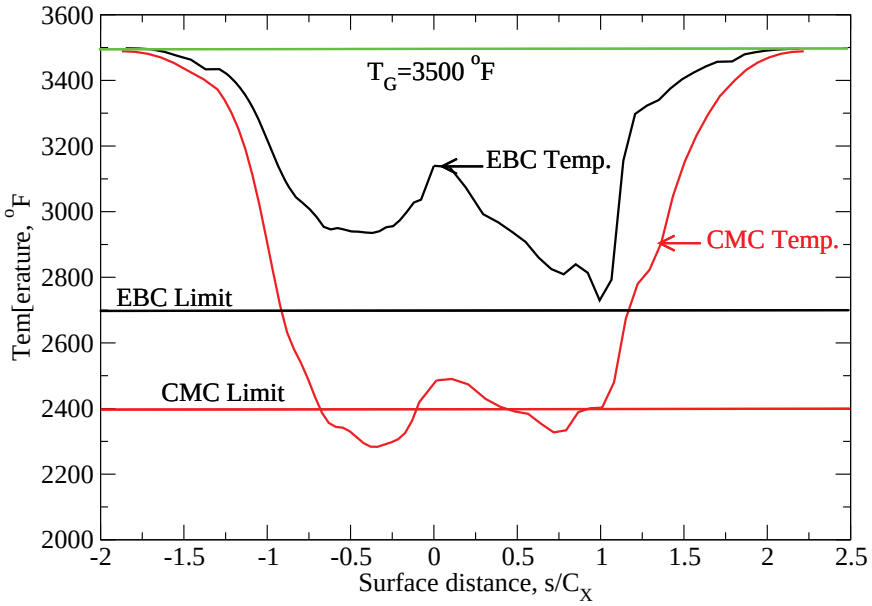

Fig. 6.1.1.4 CMC and EBC temperatures - four tubes - P=30 atm. - $T_{\mathrm{G}} = 3500°F$ - $h_{\mathrm{I}} = 5000W/m^2 -° K$ - no film cooling

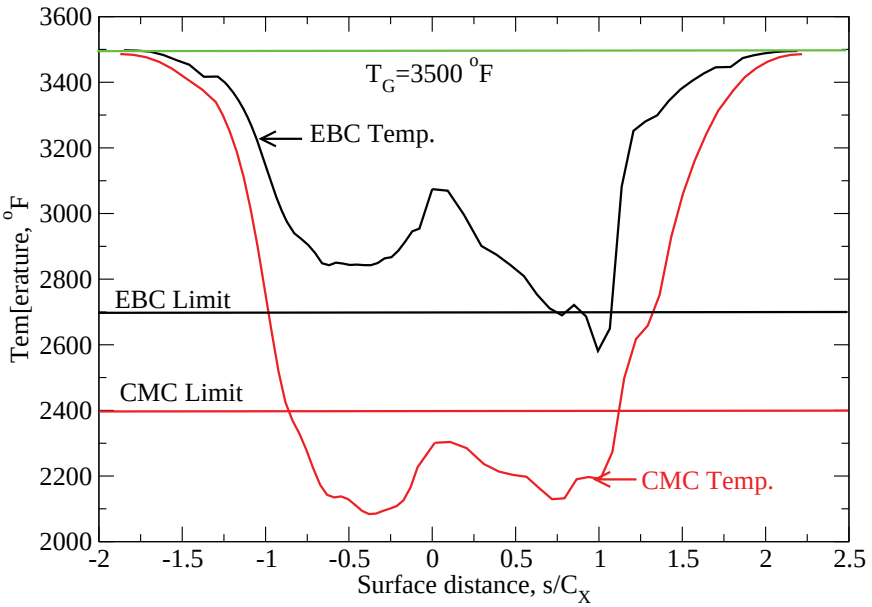

Fig. 6.1.1.5 CMC and EBC temperatures - four tubes - P=30 atm. - $T_{\mathrm{G}} = 3500°F$ - $h_{\mathrm{I}} = 8000W/m^2 -° K$ - no film cooling

These two figures show that, even away from the trailing edge region, radial cooling alone is insufficient to maintain EBC and CMC temperature at acceptable values. Away from the trailing edge region EBC temperatures are unacceptably high. While a higher internal heat transfer coefficient allows acceptable CMC temperatures in the forward part of the vane, EBC temperatures are unacceptably high. Reducing the EBC thickness below 0.127mm(5mil) would lower the maximum EBC temperatures. However if this was done to lower maximum EBC temperature to acceptable levels, the maximum CMC temperature would be unacceptable.

Figures 6.1.1.4 and 6.1.1.5 illustrate the importance of the internal film cooling heat transfer coefficient. Because the radial tubes have a small diameter, they may not be hydraulically smooth. Tube heat transfer coefficients increase as surface roughness increases. The penalty for increased surface roughness is increased tube pressure losses. Kays and Crawford[26] discuss smooth and rough tube heat transfer rates in terms of Nusselt numbers, Nu. $Nu = hD/k$, where h is the tube heat transfer coefficient, D is is the tube diameter, and k is the thermal conductivity. For a smooth tube with fully developed flow Nu is given by:

$$Nu = 0.022 Pr^{0.5} Re^{0.8}$$

Pr is the Prandtl number, and Re is the tube Reynolds number. It is convenient to express the Reynolds number in terms of the tube Mach number, M.

$$Re = \frac{P}{RT\mu} M \sqrt{\gamma RT} D$$

where P is pressure, R is the gas constant, T is the absolute temperature, μ is the dynamic viscosity, and γ is the specific heat ratio. μ and k are both proportional to T^n, where n is approximately 0.7. Consequently Nu is almost independent of temperature, but h increases somewhat with temperature. Also, h increases slightly at the diameter, D, decreases. For P equal to 17 atm., T equal to $650°K(710°F)$, M equal to 0.3, and D equal to 2.54mm(100mil), Nu is 196. The tube heat transfer coefficient, h is $3725 W/m^{2\circ}K$.

When tubes are not hydraulically smooth, roughness can increase tube heat transfer by up to a factor of 2.5(Kays and Crawford[26]). They also state that this increase comes at the expense of a four fold increase in tube friction factor, and thus a four fold increase in tube pressure drop.

The expected length-to-diameter,(L/D), ratios for radial cooling tubes is between 10 and 20. Even at an $L/D = 20$, the average smooth tube Nu will be somewhat greater than the Nu for fully developed flow. This is due to an entrance effect, and the degree of heat transfer augmentation is highly dependent on the specific entrance configuration. Overall, the consequences of possible tube roughness and entrance effects indicate that a tube heat transfer coefficient, h_{I} of $5000 W/m^2 -^\circ K$ for a pressure of 17 atm., and $8000 W/m^2 -^\circ K$ for a pressure of 30 atm. is conservative. However, h_{I} will be lower when coolant is extracted from the tubes for either film cooling or trailing edge ejection.

The amount of cooling flowing through the tubes was calculated to be approximately 7% for the four tube configuration. This calculation assumed a coolant-to-inlet Mach number ratio of 2, an inlet-to-coolant temperature ratio of 2.25, a span-to-axial chord ratio of 1.5, and a vane pitch-to-axial chord ratio of 1.4.

6.1.2 - Radial cooling & film cooling. It was shown by Arts[32] that just the presence of film cooling holes causes laminar boundary layers to become turbulent. When a laminar boundary layer is tripped and becomes turbulent there is a rapid increase in the heat transfer coefficient. If the flow upstream of a cooling row is already turbulent, there is only a small increase in heat transfer coefficients downstream of the film cooling row. Heat transfer in the leading edge region is always laminar like because of strong favorable pressure gradients, which increase as the leading edge diameter decreases. In this region heat transfer coefficients increase dramatically in the presence of film cooling rows as shown by Reiss and Bolcs[18], and by Ou and River[33]. Augmentation factors as great as a factor of four have been reported. However, augmentation factors are relative to a solid leading edge with low to moderate freestream turbulence. The high turbulence at the combustor outlet is expected to increase solid vane leading edge region heat transfer coefficients by 50% or more. However, because of low Reynolds numbers associated with vanes for turboshaft engine applications, turbulence alone will not cause transition to turbulent flow in this region.

Figure 6.1.2.1 shows CMC and EBC temperatures for the vane with two assumptions regarding transition in the leading edge region. Figure 6.1.2.2 shows the Nusselt number distributions corresponding to these two assumptions, and also shows results for a transitioning flow model with a vane inlet turbulence intensity of 10%. The first assumption is that flows are fully turbulent, and the second delays transition to locations downstream of the leading edge. The second assumption was made to better account for the heat transfer augmentation factors that are present in the Reiss and Bolcs[18] leading edge film cooling model. Figure 6.1.2.2 shows significantly different leading edge heat transfer coefficients between the fully turbulent and delayed transition models. However, figure 6.2.2.1 shows that the effect of these two model assumptions on both EBC and CMC temperature is relatively small. With film cooling CMC temperatures are acceptable throughout the entire vane. However, EBC temperatures are excessive in the leading edge region. Temperatures may be over estimated because any heat transfer within the CMC vane to the cooling holes was neglected. Leading edge region film holes are closely spaced, and are relatively long because these holes are steeply angled in the spanwise direction. An indication that heat transfer into the film cooling holes should be considered in a future analysis is that the temperatures in the leading edge region were nearly the same with and without film cooling.

Only three rows of film cooling holes were used in addition to the leading edge film cooling. Two rows were on the pressure surface, and one on the suction surface. The coolant fraction was calculated to be 16% of mainstream flow. Only three rows of film cooling holes were sufficient because the minimum cooling hole size is independent of the vane size. The smaller the vane, the fewer rows of film cooling holes are required.

6.1.3 - Single cavity & trailing edge ejection. Film cooling is very effective away from the vane leading edge region. Nusselt numbers are lower in the leading edge region if there is no film cooling. Trailing edge ejection was effective in the trailing edge region. A thermal analysis was done for a solid vane with trailing edge ejection. At most there would be room for only a single cavity in the half scale EEE vane. The configuration analyzed here is geometrically similar to the single cavity configuration discussed in section 5.2.4. The configuration analyzed has no film cooling. The internal heat transfer coefficients will vary significantly, depending on the internal cooling arrangement. For comparison purposes the internal heat transfer coefficient was assumed to be $5000 W/m^{2\circ} K$. The trailing edge ejection tube heat transfer coefficient was determined based on the assumed inlet-to-exit pressure ratio.

Figure 6.1.3.1 compares CMC and EBC outer surface temperatures for the four tube radial cooling configuration with those for the single cavity with trailing edge ejection tube configuration. Neither configuration employs film cooling. The single cavity configuration has acceptable CMC temperatures over much of the vane surface. However, on both the suction and pressure surfaces CMC temperatures exceed the temperature limit by more than $180°F (100°C)$. EBC temperatures exceed the desired maximum EBC temperature over much of the vane surface. The single cavity configuration yields lower EBC temperatures than does the four radial tube configuration.

Figure 6.1.3.2 shows that decreasing the pitch-to-diameter ratio of the trailing edge ejection tube is an effective means of maintaining CMC temperatures less than the maximum allowable CMC temperature. Unfortunately, decreasing the pitch-to-diameter ratio has little effect on the EBC outer surface temperatures.

The outer surface temperature of the EBC can be lowered by reducing the thickness of the EBC coating. However, reducing the EBC thickness raises the outer surface temperature of the CMC vane. Figure 6.1.3.3 shows the effects of varying the EBC thickness. For illustration purposes the EBC coating has a uniform thickness. These results were calculated for a trailing edge ejection tube pitch-to-diameter ratio of 1.67. Unfortunately, near the aft portion of the vane, where EBC temperatures are most in excess of the EBC temperature limit, reducing the EBC thickness does not significantly reduce EBC temperatures. In the leading edge region EBC temperatures also exceed the EBC temperature limit. In this region reducing the EBC thickness is somewhat more effective than in the trailing edge region.

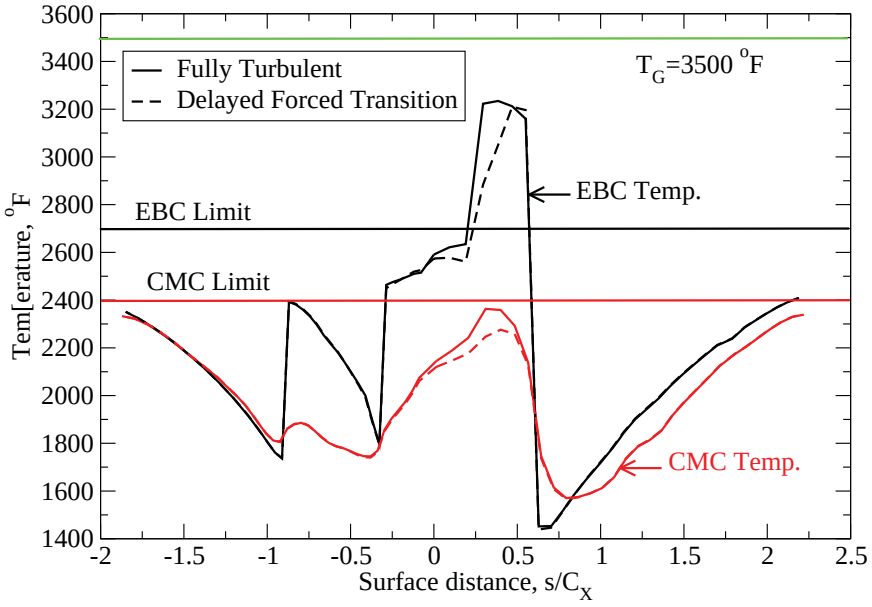

Fig. 6.1.2.1 CMC and EBC temperatures four tubes - P=30 atm. - $T_{\mathrm{G}} = 3500°F$ - $h_{\mathrm{I}} = 5000W/m^2 -° K$ - film cooled

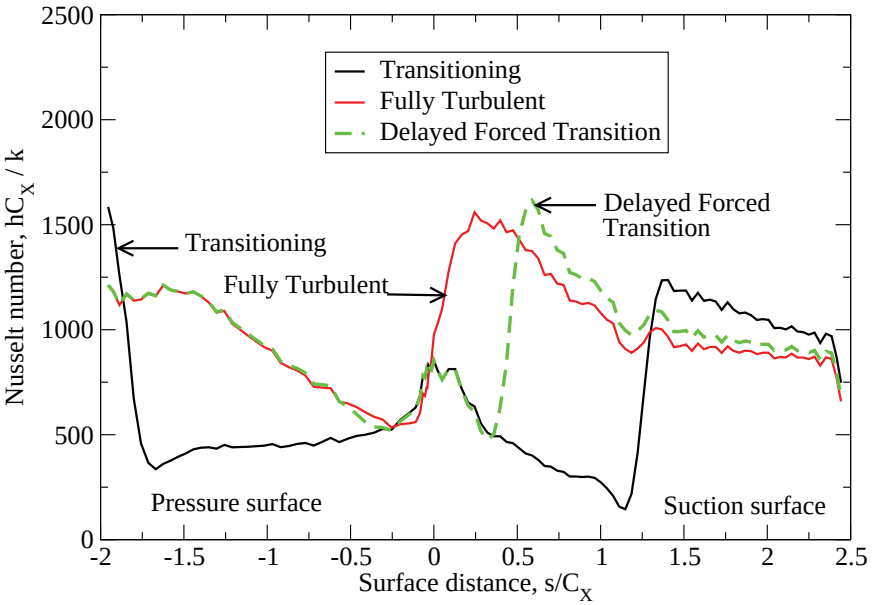

Fig. 6.1.2.2 Midspan Nusselt number distributions - P=30 atm.

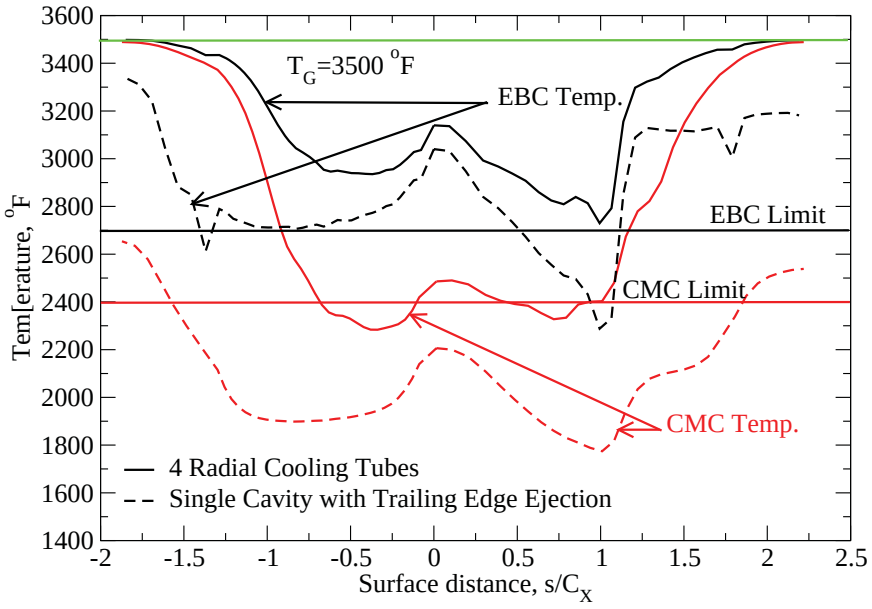

Fig. 6.1.3.1 Comparison of radial tube and single cavity CMC and EBC temperatures - P=30 atm. - $T_{\mathrm{G}} = 3500°F$ - $h_{\mathrm{I}} = 5000 W/m^2 -° K$

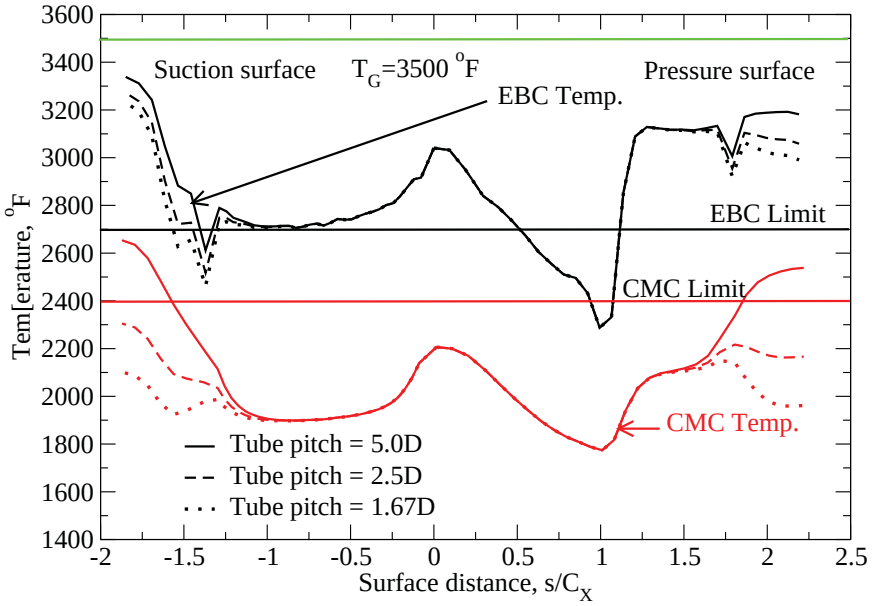

Fig. 6.1.3.2 Effect of trailing edge ejection tube pitch-to-diameter ratio on CMC and EBC temperatures - P=30 atm.

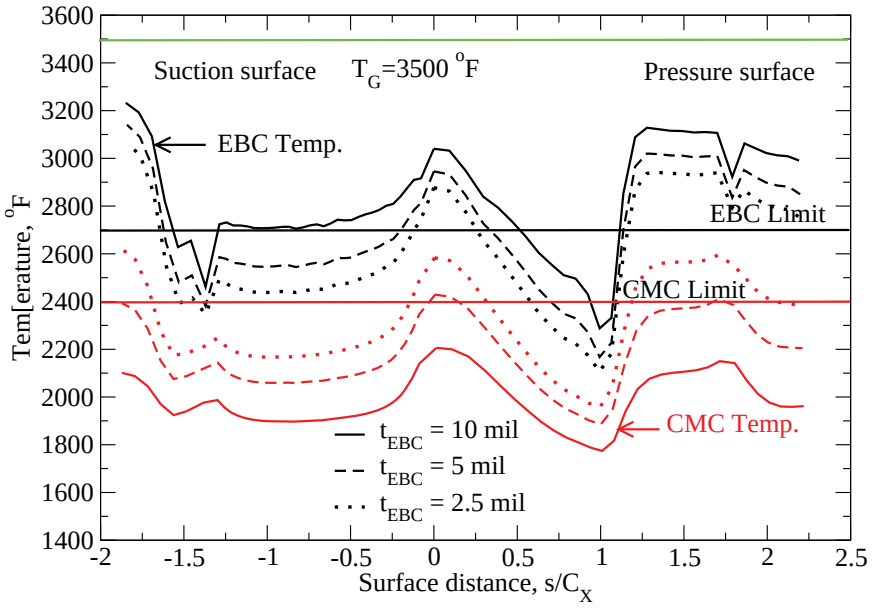

Fig. 6.1.3.3 Effect of EBC thickness on CMC and EBC temperatures - P=30 atm.

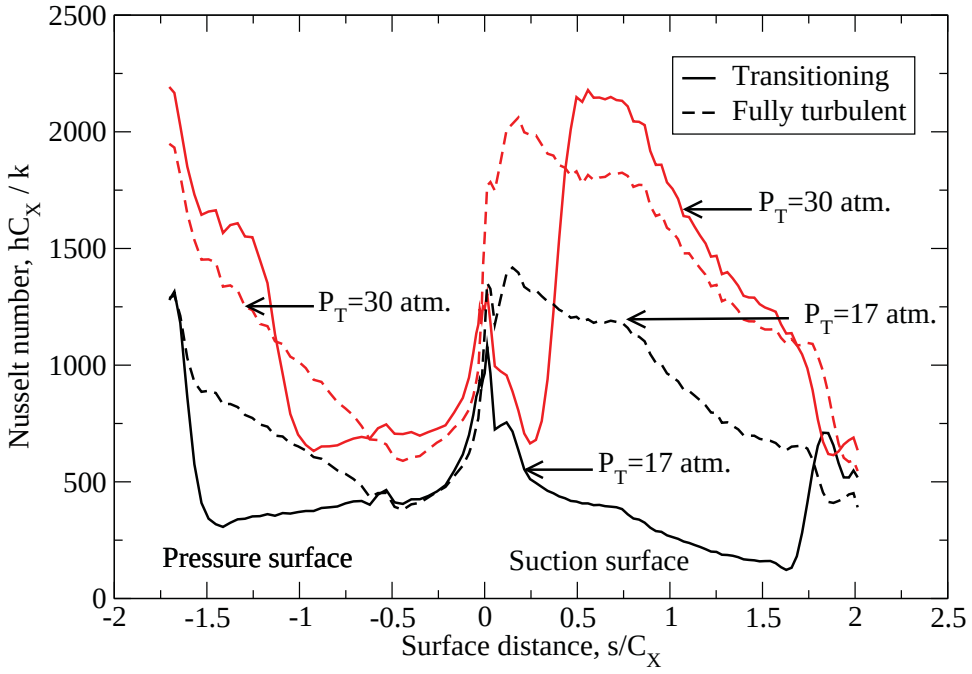

Fig. 6.2.0.1 Midspan Nusselt number distributions - NASA vane

6.2 - NASA vane

Figure 6.2.0.1 shows Nusselt number distributions for the NASA vane. The profile and pressure distributions for this vane were shown in figures 6.0.1 and 6.0.2. The Nusselt number distributions for this vane can be compared with those shown in figure 6.1.0.1 for the half scale EEE vane. The higher maximum Nusselt numbers for the NASA vane compared with the maximum Nusselt numbers for the half scale vane do not represent higher heat transfer coefficients. As shown in figure 6.0.1, the NASA vane has a longer axial chord, C_{X}, and h is proportional to Nu divided by C_{X}. Suction surface transition is very different between the NASA vane and the half scale EEE vane. Figure 6.1.0.1 for the half scale EEE vane showed that increasing the inlet total pressure from 17 to 30 atm. caused suction surface to move forward from 2/3 to 1/2 of the surface distance. Figure 6.2.0.1 shows that the NASA vane at a pressure of 17 atm. has suction and pressure surface transition occurring close to the trailing edge. At 30 atm., however, suction surface transition is relatively close to the leading edge, and after transition the maximum Nusselt number exceeds the maximum fully turbulent Nusselt number. Figure 6.0.2 shows that the NASA vane has a less favorable suction surface pressure gradient. Consequently, at a pressure of 30 atm. suction surface transition occurs further forward on the NASA vane compared with the half scale EEE vane.

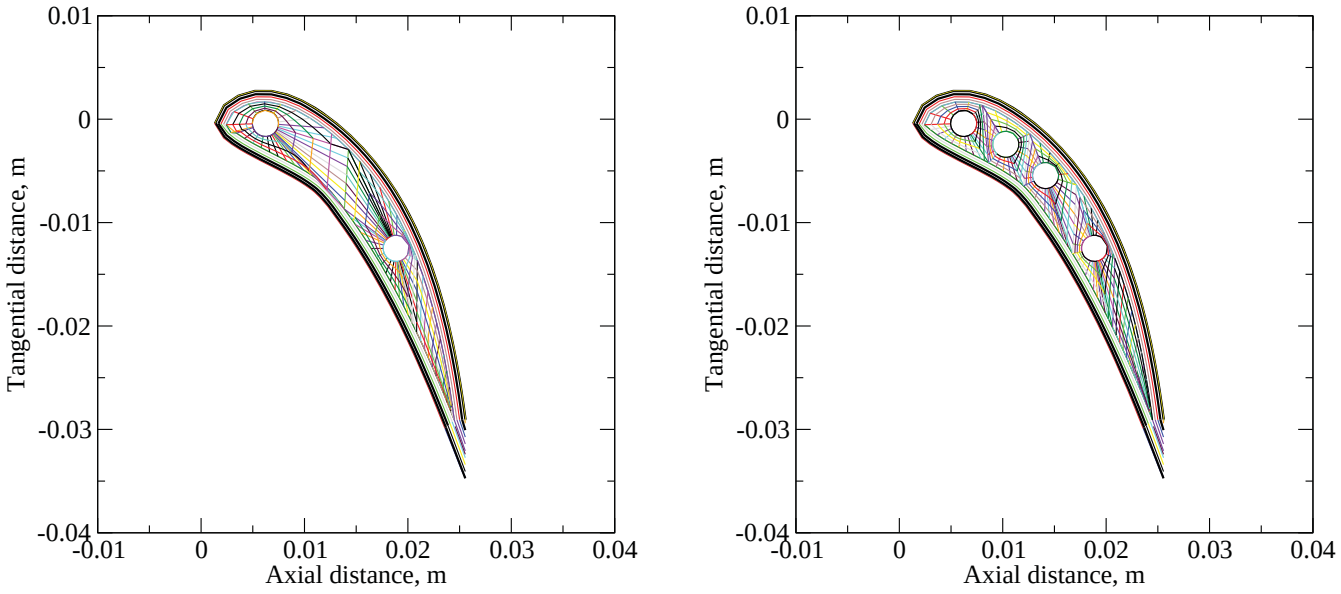

Fig. 6.2.1.1 NASA vane with two radial cooling hole configurations.

6.2.1 - Radial cooling tubes - no film cooling. Figure 6.2.1.1 shows two and four hole configurations for the NASA vane. Since cooling of the trailing edge is an issue, the two radial tube configuration has the aft tube further aft than the two hole configuration of the half scale EEE vane shown in figure 6.1.1.1. The radial cooling tubes are 2.54mm(100 mil) in diameter.

Figure 6.2.1.2 shows outer EBC and CMC temperatures for the two and four radial tube configurations. The results are for a gas temperature of $1700°K(2600°F)$, and an EBC thickness of 0.127mm(5 mil). Temperatures were calculated for a heat transfer coefficient within the tubes of $5000W/m^{2\circ}K$, which at a pressure of 17 atm. may be somewhat optimistic. Even at this relatively low gas temperature and external heat transfer coefficients that are mostly laminar, CMC temperatures exceed the design temperature for N24A towards the rear of the vane. Unless the CMC temperature limit is raised, radial cooling without film cooling is insufficient at this low gas temperature.

Figure 6.2.1.3 shows EBC and CMC temperatures for a case with four radial cooling tubes. Here the gas temperature is $2200°K(3500°F)$, and the inlet total pressure is 30 atm. Increasing the inlet total pressure from 17 to 30 atm. causes the suction surface heat transfer to change from mostly laminar to mostly turbulent. There is also an increase in coolant temperature with an increase in inlet total pressure. Temperatures are shown for two values of the tube internal heat transfer coefficient, h_{I}. The lower value of $5000W/m^2-°K$ is conservative at this pressure, since h_{I} increases with pressure. Going from 5000 to $8000W/m^2-°K$ represents the expected change in h_{I} due to the total pressure increasing from 17 to 30 atm. The EBC temperatures exceed the EBC temperature limit of $1756°K(2700°F)$ almost everywhere, even for the higher h_{I} value. Along the entire suction surface CMC temperatures exceed their limit, as they do for the majority of the pressure surface.

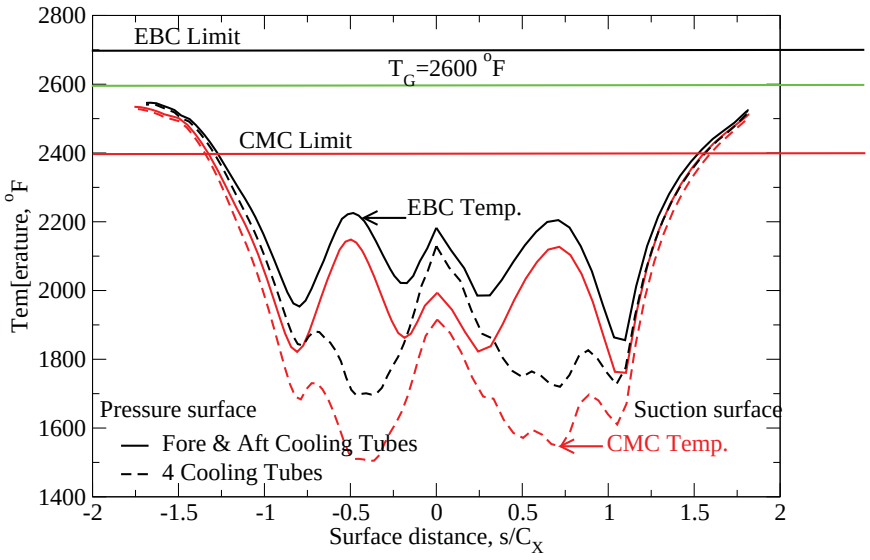

Fig. 6.2.1.2 Effect of number of cooling tubes on CMC and EBC temperatures - P=17 atm.

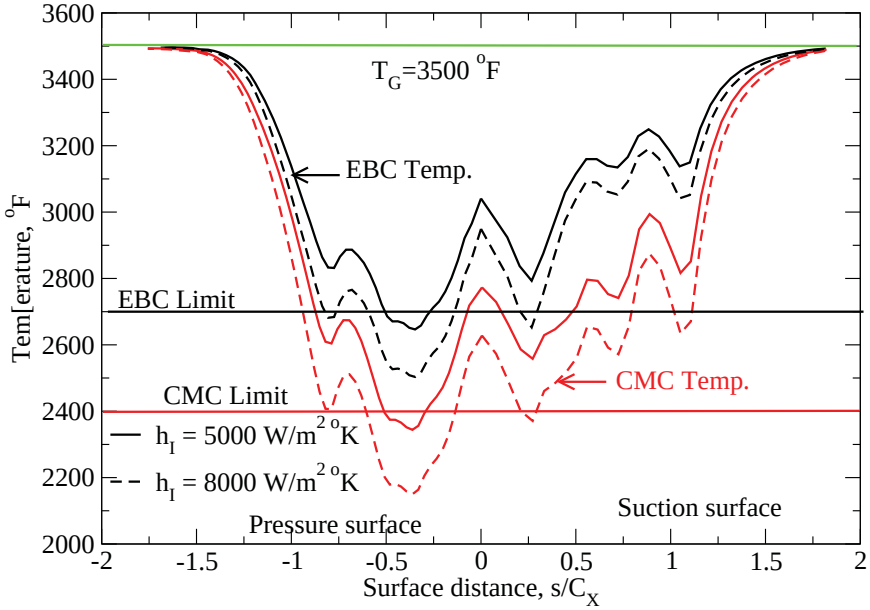

Fig. 6.2.1.3 Effect of tube heat transfer coefficient, h_I, on CMC and EBC temperatures - P=30 atm.

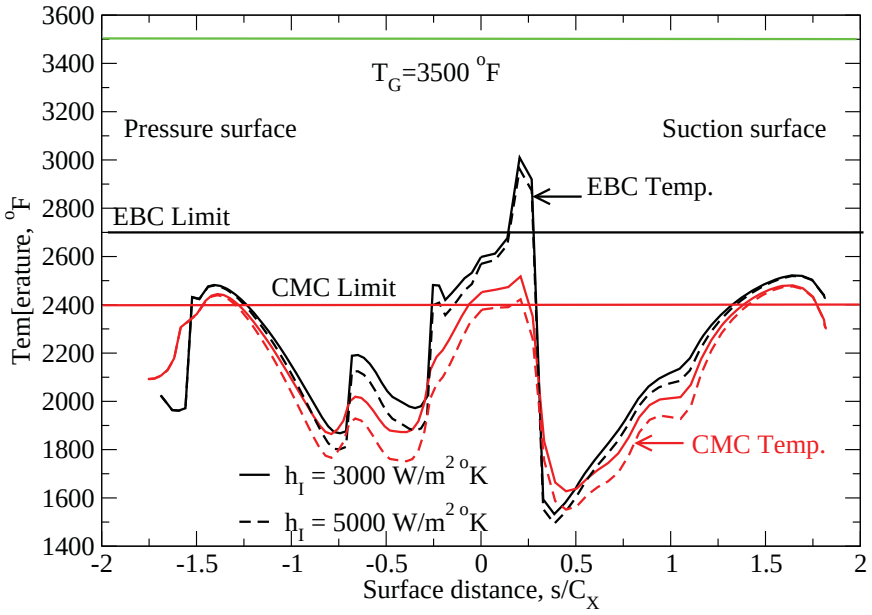

Fig. 6.2.2.1 Effect of tube heat transfer coefficient, h_{I}, on CMC and EBC temperatures - with film cooling - P=30 atm.

6.2.2 - Radial cooling & film cooling. EBC and CMC outer surface temperatures for the four radial cooling tube configuration with film cooling are shown in figure 6.2.2.1. These results are for a gas temperature of $2200°K(3500°K)$, and an inlet total pressure of 30 atm. In addition to leading edge film cooling there are three film cooling rows on the pressure surface, and one row on the suction surface. Tube heat transfer coefficients are lower when film cooling air is extracted from the tube. Therefore, results are shown for lower tube heat transfer coefficients of 3000 and $5000 W/m^2 -° K$. The effects of changing h_{I} are relatively small. However, the higher value for h_{I} is sufficient to maintain the CMC suction surface temperatures near the leading edge within the CMC limit temperature.

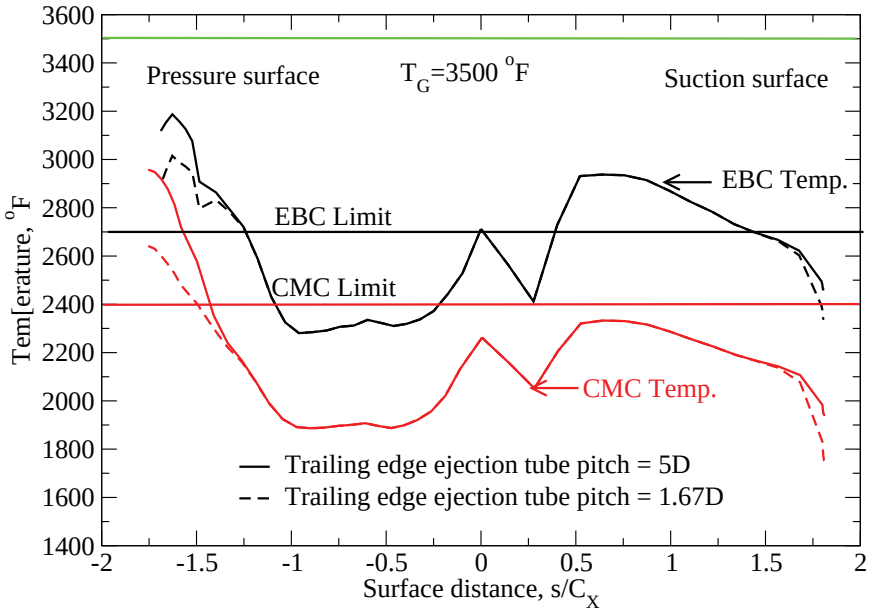

Fig. 6.2.3.1 Effect of trailing edge ejection tube heat transfer coefficient, h_I, on CMC and EBC temperatures - no film cooling - P=30 atm.

6.2.3 - Single cavity & trailing edge ejection. Figure 6.2.3.1 shows temperatures for a single cavity configuration similar to the configurations discussed in sections 5.2.4 and 6.2.3. This figure shows that acceptable CMC temperatures can be achieved with a single cavity configurations as long as there is trailing edge ejection. Except at the rear of the pressure surface, CMC temperatures are less than the CMC limit temperature of $1583°K(2400°F)$. Previous results showed that only a small amount of pressure surface film cooling would reduce CMC temperatures at the rear of this surface to acceptable values.

The difference in temperatures between results with a trailing edge ejection spanwise pitch-to-tube diameter,D, ratio of 1.67 and 5 shows the sensitivity of temperatures to the amount of heat removed via trailing edge ejection. The average heat transfer coefficient for the trailing edge ejection tube was calculated from the correlation for fully developed flow in a tube. The hydraulic diameter of the cavity is much larger than the hydraulic diameter of the radial cooling tubes, and the average inter heat transfer coefficient decreases as the hydraulic diameter decreases. Fortunately, the decrease is not linear, but only to the 0.2 power, because the radial flow is turbulent in either the cavity or radial tubes. While the assumed value of $5000W/m^{2\circ}K$ may be somewhat optimistic, it is not excessively so. CMC temperatures are acceptable, except near the trailing edge. However, EBC temperatures exceed the EBC temperature limit in the forward part of the suction surface as well as the aft portion of the pressure surface.

6.3 - Conclusions

Results were similar for both vanes analyzed for turboshaft engine applications. Pressure distributions, and consequently the heat transfer distributions, were different between the two vane geometries. Even so, both vane geometries required film cooling or trailing edge ejection to achieve acceptable temperature limits. Radial cooling alone provided insufficient cooling to avoid excessive CMC and EBC temperatures, even when the gas temperature was only $1700°K(2600°F)$.

When the gas temperature was $2200°K(3500°F)$ film cooling and trailing edge ejection provided sufficient cooling to keep CMC temperatures generally below $1589°K(2400°F)$. Even when the EBC thickness was 0.127mm(5 mil), EBC temperatures were generally in excess of their limit of $1756°K(2700°F)$ at locations where the CMC temperatures were close to their limit value. Either raising the EBC temperature limit or increasing EBC conductivity would help to alleviate this problem. The EBC thermal conductivity was assumed to be $1W/m - K$.

7.0 - References

1. Hartsel, J.E., 1972, "Prediction of Effects of Cooling Mass Transfer on the Blade Row Efficiency of Turbine Airfoils," AIAA paper 72-11.

2. Verrilli, M., Calamino,, A., Robinson, R.C., and Thomas, D.J.,2004, "Ceramic Matrix Composite Vane Subelement Testing in a Gas Turbine Environment, ASME Paper GT2004-53970.

3. Vedula, V., Shi, J., Jarmon, D., Ochs, S., Oni, L., Lawton, T., Green, K., Prill, L., Schaff, J., and Linsey, G., 2005, "Ceramic Matrix Composite Vanes for Gas Turbine Engines, ASME Paper GT2005-68229

4. Brewer, D.N., Verrilli, M., and Calomino, A., 2006, "Ceramic Matrix Composite Vane Subelement Burst Testing", ASME paper GT2006-90883.

5. Watanabe, K.-I., Suzumura, N., Nakamura, T., Murata, H., Araki, T., and Natsumura, T., 2008, "Development of CMC Vane for Gas Turbine Engine", Ceramic Engineering and Science Proceedings, Volume 24, Issue 4, (eds W. M. Kriven and H.-T. Lin), John Wiley & Sons, Inc., Hoboken, NJ, USA. doi: 10.1002/9780470294826.ch87

6. Nakamura, T., Murata, H., Takahashi, A., and Okita, Y., 2010, "Development of a CMC Turbine Vane", in Proceedings of the 7th International Conference on High Temperature CMCs(HT CMC7), pp. 559-565.

7. Marshall, D.B., and Cox, B.N., 2008, "Integral Textile Ceramic Structures," Annual Review of Materials Research, Vol. 38, pp. 425-443.

8. Halila, E.E., Lenahan, D.T., and Thomas, T.T., 1982, "High Pressure Turbine Test Hardware Detailed Design Report, NASA CR-167955, General Electric Company report R81AEG284

9. Mital, S.K., Bednarcyk, B.A., Arnold S.A., and Lang, J., 2009, "Modeling of Melt-Infiltrated SiC/SiC Composite Properties," NASA TM-2009-215806.

10. Snyder, C.A., and Thurman, D.R., 2010, "Effects of Gas Turbine Component Performance on Engine and Rotary Wing Vehicle Size and Performance," NASA TM 2010-216907.

11. Boyle, R., Miller, I., Halbig, M., DiCarlo, J., Bhatt, R., and Jaskowiak, M, 2012, "Design Concepts for Cooled Ceramic Matrix Composite Turbine Vanes," 36th Annual Conference on Composites, Materials and Structures, Cocoa Beach, FL

12. Boyle,, R., Parikh, A., Nagpal V., Halbig, M., DiCarlo, J., and Bhatt, R., 2013, "Design Concepts for Cooled Ceramic Matrix Composite Turbine Vanes," 37th Annual Conference on Composites, Materials and Structures, Cocoa Beach, FL

13. Boyle, R.J., Parikh, A.H., Halbig, M.C., and Nagpal, V.K., 2013, "Design Considerations for Ceramic Matrix Composite Vanes for High Pressure Turbine Applications," ASME paper GT2013-95104

14. Wilcock, R.C. Young, J.B., and Horlock, J.H., 2005. "The Effects of Turbine Blade Cooling on the Cycle Efficiency of Gas Turbine Power Cycles," ASME *Journal of Engineering*

for Gas Turbines and Power, Vol. 127, pp 109-120.

15. www.specialmetals.com

16. DiCarlo, J.A,, Yun, H.-M., Morsher, G.N., and Bhatt, R.T., 2004, "SiC/SiC Composites for 1200 °C and Above," NASA TM-2004-213048

17. Lee, K.N., Fox, D.S., Eldridge, J.I., Zhu, D., Robinson, R.C., Bansal, N.P., and Miller, R.A., 2002, "Upper Temperature Limit of Environmental Barrier Coatings Based on Mullite and BSAS," NASA TM-2002-211372

18. Reiss, H., and Bolcs, A., 1999, "Experimental Study of Showerhead Cooling on a Cylinder Comparing Several Configurations Using Cylindrical and Shaped Holes," ASME paper 99-GT-123.

19. Boyle, R.J., and Ameri, A.A., 2010, "A Correlation Approach to Predicting Film Cooled Turbine Vane Heat Transfer," ASME paper GT2010-23597.

20. Tacina, R., Wey, C., Laing, P., and Mansour, A., 2002, "A Low NOx Lean-Direct Injection, Multipoint Integrated Module Combustor Concept for Advanced Aircraft Gas Turbines," NASA TM-2002-211347, Presented at the Conference on Technologies and Combustion for a Clean Environment, Oporto, Portugal, July 2001.

21. Harth, S., Zarzalis, N., Bauer, H.-J., and Turrini, F., 2013, "Evaluation of a Piloted Lean Injection System in Terms of Emission Performance and Flame Structure at Elevated Pressure," ASME paper GT2013-94371.

22. Dusing, K.M., Ciani, A., Benz, U., Eroglu, A., and Knapp, K., 2013, "Development of GT24 And GT26 (Upgrades 2011) Reheat Combustors, Achieving Reduced Emissions and Increased Fuel Flexibility," ASME paper GT2013-95437.

23. Boyle, R.J., and Jones, S.M., 2009, "Effects of Precooling Turbine Cooling Air on Engine Performance," ASME paper GT-2009-60120

24 Anon., 2007, "Performance Prediction and Simulation of Gas Turbine Engine Operation for Aircraft, Marine, Vehicular, and Power Generation," NATO RTO Technical Report ATV-036.

25. Engel, T., 2013, "High-Temperature Interlaminar Tension Test Method Development for Ceramic Matrix Composites," ASME paper GT2013-94095.

26. Giel P. W., VanFossen, G. J., Boyle, R. J., Thurman, D. R., and Civinskas, K. C., 1999, "Blade Heat Transfer Measurements and Predictions in a Transonic Turbine Cascade", ASME 99-GT-125, June, 1999, also NASA/TM-1999-209296.

27. Boyle, R. J. and Jackson, R., 1997, "Heat Transfer Predictions for Two Turbine Nozzle Geometries at High Reynolds and Mach Number", ASME *Journal of Turbomachinery, vol. 119, no. 2, pp. 270-283.*

28. Florschuetz, L.W., Truman, C.R., and Metzger, D.E., 1981, "Streamwise Flow and Heat Transfer Distributions for Jet Array Impingement with Crossflow," *Journal of Heat Transfer,*

Vol. 103, pp. 337-342.

29. Kays, W.M., and Crawford, M.E., 1980, *Convective Heat and Mass Transfer,*, 2nd ed. McGraw-Hill Book Co. New York, NY.

30. Anon., 2009, "ANSYS Mechanical APDL, Release 12.1,"

31. Brauer, J.R., ed., 1993, it What Every Engineer Should Know About Finite Element Analysis, Marcel Decker Inc. New York, NY.

32. Arts, T., 1995, "Thermal Investigation of a Highly Loaded Transonic Turbine Film Cooled Guide Vane", 1^{st} European Conf. on Turbomachinery - Fluid Dynamic and Thermodynamic Aspects, Erlanger, Germany, also VKI preprint 1995-11.

33. Ou, S. and River, R., 2001, "90° Skew Leading Edge Film Cooling Effectiveness, Heat Transfer, and Discharge Coefficients for Cylindrical Film Holes at High Free Stream Turbulence," NATO pub. RTO-MP-069(I), presented at RTO-ATV Symposium on "Advanced Flow Management: Part B Heat Transfer and Cooling in Propulsion and Power Systems, held in Loen, Norway, 7-11 May 2001,